RELATIONSHIPS BETWEEN NEAR-SURFACE PLANKTON DISTRIBUTIONS, HYDROGRAPHY, AND SATELLITE MEASURED SEA SURFACE THERMAL PATTERNS

by

Andrew Charles Thomas

B.Sc., McGill University, 1979

M.Sc., University of British Columbia, 1982

A Thesis Submitted in partial fulfillment of the requirements for

the degree of Doctor of Philosophy.

in

The Faculty of Graduate Studies

Department of Oceanography

We accept this thesis as conforming to the required standard

The University of British Columbia

December, 1987

In presenting this thesis in partial fulfilment of the requirements for an advanced degree at the University of British Columbia, I agree that the Library shall make it freely available for reference and study. I further agree that permission for extensive copying of this thesis for scholarly purposes may be granted by the head of my department or by his or her representatives. It is understood that copying or publication of this thesis for financial gain shall not be allowed without my written permission.

Department of Oceanography

The University of British Columbia
1956 Main Mall
Vancouver, Canada
V6T 1Y3

Date 27 Jan 1988

Abstract

In-situ measurements of surface chlorophyll and zooplankton concentration are compared with in-situ hydrographic measurements and infrared satellite images of the west coast of British Columbia. Their relationships are quantified for a mid-summer and an early winter study period. Winter in-situ hydrographic data showed the shelf to be dominated by Vancouver Island Coastal Current water near-shore, Davidson Current water over the middle shelf, a frontal zone separating these regimes, and North Pacific water over the shelf break. The summer shelf was dominated by topographically induced upwelling in the southern portion of the shelf and stratified regions over the outer shelf and shallow banks further north. Strong northwest winds late in the summer study period induced upwelling along the entire shelf. The surface thermal signature of each of these regimes was identifiable in the satellite imagery.

Maximum winter concentrations of chlorophyll and zooplankton were associated with Vancouver Island Coastal Current water and southern portions of the frontal zone. Davidson Current water consistently had the lowest chlorophyll concentrations in the winter study area. Zooplankton concentrations decreased with increasing temperature and distance from shore. The correlation of $\log_e$ transformed zooplankton concentrations with surface temperature allowed the satellite imagery to explain 49% of the sampled variance. The association of specific chlorophyll concentrations with each hydrographic regime enabled the satellite imagery, in conjunction with an image derived salinity model, to explain 55% of the sampled variance. Image derived plankton models allowed a spatial representation of predicted plankton concentration and the model error.

Summer zooplankton concentrations were not consistently related to satellite measured surface temperature but showed a qualitative association with higher chlorophyll concentrations around the outer edge of the upwelling area. Minimum chlorophyll concentrations were found in warm, stratified surface water and intermediate concentrations in the coldest, most recently upwelled water. Maximum concentrations oc-

curred at intermediate temperatures. A least squares fit non-linear equation showed the satellite measured surface temperature patterns explained 72% of the sampled $\log_e$ transformed chlorophyll variance. Distributions of both zooplankton and chlorophyll concentration retained their association with patterns of sea surface temperature during a wind driven upwelling event.

Multivariate cluster analysis of zooplankton taxonomic groups during both winter and summer showed spatial patterns of community composition matched satellite measured patterns of sea surface temperature over the middle and inner shelf. Over the outer shelf, spatial patterns of community structure appeared more closely associated with depth than surface thermal patterns.

Contents

List of Tables

List of Figures

Acknowledgements

I would like to acknowledge the support of my supervisor, Bill Emery, who initially convinced me that a biological oceanographer with a background in remote sensing would be a useful person, and then provided continual encouragement throughout this research. Dave Mackas of I.O.S. introduced me to continual sampling of multiple variables at sea and gave me access to to his high resolution sampling system. Bruce Dilke of Broccoli Bros., Sidney, B.C., provided technical assistance in its use at sea, and did the initial data processing. Gary Borstad of Borstad Associates Ltd. provided the cooperative support for my B.C. Great award and spent much time explaining the intricacies of satellite measurements. I thank my colleagues Paris Vachon, Hae Yong Shin and Michael Collins for their mathematical help and patient introductions to digital image processing. Denis Laplante and Paul Nowlan of the Satellite Oceanography Laboratory were a continual cheerful source of software and hardware debugging help and without whose tireless assistance I would still be trying to sign on to the Vax. I acknowledge those vintners throughout the world whose splendid products have helped maintain my sense of priorities, even at the most discouraging of times. My parents, although they still aren't sure what an oceanographer does, have always encouraged me to pursue what I enjoy doing. Most importantly, I thank my wife, Maura, whose love, support, and companionship is a constant source of happiness and stability.

RAHTID!

Chapter 1

INTRODUCTION

1.1 Overview and Objectives

The distribution of plankton in the marine environment is a result of interactions between physical, chemical and biological processes. In general, physical processes become more important in determining distributions when their time scales to produce a given biotic gradient become similar to, or less than, the time scales of such biological processes as growth rates, nutrient uptake, and reproduction *(Mackas et al. 1985; Okubo 1978)*. Numerous previous authors *(e.g. Simpson et al. 1978; Pingree et al. 1976; Chelton et al. 1982; Hayward and McGowan 1985; Wishner and Allison 1986)* have described the temporal or the spatial distribution of plankton in terms of interaction with various physical regimes. Temperature is an important component of the physical regime both as a quasi-conservative tracer of mixing, and because of it's role in the density equation of seawater. An accurate indication, if not identification, of many of the physical processes potentially responsible for plankton distributions is possible from a description of the three dimensional temperature structure of the water column. Furthermore, those processes with surface ramifications can often be identified and monitored on the basis of the two-dimensional surface temperature field. Numerous studies have used temperature as an indicator of the physical regime for comparison with plankton distributions *(e.g. Denman and Platt 1975; Denman 1976; Fasham and Pugh 1976; Fournier et al. 1979)*. These studies demonstrate that significant correla-

tions exist between the thermal regime of the ocean and plankton distributions. These correlations can result from a direct causal relationship. *Eppley (1972)* has shown that phytoplankton growth rates can be a logarithmic function of temperature. Over coarse to mesoscale areas, however, especially in coastal environments, the plankton community is most likely quite eurythermal. In general, plankton correlations with temperature arises due either to direct interaction with mixing and advective processes, or indirect interactions through trophic relationships *(e.g. Lekan and Wilson 1978; Steele and Henderson 1979; Pomeroy et al. 1983; Smith and Vidal 1984).*

In the past, mapping of plankton distributions and models relating them to physical oceanographic processes, especially in complex and dynamic continental shelf regions of the ocean, have suffered from the unavoidable non-synoptic nature of ship sampling. The problem of sampling an environment which changes in four dimensions (three spatial dimensions and time) continuously, imposes serious constraints on the design of an optimum cruise plan. It is extremely difficult, especially with non-conservative biological variables, to separate spatial variability from temporal variability. Automated sampling systems attempt to address this problem through the collection of both physical and biological measurements at a sufficient rate to allow at least quasi-synoptic surface coverage of localized areas by a single ship.

Remote sensing by satellite allows, for the first time, a truly synoptic representation of oceanographic variables. Satellite images of sea surface temperature have the potential to provide synoptic maps with sufficient spatial resolution to resolve all but the smallest scale features, and repeat coverage allowing temporal resolution of all but the highest frequency processes *(Atkinson et al. 1986).* In practice, their effectiveness is often reduced by cloud cover, and a sampling bias can be introduced by weather patterns *(Kelly 1983).* Satellite images of sea surface temperature provide a means of mapping and monitoring, in a suitably synoptic manner, the surface signature of many of the physical processes which potentially have important biological implications.

This poses the question, and the central motivation behind this thesis, of the extent

to which satellite images of sea surface temperature reflect distributions of phytoplankton and zooplankton. As the satellite sensor measures only the surface ramifications of physical processes, it is unreasonable to expect satellite images to reflect the three dimensional distributional patterns of plankton patchiness. However, to the extent that plankton spatial patchiness is a direct or indirect result of physical processes, surface distributions of phytoplankton and zooplankton might be correlated with thermal features visible in satellite imagery. If this is so, satellite images of sea surface temperature contain valuable biological information on the spatial and temporal distribution of surface plankton. On this basis it is possible to state a hypothesis which this thesis will test. Relationships between phytoplankton and zooplankton distributions and physical processes are sufficient to allow satellite images of sea surface temperature to interpolate spatial patterns of plankton distribution from ship samples. The study area chosen to test this hypothesis was the southern continental shelf of British Columbia. This region is known to be physically dynamic and therefore likely to have strong surface thermal gradients, and also to have a productive and heterogeneous plankton regime. These aspects of the study area will be reviewed in the next sections.

An early winter and a mid summer sampling period were used to investigate relationships between satellite thermal patterns and in-situ plankton distributions. The study area and relevant bathymetry are shown in Figure 1.1. Surface distributions of chlorophyll concentration and zooplankton concentration were compared with both in-situ measured hydrographic variables and satellite images of sea surface thermal patterns. Previous work in both the terrestrial and aquatic environments has shown that the biological response to environmental gradients occurs not only as changes in biomass, but often as, and often only as, changes in species composition *(Odum 1971)*. This was investigated by comparing patterns of zooplankton community composition with satellite measured sea surface thermal patterns.

The hypothesis presupposes a number of relationships which must be demonstrated in order to address the hypothesis, each of which is an important investigation in its

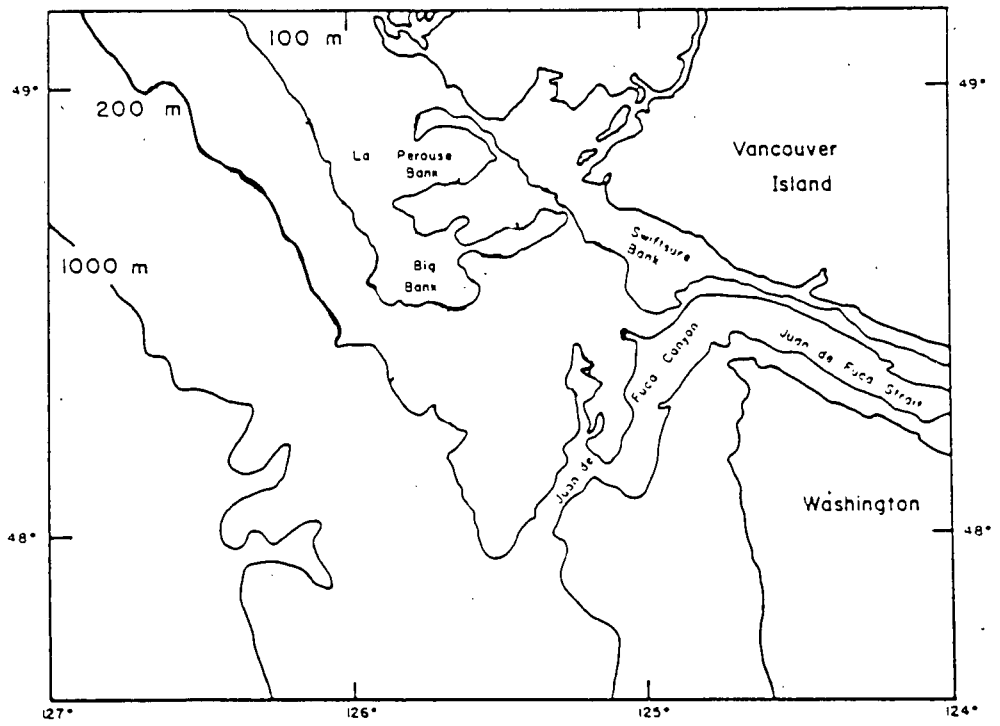

Figure 1.1: The study area on the southern British Columbia continental shelf, showing bathymetry and relevant geographic features.

own right. The relationship between satellite measured surface temperatures and ship measured temperatures is not always straightforward (see Section 1.3). In addition, the relationship between thermal patterns visible in satellite images and the physical processes within the water column which cause them is an active area of research (Section 1.3). It is these physical processes, however, which are most likely to influence the spatial distribution of plankton, rather than surface temperature *per se*. Although previous authors have discussed relationships between summer plankton distributions and physical processes on the British Columbia west coast (see Section 1.4), to date, there has been no work correlating these distributions with features seen in infrared satellite imagery. Furthermore, both winter hydrographic properties and plankton distributions remain poorly studied. For these reasons, research chronology proceeded along a series of logical steps:

1. identification of thermal regimes on the southern B.C. continental shelf vis-

ible in satellite images

2. an investigation of the relationship between these regimes and hydrographic features measured by in-situ surface and subsurface data
3. a description of surface plankton distributions for both winter and summer,
4. a qualitative and then quantitative comparison of plankton concentrations and in-situ hydrographic properties during both winter and summer,
5. qualitative and then, where possible, quantitative estimates of the similarity between patterns of satellite measured sea surface temperature and plankton distributions.

This study extends the application of infrared imagery from its traditional role of monitoring physical processes into a biological context. The continuing availability, low cost, rapid processing time and quality of the satellite imagery make its maximum exploitation for both physical and biological oceanography expedient. Restated as a sampling problem, the hypothesis has implications for both future research sampling programs and coastal monitoring. If it can be demonstrated that consistent relationships between surface temperature and plankton concentrations exist along transects sampled by ships, then satellite images, which map surface temperature in the study area in two dimensions, can be used to interpolate plankton concentrations between transects. This would provide a two dimensional estimation of the plankton distribution.

Specific questions which the thesis will address are summarized below.

- To what extent are winter and summer hydrographic features, measured in-situ, related to surface thermal features visible in infrared satellite images?
- Are there spatial similarities between the location of surface hydrographic features and surface plankton distributions?

- Do these similarities extend to relationships between thermal patterns in infrared satellite images and plankton distributions?
- If so, is it possible to quantify these relationships?
- Over what time periods might these relationships be valid?
- Do patterns of zooplankton community structure map coherently with satellite measured sea surface temperature features?

1.2 Hydrography

Early studies of the physical oceanography of the southern British Columbia continental shelf by *Tully (1942)* and *Lane (1961)* established the area as a dynamic and complex oceanographic region. *Hickey's (1979)* review of the physical oceanography of the North American west coast shows the Vancouver Island shelf to be part of the California Current System. Alongshore coherence of currents between Oregon, Washington, and Vancouver Island *(Hickey 1981)* support this observation. In general, surface currents are alongshore and to the southeast during the summer, and to the northwest during the winter under the influence of the dominant wind stress *(Hickey 1979)*. Transitions between the two regimes can be abrupt *(Huyer et al. 1979; Freeland and Denman 1982)* and usually occur in late October and in March. Data presented in this thesis represent winter and summer conditions only, and make no attempt to describe a seasonal cycle, or the transitions. A review of the hydrography of the shelf will be restricted to summer and winter conditions.

The surface current regime on the continental shelf is dominated by the tidal streams *(Freeland et al. 1984)*, and in the summer by currents induced by a cyclonic eddy over Juan de Fuca Canyon. Only through non-linear interactions and topographic rectification will tidal currents accomplish any significant property transport. The lower frequency mean current and those associated with the eddy will be more effective

in changing hydrographic properties and contributing to advection *(Freeland et al. 1984; Emery et al. 1986)*. Because cruise sampling, by necessity, integrates over many tidal cycles, and the frequency of satellite image reception is insufficient to resolve tidal advection, tidal currents and their effects will not be discussed.

Freeland et al. (1984) observe that after elimination of the tidal component, residual current time series over much of the B.C. shelf are dominated by the annual cycle. Descriptions of the winter surface temperature regime given by *Douglas and Wickett (1978)* and *Dodimead and Ballantyne (1980)* show a cross-shelf thermal gradient from colder to warmer values with increasing distance from shore. Warm water originating in the south, flowing along the shelf break near the surface has been identified as the Davidson current along the Oregon and Washington coasts *(Hickey, 1979)*. *Ikeda et al. (1984a)* identify the Davidson Current in winter satellite imagery off Vancouver Island and *Hickey (1981)* shows the coherence of northward winter velocity vectors as far north as Tofino. High current velocities close to shore in winter indicate the presence of a coastal current *(Freeland et al. 1984)*, probably driven by freshwater buoyancy input from Juan de Fuca Strait and/or coastal rivers. Current meter records reported by these authors indicate that the coastal current, which they call the Vancouver Island Coastal Current, is shallow and does not reach the bottom except in shallow areas. The dominant winter southeast winds induce an onshore Ekman transport *(Emery and Mysak 1980)* which probably plays a role in confining the lower density Coastal Current water to the inner shelf. Winter surface currents on the shelf also show the confluence of the northward flow near La Perouse Bank, indicating deflection of the current by this large topographic feature *(Freeland et al. 1984)*.

The summer shelf is dominated by a northwest mean wind direction and southeast mean flow of the California Current System *(Hickey, 1979)*. This wind creates an offshore Ekman transport which is responsible for episodic wind driven upwelling events along the Oregon, Washington and California coastlines, as well as the Vancouver Island shelf *(Huyer 1977; Freeland et al. 1984; Thomson 1981)*. *Ikeda and Emery (1984)*

show that the cold surface region develops near the coast within a day of the onset of upwelling favourable winds, and propagates offshore as a front at a rate of about $10\text{km} \cdot \text{day}^{-1}$. Colder and more saline water is thus brought to the surface over much of the continental shelf, and warmer, stratified water is advected offshore. Along the inner shelf, Hickey et al. (in prep.) show that the Vancouver Island Coastal Current persists during the summer as a near-surface , low salinity northwestward flow.

Freeland and Denman (1982) have shown that the interaction of bottom topography in the Juan de Fuca canyon region (see Figure 1.1), and the summer large scale coastal current system induces upwelling of cold subsurface water. This forms a cold, cyclonic eddy which is present for much of the summer off the mouth of Juan de Fuca Strait.

Juan de Fuca Strait essentially behaves as a large estuary, with minimum surface salinity during the summer produced by the seasonal peak in Fraser River discharge *(Herlinveaux and Tully 1961)*. Upper layer transport provides a large local source of cold, relatively fresh surface water to the southern shelf *(Freeland and Denman 1982)*. *Freeland et al. (1984)* state that during summer months, the dominant contributor of buoyancy and energy to the Vancouver Island Coastal Current is probably Juan de Fuca Strait, but at other times coastal rivers may dominate.

Numerous studies have emphasized the intense mesoscale instabilities which characterize the summer flow regime along the west coast of Vancouver Island. *Emery and Mysak (1980)*, *Ikeda et al. (1984a)*, and *Ikeda et al. (1984b)* show the existence of meanders in the California Current System with characteristic wavelengths of 75-80 km in the summer. They use a non-linear model to show that topographic features along the shelf break initiate the meanders which then grow as a result of baroclinic instability. *Thomson (1984)* describes a cyclonic eddy at the shelf break generated by baroclinic instability with isopycnal surfaces domed upward by 50 meters and a core of relatively warm, saline, and low dissolved oxygen water. The source of this upwelled water appeared to be the California Undercurrent. *Thomson and Gower (1985)* show that mesoscale eddies might also be initiated near the shelf break by local along-shore

winds and point out that the surface thermal signature of these features is often masked by solar heating of the surface layers.

1.3 Remote Sensing of Sea Surface Temperature

The Advanced Very High Resolution Radiometer (AVHRR) aboard the National Oceanographic and Atmospheric Administration (NOAA) satellite series measures upwelling radiation in either four or five relatively wide bandwidth channels. NOAA satellites are launched into a sun-synchronous, polar orbit, passing over a target at approximately the same local time each day, twice per day, once in an ascending mode, and once in a descending mode. NOAA generally keeps two satellites in operation at any time making it possible to image a particular region of ocean up to four times per day. The AVHRR is a scanning radiometer with a swath width of approximately 2600 km, and a spatial resolution of 1.1 km at nadir. Ten bit quantization of the sensor signal gives a thermal resolution of approximately 0.2°C in the infrared channels. In oceanographic applications, visible and reflected near-infrared data in channels 1 and 2 are used to identify water/land and water/ice boundaries, as well as cloud, fog, and haze. These channels are obviously only useful for daylight images. Channels 3, 4 and 5 measure radiation in the infrared portion of the spectrum. The AVHRR aboard NOAA 7 and 8, which were used for this study, had severe noise problems in channel 3, rendering it virtually useless without time consuming rectification *(Lynn and Svejkovsky 1984)*.

In general, channels 4 and/or 5 are used for ocean surface temperature measurement. Each measures the total radiation within its spectral bandwidth and within its Instantaneous Field of View (IFOV). The IFOV includes energy radiated, reradiated and backscattered from the atmospheric column between the satellite and the target, as well as the energy from the target. The primary atmospheric component responsible for attenuation of the surface energy in the infrared region of the spectrum is water vapour *(Maul and Sidran 1973; Walton 1980; Pathak 1982)*. AVHRRs with dual ther-

mal infrared channels (4 and 5) allow a *split-window* correction for this attenuation by utilizing the radiance differences at the slightly different wavelengths *(McMillan 1980; McClain et al. 1982, 1983)*. Atmospheric correction is discussed further in Chapter 2.

The AVHRR receives electromagnetic radiation only from the upper few microns of ocean surface. The response of this *skin* to environmental forcing from wind and solar heating is often independent of slightly deeper layers of the upper ocean *(Katsaros 1980)*. Accuracy of the AVHRR temperature measurement is therefore a somewhat ambiguous quantity. Ship measurements of surface temperature are taken at depths of up to a meter, and often integrate vertically over many centimeters creating an obvious bias (*Schuessel et al. 1987*). In addition, this bias is subject to diel changes caused by surface evaporation, cooling and warming *(Katsaros 1980; Lynn and Svejkovsky 1984)*. Published accuracies of the sea surface temperature product from multi-channel correction algorithms are on the order of 0.5°C RMS deviation from in-situ measured temperatures *(McClain et al. 1985; McClain 1981)* and have a bias of -0.3°C.

AVHRR imagery has been used to study a wide variety of physical oceanographic processes, many of which have important biological implications. *Simpson et al. (1978)* and *Holligan et al. (1984)* used infrared imagery to identify tidally generated frontal zones and *Roden and Paskausky (1978)* to identify oceanic frontal zones. *Legeckis (1978)* reviewed the infrared imaging of frontal zones in general. *McClain et al. (1984)* and *Ikeda and Emery (1984)* identified zones of wind driven upwelling and *Gagliardini et al. (1984)* studied river / ocean interactions. Satellite imagery has been used to measure spatial scales of surface temperature variability *(Lutjeharmes 1981; Deschamps et al. 1981)*, and map areas affected by specific advective processes *(LaViolette 1984; Legeckis and Cresswell 1981)*. The temporal resolution afforded by the repeat coverage of a target makes it possible to measure rates of advective processes and changes in the physical regime over time. *Brown et al. (1983)* and *Kasamura et al. (1986)* studied temporal variations in warm core ring structure in the Gulf Stream and the Kuroshio respectively, and *Ikeda and Emery (1984)* and *Brown et al. (1980)* measured the rate

of offshore propagation of upwelled water. On longer time scales, *Fiedler (1984)* studied the 1982-83 El Niño event on the west coast of the United States and *Legeckis (1986)* differences in surface thermal patterns in the eastern equatorial Pacific. *Legeckis and Pichel (1984)* and *Legeckis and Reverdin (1987)* showed low frequency long waves (24 days and $\approx$ 100 km) in the displacement of fronts in the Pacific and Atlantic, respectively.

Previous authors have used infrared satellite imagery to study the physical oceanography of the west coast of Vancouver Island. Early work by *Tabata and Gower (1980)* showed the relationship between ship measured temperature and satellite infrared imagery. *Emery and Mysak (1980)* used a time series of infrared images to provide evidence of baroclinic waves in the California Current System. More recently, *Ikeda et al. (1984a, 1984b)* have modelled meanders in frontal zones observed in infrared image series to show their seasonal variability, wavelength, and topographic dependence. *Ikeda and Emery (1984)* showed that infrared imagery identifies and monitors wind driven upwelling events along the Vancouver Island coast. Images of sea surface temperature showed mesoscale eddy formation which was correlated with current measurements and in-situ hydrographic variables *(Thomson 1984, Emery et al. 1986).*

Remotely sensed sea surface temperature data used in conjunction with concurrently measured biological variables provides valuable insights into their interrelationship *(Campbell and Esaias 1985).* Especially in dynamic areas, the synoptic capability of infrared satellite images is valuable in showing the spatial relationships between physical features and plankton distributions *(Traganza et al. 1983; Simpson et al. 1986; Abbott and Zion 1985).* These relationships have been shown to apply not only to chlorophyll distributions, but also to zooplankton distributions *(Wiebe et al. 1985; Haury et al. 1986; Boyd et al. 1986)* and fish distributions *(Breaker 1981). Lasker et al. (1981)* used infrared satellite imagery and in-situ measurements of anchovy egg distributions to show avoidance of certain water regimes by spawning adults. *Larsen (1985)* described relationships between satellite observed frontal zones caused by tidal

mixing and benthic invertebrate distribution. Correlations between albacore tuna catch and sea surface features seen in both infrared and colour imagery *(Laurs et al. 1984)* demonstrated a connection between biological variables of commercial importance and features seen from space.

1.4 Plankton Distributions

Spatial heterogeneity of both plankton biomass and species composition, especially in complex and dynamic coastal regions, is an accepted component of our understanding of the biology of the ocean *(Steele 1978; Longhurst 1981)*. The importance of physical processes in determining the patterns and dominant spatial scales of biological variability was reviewed by *Denman and Powell (1984)*, *Mackas et al. (1985)*, and *Legendre and Demers (1984)*. Numerous studies have provided quantitative links between the horizontal distribution of surface temperature, phytoplankton and zooplankton using in-situ measurements *(Denman and Platt 1975; Denman 1976; Steele and Henderson 1979; Lekan and Wilson 1978; Fasham and Pugh 1976; Herman et al. 1981)*. More recently, the ability of satellite sensors to image both surface temperature and ocean colour on synoptic scales has led to their use in comparing physical and biological regimes *(Traganza et al. 1983; Fiedler 1984; Abbott and Zion 1985; Simpson et al. 1986)*.

Previous work has shown the summer southern B.C. continental shelf to be dominated by intense spatial and temporal patchiness of both phytoplankton and zooplankton biomass and community structure *(Mackas et al. 1980; Denman et al. 1981; Mackas and Sefton 1982; Mackas 1984)*. Satellite images of ocean colour along the shelf edge demonstrate the patchy nature of the phytoplankton distribution and their general relationship to flow patterns *(Thomson and Gower 1985)*. *Mackas et al. (1980)* and *Denman et al. (1981)* showed that summer zooplankton and phytoplankton concentrations were relatively high inshore of a salinity front, but lower seaward of this front, over the middle shelf. Localized peaks in both phytoplankton and zooplankton

biomass were present over shallow banks and centered over the outer shelf edge. These authors stated that the actual nutrient enrichment mechanism responsible for the high levels of production is unclear. Wind driven upwelling is known to occur *(Ikeda and Emery 1984)*, however, *Denman and Freeland (1984)* showed that the wind forcing is often uncoupled from the arrival of deep, nutrient rich water on the shelf. They argued that this upwelling is most likely topographically induced by a submarine canyon. Tidal mixing over the irregular bottom topography, estuarine outflow of Juan de Fuca, wind driven upwelling, and topographically induced upwelling within the eddy probably all play a role *(La Perouse Project 1986)*.

Mackas and Sefton (1982) showed the geographic pattern of zooplankton and phytoplankton community structure to be relatively stable during summer months. The authors suggested that patterns of community structure conform to both local bathymetry and physical circulation. Temporal changes in the actual species composition within the patterns indicated that nonlocal succession and advection determine the species composition on the shelf. Dissimilarity correlograms calculated by *Mackas (1984)* showed that plankton patchiness patterns are stretched parallel to the bathymetry with cross shelf correlation scales three times shorter than the along shore scales. The zooplankton community pattern showed the longest correlation scales followed by the phytoplankton biomass. Shortest correlation scales were found for zooplankton biomass and phytoplankton community structure. Because each of these characteristics of the biological regime are subjected to the same turbulent dissipation forces over the shelf, *Mackas (1984)* concluded that these length scale differences result from intrinsic biological processes.

Each of the above studies were conducted on data collected during the late spring and summer. Data analyzed for this thesis represent the first detailed description and analysis of winter plankton distributions on the southern B.C. continental shelf.

Chapter 2

DATA COLLECTION AND PROCESSING

Data collection produced two series of infrared satellite images concurrent with in-situ physical and biological oceanographic measurements. In-situ sampling strategy was designed to collect the most synoptic measurements possible of the study area, while still providing the necessary spatial and vertical coverage for comparison with the imagery. This chapter discusses the collection of these data and initial processing steps.

2.1 Satellite Data

2.1.1 Reception

NOAA AVHRR satellite images of the west coast of Vancouver Island were received and processed at the U.B.C. Satellite Oceanography Laboratory. During the winter (1983) and summer (1984) study periods, two NOAA satellites, NOAA 7 and NOAA 8, were in operation. A maximum of three images per day was recorded. Collection began a few days prior to each cruise, continued at maximum capability during the cruise, and ended a few days after sampling had finished. Cloud-free weather in the study area during much of both sampling periods resulted in two image series concurrent with the in-situ data.

Ten infrared images of the study area were collected during the November-December 1983 sampling period and fifteen infrared images were collected during the July 1984 sampling period. Their chronology in relation to in-situ sampling procedures and orbit numbers are presented in Figure 2.1. This figure shows that the summer in-situ sampling period was approximately twice as long as the winter sampling period. This was unavoidable due to ship time-sharing and bad weather.

2.1.2 Processing

Raw satellite data were processed into 512 × 512 pixel navigated images of maximum spatial resolution (1 pixel = 1.1 km) using a U.B.C. developed image navigation procedure *(Emery and Ikeda 1988)*. Using high quality satellite ephemeris data supplied by the U.S. Navy, this procedure corrects distortions in the image due to earth curvature and rotation and relocates each pixel making image geography match a specified geographic projection. Navigated images were displayed on a raster screen and overlayed with a digitized coastal outline map. A final linear translation of each image was necessary to co-register it exactly with the digitized map. This navigation error was due to slight inaccuracies in the clock of the recording computer. Final navigational accuracy was usually within two pixels over the entire 512 × 512 image. Each image was then reduced by truncation to a 256 × 256 pixel image centered on the study area. Over this reduced area, navigational accuracy (by comparison with the digitized map) was within one pixel (1.1 km).

A two stage masking process flagged land pixels and cloud contaminated pixels in each image. Subtraction of a binary land mask from each image left ocean pixel values unchanged, but reduced all land pixels to a uniform value of 0. A subjective cloud mask for each image was produced by visual inspection of brightness values in Channels 1, 2 (for daytime images only) and 4, and comparison of patterns over each time series of images. Ocean pixels considered contaminated by cloud were then masked to a value of 255.

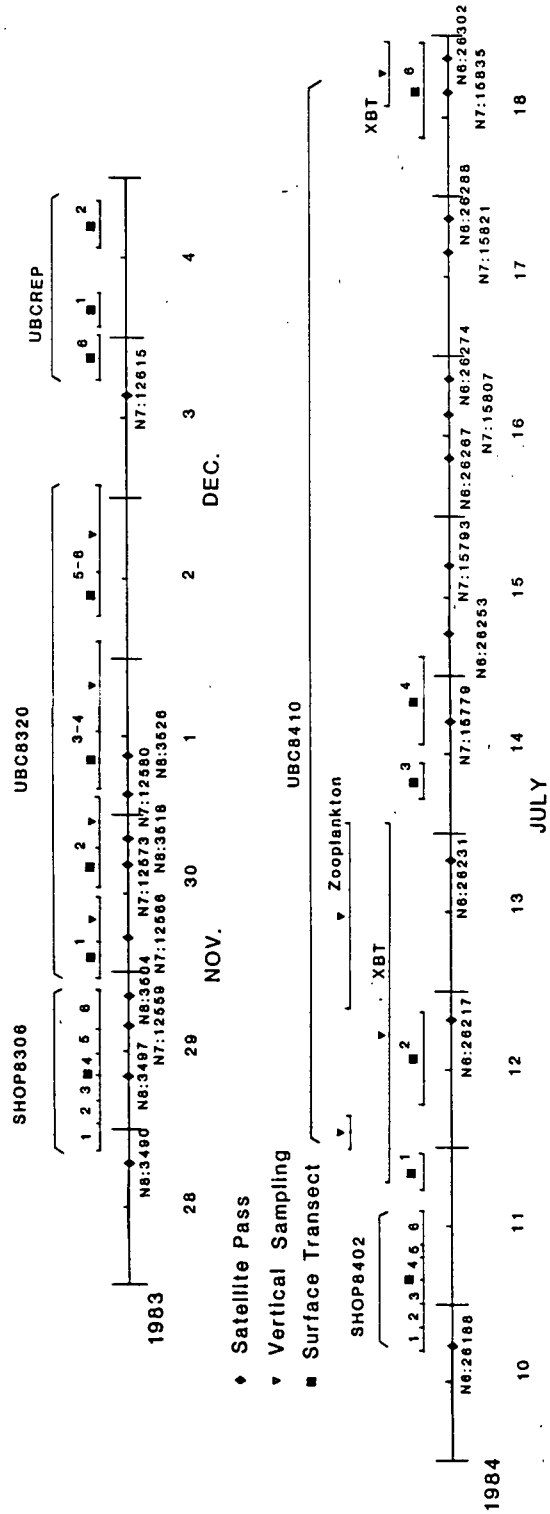

Figure 2.1: Chronology of winter and summer in-situ sampling and satellite image reception.

On-board calibration for the three infrared AVHRR channels is provided by four platinum resistance thermometers (PRT's) which monitor the instrument housing, which is designed to maintain a relatively constant blackbody temperature. Upwelling radiance for each pixel is measured in each channel (see Chapter 1) and digitized to a 10 bit count for transmission by the (High Resolution Picture Transmitter) HRPT. The AVHRR scans deep space, each PRT target and then the earth on each scan line. Coefficients provided by NOAA allow a conversion from PRT measurements to temperatures. The measurement from deep space is used as a zero value. The PRT temperatures are averaged to provide an average target temperature. Assuming the output of each channel is a linear function of radiance, the radiance in each channel is related to the 10 bit count by

$$N = G \cdot x + I$$

where N is the target radiance, x the 10 bit count, I the linear intercept, and G the channel gain. The gain, G, is given by

$$G = \frac{N_{space} - N_{target}}{x_{space} - x_{target}}$$

where N_{space} is the radiance of space, N_{target} is the radiance of the PRT target and x_{space} and x_{target} are the output counts of space and the PRT target. The intercept I,is given by

$$I = N_{space} - G \cdot x_{space}.$$

In reality, the response of channels 4 and 5 on the AVHRR is slightly non-linear, and a correction factor supplied by NOAA is applied.

The emitted radiation at frequency $\nu(Hz)$ by a blackbody (a perfect emitter) is related to temperature $T(^\circ K)$ by the Planck function

$$B\nu(T) = \frac{2h\nu^3}{c^2} \frac{1}{exp(h\nu/kT) - 1}$$

where $B\nu$ is the spectral brightness per frequency band, h is Planck's constant, ν the frequency of radiation, k is Boltzmann's constant, and c the velocity of light. Seawater emissivity approximates that of a blackbody at visible and infrared wavelengths.

In practice, the Planck function was solved backwards to calculate a radiance for each temperature in a table of temperature values. Using the satellite provided calibration values, an image specific gain and intercept was used to convert each of these radiance values to a 10 bit count. This created a Look Up Table relating temperature to radiance and finally to 10 bit count for each infrared channel of each image.

The image recording hardware in use at the U.B.C. SOL at the time of the study (a Weather Image Processing System (WIPS), provided by MacDonald, Dettwiler and Associates Ltd.) was unable to process 10 bit HRPT satellite transmissions and recorded only 8 bit data. A Look Up Table function converted the incoming 10 bit data into 8 bit data maintaining a near unit gain in the count ranges typical of ocean temperatures, and considerably less than unity for counts representative of extremes in temperature. In this way, very little ocean thermal resolution was lost. The 8 bit counts recorded by the WIPS were converted back to their original 10 bit values by inverting the WIPS function. Temperature values for these 10 bit counts were then obtained from the Look Up Table generated by the Planck function.

Temperatures measured by each of the infrared channels of the AVHRR, represent the brightness temperature of the total radiance within the IFOV. This total radiance is a summation of both the integral of the radiance emitted and absorbed by the atmosphere between the ocean and the satellite in the direction of the satellite, and the radiance of the ocean itself. This atmospheric contamination (attenuation) of the signal causes the ocean to appear colder than it actually is and must be subtracted to obtain an accurate SST measurement. An attempt to use the split-window algorithm described by *McClain et al. (1982)* to produce an atmospheric correction for the images used in this study resulted in an unacceptable increase in the spatial variance of the resultant temperature signal (Figure 2.2). This variance was most likely due to uncorrelated noise in the two channels. Although spatial filters would reduce this noise, they would also blur small scale thermal patterns and gradients and the split-window technique was not pursued.

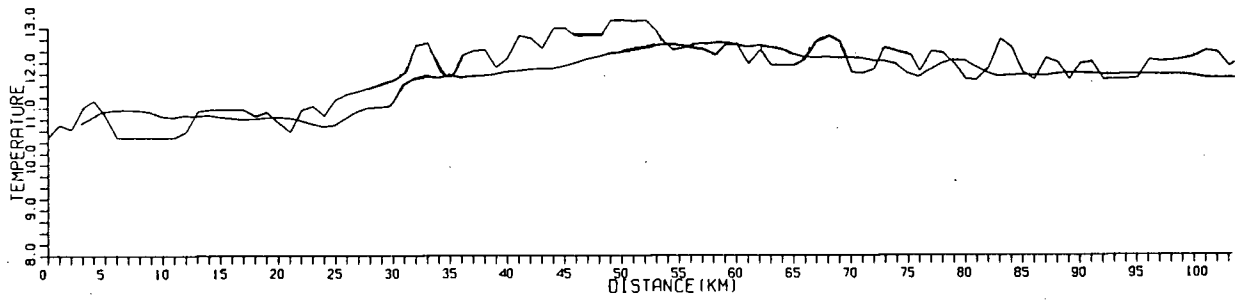

Figure 2.2: In-situ temperature and satellite split-window temperature along the same transect showing the greater variance of the split-window satellite signal.

In-situ near-surface temperature measurements (see Section 2.2) were used as ground truth data to provide the equivalent of an atmospheric correction for a single infrared channel of each satellite image (Channel 4). If we assume a horizontally homogenous atmosphere and attenuation coefficient, we can use surface data from specific sample sites within the image area to estimate the correction factor applicable to the whole image. Over relatively small areas such as the 256 $\times$ 256 pixel images used in this study, such an assumption is valid provided pixels contaminated with cloud or fog are avoided. A further advantage of this approach is the avoidance of diurnal surface skin temperature fluctuations. Treating the satellite image as a spatially varying random signal to be correlated with in-situ data, masks any diurnal surface thermal changes seen by the satellite, but not sampled by the ship.

Satellite and ship measurements of surface temperature made at the same geographic locations were compared. A mean bias was calculated for a complete transect and subtracted from the satellite data to produce two data sets of minimum RMS difference. The in-situ transect used to calculate the mean bias for each image was that sampled as close as possible in time to that of the satellite overpass to avoid errors induced by advection. Timing differences between the satellite passes and the sampling of in-situ data are shown in Figure 2.1. Subsampling of the images at a specific latitude and longitude to provide satellite temperature transects relied on image specific navigation coefficients which translate latitude and longitude to x,y coordinates and a

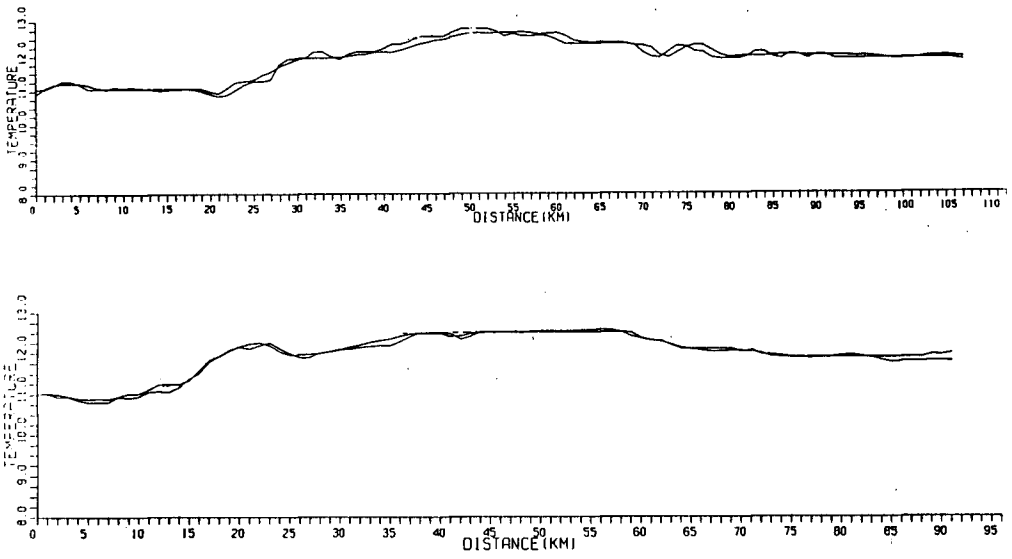

Figure 2.3: Satellite (Channel 4) temperature and in-situ temperature from two different images, along two representative transects after the subtraction of the mean bias.

bilinear interpolation algorithm given by

$$T(x,y) = dydxP_1 + dy(1-dx)P_2 + dx(1-dy)P_3 + (1-dx)(1-dy)P_4$$

where P_{1-4} are the satellite temperatures of the four pixels nearest the x, y location and dx and dy are the differences between their integer addresses in the image matrix and the x, y coordinates. This returned a single satellite measurement for each ship sample site along a transect. Examples of temperature values from the ship and satellite for two winter images and their corresponding transects are given in Figure 2.3. Correlations between satellite and ship measured temperature were high (Figure 2.4). Their variances appear similar and considerably less than that produced by the split window algorithm (Figure 2.2). The mean bias between the two signals was then subtracted from the entire satellite image.

It should be emphasized that this is not an atmospheric correction. The atmospheric attenuation component was neither measured or subtracted. While this approach made the two data sets readily comparable, the satellite image was no longer an independent measurement of sea surface temperature.

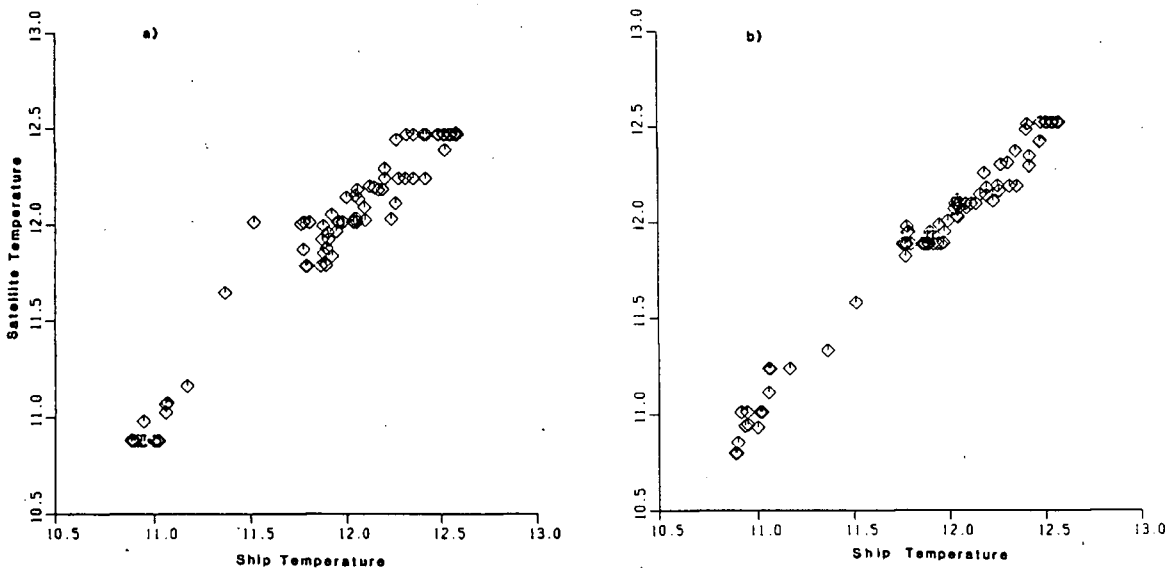

Figure 2.4: Ship measured surface temperature and channel 4 AVHRR temperature from the same location after the subtraction of the mean bias, for two representative transects. Correlation coeficients are a) 0.978 and b) 0.992.

Following ground truth calibration, each image within a season was enhanced using a single linear enhancement function given by

$$g(x,y) = \{(f(x,y) - m)/(M - m)\}(N - n) + n$$

where (M, m) are the maximum and minimum in the range of ocean temperature values $f(x,y)$ in the study area, and (N, n) are the maximum and minimum in the resultant range of 8 bit values $g(x,y)$. This transformed pixel values representative of ocean temperatures in the study area to the full 8 bit resolution of the raster display screen. Within each season, a particular temperature was represented by a single 8 bit value between 1 and 254 inclusive (0 and 255 were assigned to land and cloud pixels).

2.2 In-situ Data

Data from four cruises, two from early winter 1983, and two from mid-summer 1984 are used in this study (Figure 2.1). The two Ship of Opportunity (SHOP) cruises

were conducted by Broccoli Bros. Inc. of Sidney B.C., under contract to the Department of Fisheries and Oceans (Ocean Ecology Group). On board data collection and subsequent processing steps were similar for all four cruises. Each cruise sampled a series of cross-shelf transects making continuous measurements of surface temperature, salinity, fluorescence, and zooplankton-sized particle abundance. These data were supplemented by XBT and CTD profiles to provide an estimate of vertical hydrographic structure and vertical net hauls and bottle casts to provide a more complete description of subsurface variables.

2.2.1 Surface Data

The transects sampled during each cruise (Figure 2.1) are shown in Figures 2.5 and 2.6. Good weather during both SHOP cruises and UBC8320 allowed a regular grid to be sampled. Heavy seas, high winds and a less sea-worthy ship during UBC8410 necessitated modifications.

Near surface measurements of temperature, salinity, fluorescence, and particle number were made along each transect using a continuous flow, high resolution, automated sampling system. A detailed description of the apparatus and its use is given by *Mackas et al. (1980)* and will not be repeated here. Sampling depth was 1.5 meters during the winter cruises when the automated sampling system was linked to the ship's sea chest. Different plumbing aboard the summer research vessel did not allow a similar linkup and water was sampled from ≈ 0.5 meters depth through a towed hose attached to a worm-gear pump. Logistics, and the availability of a direct data linkup to a micro-computer necessitated the use of a different prototype of the automated sampling system for the two sampling periods. Their method of operation and basic design was similar and follows that given by *Mackas et al. (1980)*. Discrete samples were withdrawn from the sampling apparatus at half-hourly intervals and used for instrument calibration and later nutrient analysis. Fluorescence was converted to chlorophyll concentration by regression and used as a measure of phytoplankton biomass. The re-

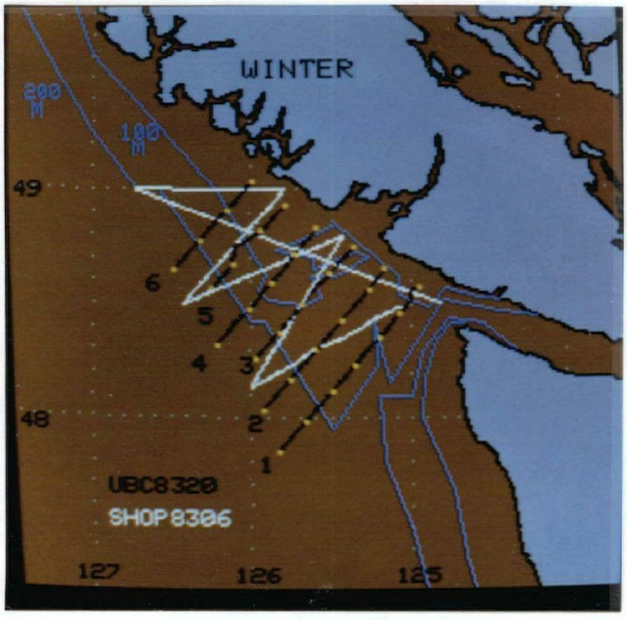

Figure 2.5: Surface sampling legs for the winter study period, representing the three sampling sequences SHOP8306, UBC8320 and UBCREP. Yellow squares indicate vertical sampling stations. UBC8320 sampling Legs are numbered. UBCREP comprised three legs, exact replicates of the longest (NW–SE) SHOP8306 leg and UBC8320 legs 1 and 2. Images in following chapters do not have lines of latitude and longitude. The scale throughout remains the same, however, and $1cm \approx 20km$.

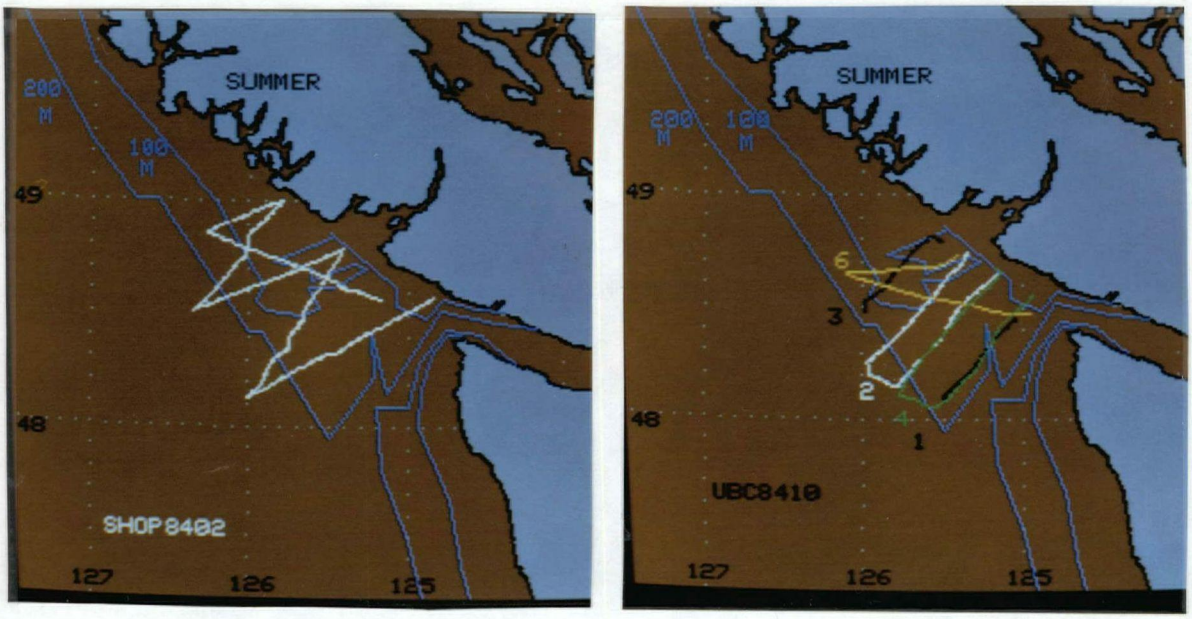

Figure 2.6: Surface sampling legs for the summer study period, for a) SHOP8402 and b) UBC8410 (Legs 1–4, and 6).

lationship between fluorescence and chlorophyll is not constant as a result of changes in species composition. However, the discrete samples allow regression lines to be constructed for different portions of the cruise. In this manner, the relationship between fluorescence and chlorophyll was optimized. Examples of changes in this relationship for the study area are shown by *Mackas et al. (1980)*. Particle counts were used as an estimation of zooplankton abundance. The instrument functions in a similar manner to a Coulter-Counter, counting particles in the water presented to it in the size range 0.3 to 3.0 millimeters. Although this is the smaller end of the zooplankton size spectrum, it does represent the numerically dominant portion of the population. The counts thus give a biased representation of biomass distribution, but a more realistic estimate of the relative numbers of small zooplankton. Nutrient samples were frozen on board and later analysed for nitrates (plus nitrites) and phosphates using an Auto-Analyser according to the methods described by *Armstrong et al. (1967)* and *Hagar et al. (1968)*.

nificant (0.5°C) positive offset caused by warming in the ship's plumbing system (see *Mackas et al. 1980*). As this bias was constant, and emphasis in this study is on relative temperatures and spatial patterns, no attempt was made to correct the offset and it is included in the satellite temperature correction described in Section 2.1.2. The bias was not measured during the summer cruises; however, the towed hose and direct linkup to the automated sampling system would have reduced any offset.

Initial processing of all the automated sampler surface data was carried out by Broccoli Bros. Inc.. At a cruising speed of approximately $18.5\text{km} \cdot \text{hr}^{-1}$, the spatial resolution of the data was $\approx$ 300 meters. This data record was first manually despiked and then averaged into one kilometre bins. This smoothing procedure eliminated small scale structure, but reduced the noise level producing an in-situ data set with a similar spatial resolution to the AVHRR data.

To reduce apparent spatial patchiness in the zooplankton data caused by diurnal vertical migrations, each of the UBC8320 transects, and each of the UBC8410 transects except part of Leg 4 were sampled during daylight. The continuous nature of the SHOP cruises did not allow such a procedure. A visual inspection of these data was made to look for any obvious increases or decreases which coincided with dusk or dawn. Visual inspection of the SHOP data sets, and comparison of UBC8410 Leg 4 with other UBC8410 transects indicated that any diurnal changes in zooplankton biomass were indistinguishable from variability within the zooplankton data as a whole.

2.2.2 Subsurface Data

Vertical profiles of temperature and salinity were obtained with a Guildline CTD at stations 18.5 km apart along each of the UBC8320 transects (Figure 2.5). These data were despiked, smoothed, and then resampled at 1 meter intervals using U.B.C. Department of Oceanography software. No CTD data were collected during UBC8410 due to a ruptured hydraulic line but vertical profiles of temperature were obtained by XBT. Summer station spacing was either 9.25 or 18.5 km across-shelf and 18.5 km along-shelf.

The geographic locations of these stations are given in Chapter 3 in relation to relevant surface thermal patterns. Temperature profiles from the XBT recording charts were digitized every 10 meters and at every change in slope of the profile. Subsurface data collected during the two SHOP cruises was not analysed in this study.

Subsurface oxygen data were collected during the summer cruise with NIO bottles set at standard depths. Stations occupied will be shown in Chapter 3 in relation to surface thermal patterns. Oxygen concentration was determined on board by Winkler titration.

Zooplankton samples for taxonomic analysis were collected with a vertically hauled, black nylon net of 0.5m diameter and 0.233mm mesh size. Samples were taken from 200m or near bottom, whichever was shallower, and preserved in 5% buffered formalin for later analysis. Sampling times for the stations occupied are shown in Figure 2.1. Station locations and names are presented in Chapter 5.

Chapter 3

SHELF HYDROGRAPHIC ZONATION

This chapter provides a descriptive analysis of the physical regime on the southern B.C. continental shelf during the winter and summer study periods. The infrared satellite data are discussed and interpreted in terms of shelf thermal zonation and temporal variation. Surface and subsurface in-situ hydrographic data are presented and described. The spatial distribution of these hydrographic characteristics are compared with the infrared images to infer physical processes in the study area which result in the thermal patterns identifiable in the imagery. These data are used to divide the shelf into distinct surface thermal zones for later comparison with surface plankton distributions.

3.1 Satellite Measured Surface Thermal Patterns

3.1.1 Winter

Visual analysis of the winter image series showed the overall pattern of sea surface temperature remained nearly constant over the image sequence. Larger scale features did not change either shape or position significantly, and most of the inter-image variability was at smaller scales (order 1–4 pixels or 1–5 km). Furthermore, the actual temperature in each region also remained approximately constant. The correlation of winter

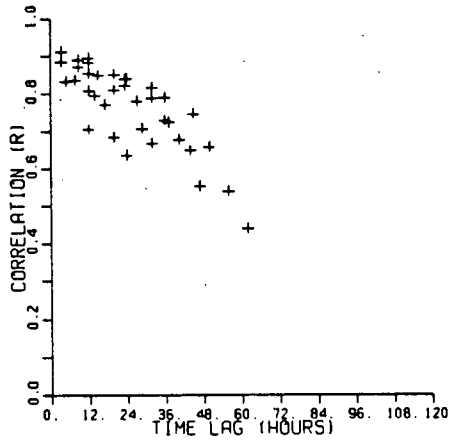

Figure 3.1: Temporal correlation of winter surface thermal patterns in the study area, measured by satellite.

image thermal patterns over time is shown in Figure 3.1. Over the sequence of winter images, surface thermal patterns remained highly correlated. These data support the extrapolated structure functions of *Denman and Freeland (1985)* which show surface thermal patterns on the shelf over time periods of a single cruise can be considered synoptic. Correlations (Figure 3.1) were calculated between all possible pairs of images using image subsamples ($\approx 150 \times 150$ km) centered on the shelf study area and plotted as a function of their temporal separation. A large component of a simple correlation between images will be due to the dominant cross-shelf gradient in temperature which was present in each image. To isolate and examine underlying thermal patterns, this gradient was removed from each image subsample by calculating and subtracting the least squares fit plane (in $x, y, T°C$ space) of each image from itself. Correlation calculations shown in Figure 3.1 were then made on the residual thermal pattern. The winter image sequence, however, covered only the time period during which SHOP8306 and UBC8320 were sampled. No images coincided with the sampling of UBCREP (see Figure 2.1).

The high correlation of thermal patterns over time periods of less than 48 hours permits a mean image to represent the winter surface thermal regime present during the winter cruises. Figure 3.2 shows the winter mean image calculated as the arithmetic

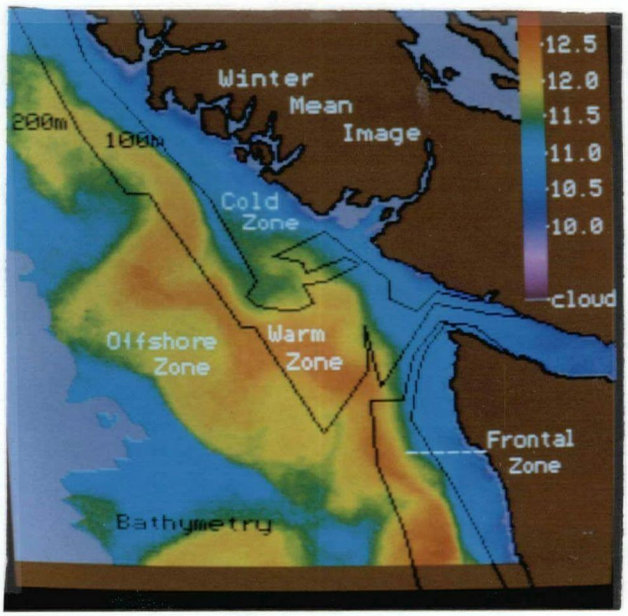

Figure 3.2: Winter mean sea surface temperature image showing the four major surface thermal zones. The image is a mean of the nine most cloud-free images.

mean of the nine most cloud-free images. Only pixels which were cloud free in five or more images were used to calculate a mean temperature; pixels failing this criterion were classified as cloud. In general, a large portion of the actual study area was cloud-free in all nine images. While not a statistically robust representation of winter conditions, Figure 3.2 does represent the mean thermal field over the majority of the sampling period.

The mean image shows the study area can be divided into four major surface thermal zones. The dominant feature of the image was a region of warmest water over the middle and outer shelf, with temperatures above 12.2°C(warm zone). Cross-shelf variability in the position of this warm water resulted in an on-shore penetration in the southern portion of the shelf, immediately south of La Perouse Bank. At La Perouse Bank, the warm water curved offshore, away from the shelf. Coldest surface water was present as a continuous zone closest to shore, with temperatures below 11.5°C(cold zone). A distinct feature of this coastal zone was a tongue extending away from shore in a

southward direction in the vicinity of La Perouse Bank. Surface water seaward of the warmest band, over the shelfbreak, formed a third thermal zone with intermediate temperatures of 11.6°C(offshore zone). Water seaward of this zone was colder (11.0°C in the satellite image) but was never sampled by the ship. Although this water clearly formed another surface thermal zone, it will not be treated in this study as no in-situ data was available for comparison. A fourth thermal zone within the study area was created by the strong surface thermal gradient separating the cold coastal water from warmer water over the middle and outer shelf. Figure 3.3 shows the magnitude and position of surface gradients in the study area. Surface temperature gradients were computed using an unweighted central difference, the magnitude of which is given by

$$|T_{(x,y)}| = \frac{1}{2\triangle h}\{[T_{(x-\triangle h,y)} - T_{(x+\triangle h,y)}]^2 + [T_{(x,y-\triangle h)} - T_{(x,y+\triangle h)}]^2\}^{1/2}$$

where T is the surface temperature at position x, y and $\triangle h$ is a spatial separation. The largest gradients formed a frontal zone which was strongest in the southern portion of the study area, off the mouth of Juan de Fuca Strait, and further north over the outer edge of La Perouse Bank. Surface gradients were weakest and most diffuse in the central portion of the study area, over southern La Perouse Bank. Gradients calculated from the mean image will underestimate gradient magnitude and overestimate width due to temporal variability in the frontal position. For this reason, Figure 3.3 was calculated from a single image (N7 12566, see Figure 2.1) near the middle of the UBC8320 sampling sequence.

The spatial pattern of variance associated with the mean image (Figure 3.4) is shown in support of the decision to divide the study area into separate thermal zones in which temperatures remained relatively stable. This image shows relatively low thermal variance within colder water near the coast, in the warmest region, and in cooler water southwest of this warm water. Maximum thermal variance was associated with frontal zones. In these regions, minimal spatial and/or temporal changes in the gradient position or magnitude would create maximum surface thermal variability.

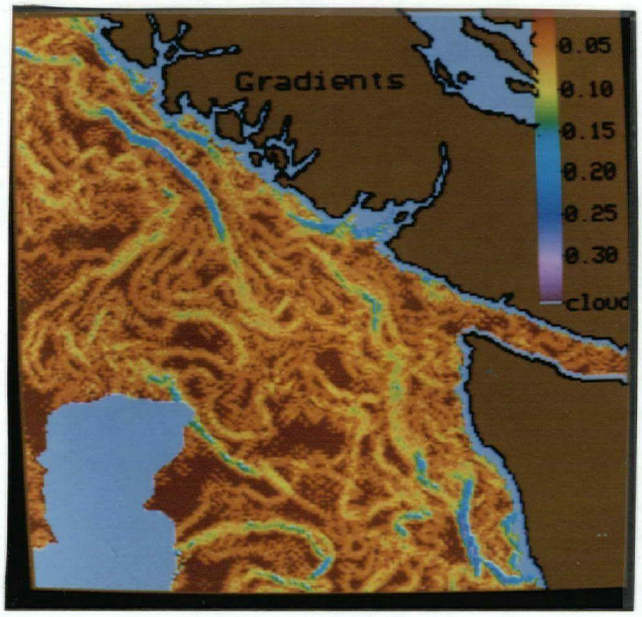

Figure 3.3: Winter sea surface temperature gradients in $°C \cdot km^{-1}$ for Nov. 30, 1983 (N7.12566).

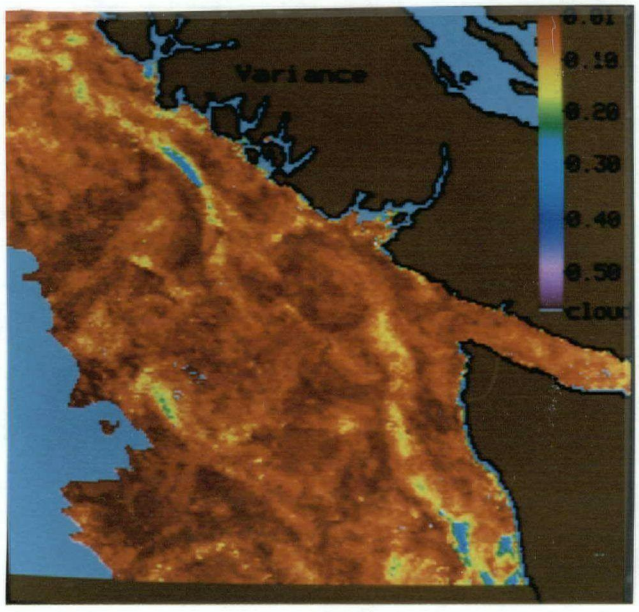

Figure 3.4: Spatial patterns of winter sea surface temperature variance.

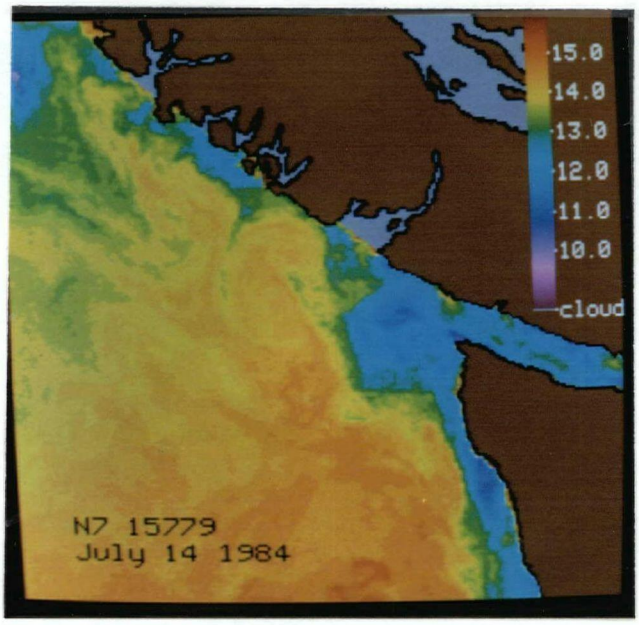

Figure 3.5: N7 15779, recorded July 14, early in the summer sampling period.

3.1.2 Summer

Visual analysis of the summer image series revealed significant changes in the overall surface thermal pattern in the study area over the time period of in-situ sampling. A mean image for the entire series would not be meaningful, and all in-situ data cannot be considered synoptic. Figure 3.5 provides an example of sea surface temperature patterns early in the sampling period, and Figure 3.6 shows patterns present during the latter period of sampling.

The summer study area was divided into two regions based on thermal patterns seen in the imagery. The shelf area south of La Perouse Bank and over Juan de Fuca Canyon remained relatively cold throughout the study period with thermal patterns retaining a generally circular shape. Mean surface temperatures in this region ranged from 11.5 to 12.6°C. The shelf areas seaward and also north of this region, over La Perouse Bank, were relatively warm in the early portion of the study period with mean surface temperatures ranging from 13.5 to 15.5°C. The region over La Perouse Bank, however, cooled rapidly later in the study period. These temporal changes are

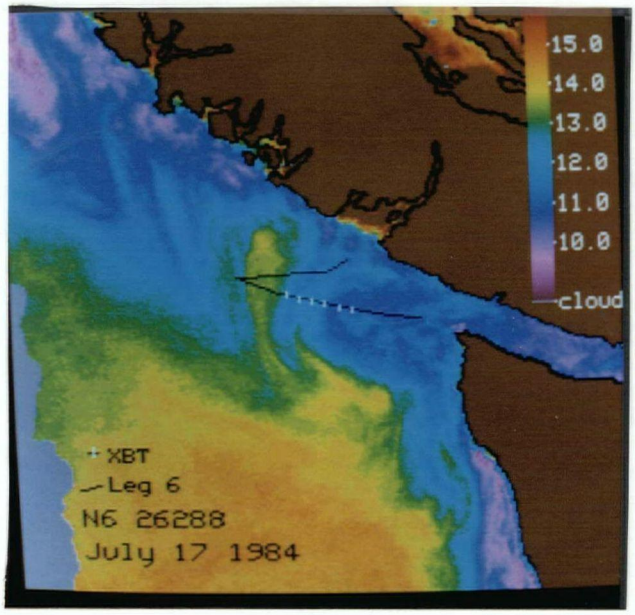

Figure 3.6: N6 26288, recorded July 17, late in the summer sampling period. This figure also shows the ship transect (UBC8410 leg 6) sampled for surface data, and the location of stations sampled for subsurface profiles of temperature.

shown quantitatively in Figure 3.7. Mean surface temperatures in these two areas were calculated from subsamples of each image and plotted over the study period. Temperature variation in the colder region over Juan de Fuca Canyon was relatively small, with a total range of 1.2°C. A decrease of 0.8°C occurred in 18 hours between July 16 and 17. In contrast, the mean temperature range over La Perouse Bank was greater than 2.0°C with a decrease of 1.2°C over the same 18 hour period on July 16-17. Figure 3.7 shows that cooling in this northern region began approximately 24 hours before any changes took place in the mean surface temperature of the colder water, and continued for an additional 24 hours.

Temporal correlation calculations show that the lack of synopticity in summer in-situ data was due to the longer sampling period rather than greater temporal variability in thermal patterns. The correlation of summer surface thermal patterns in the study area over time (Figure 3.8) was calculated from detrended images in a similar manner to the winter sequence. A comparison with winter image correlations (Figure 3.1)

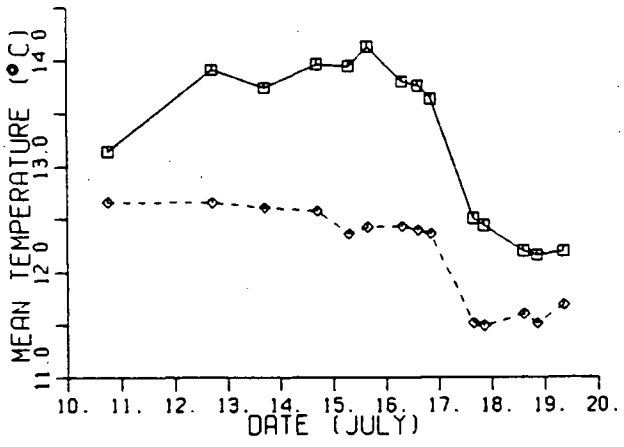

Figure 3.7: Changes in satellite measured mean sea surface temperature for the northern (La Perouse Bank) (solid line) and southern (Juan de Fuca Canyon) (dashed line) regions of the shelf during the summer sampling period. Symbols show the times of satellite overpass.

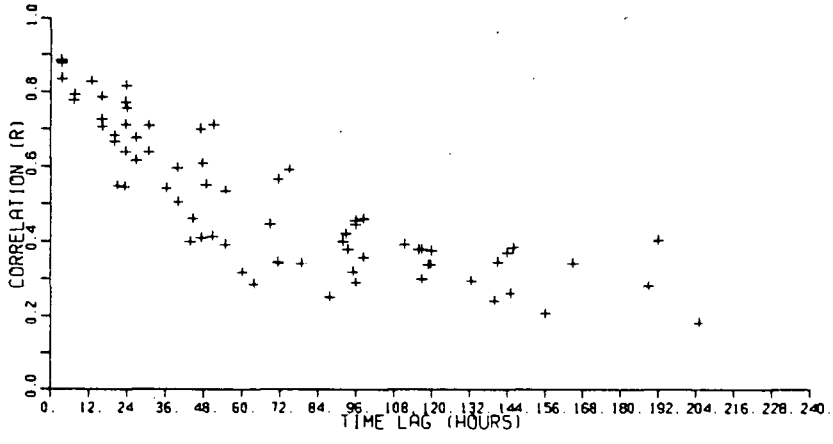

Figure 3.8: Temporal correlation of summer surface thermal patterns in the study area.

shows that the rate of decorrelation in both seasons is approximately the same. Over time periods less than 36 hours, surface patterns remained highly correlated. At separations greater than 24 hours, however, the summer range in correlation values began to increase. At 48 hours separation, correlations range from 0.72 to 0.38. This reflects the short time scale "event" which rapidly changed surface temperatures and patterns on July 16-17. Prior to this event, image patterns remained similar, and significant correlations in Figure 3.8 extend to separations as long as 72 hours. Extrapolated structure functions from data averaged over 25 cruises *(Denman and Freeland 1985)* show near-surface thermal patterns might be considered synoptic for time scales of less than 10 days. Although the satellite measured surface skin temperature can be expected to less conservative than the integrated upper layers measured by these authors, data presented here suggests that, at least in this case, specific events can make time scales of synopticity considerably shorter than this 10 day mean. Figure 3.8 provides evidence of both situations. High correlations ($r > 0.6$) extend for as long as 72 hours, yet there are correlations less than 0.6 at temporal separations as short as 20 hours. Figures 3.7 and 3.8 emphasize the ability of satellite images to monitor changes in the surface physical regime over 'event' scale time periods.

The summer image sequence was divided into two periods. A mean image (Figure 3.9) calculated from the five satellite images recorded prior to the cooling event represents sea surface thermal patterns for this period and was considered concurrent with SHOP8402 data and UBC8410 data from Legs 1-4. Only those pixels which were cloud free in three or more of the images were used to form the mean. In general, the entire study area was cloud-free over the image sequence used to calculate this mean. A single image (Figure 3.6) was used to represent surface thermal patterns during the wind event sampled by UBC8410 Leg 6 (see Figure 2.1). The spatial pattern of variance associated with the mean image (Figure 3.10) shows maximum temporal thermal variations were associated with the frontal region separating the cold near-shore water from warmer water over the outer shelf and the northern portion of the study area.

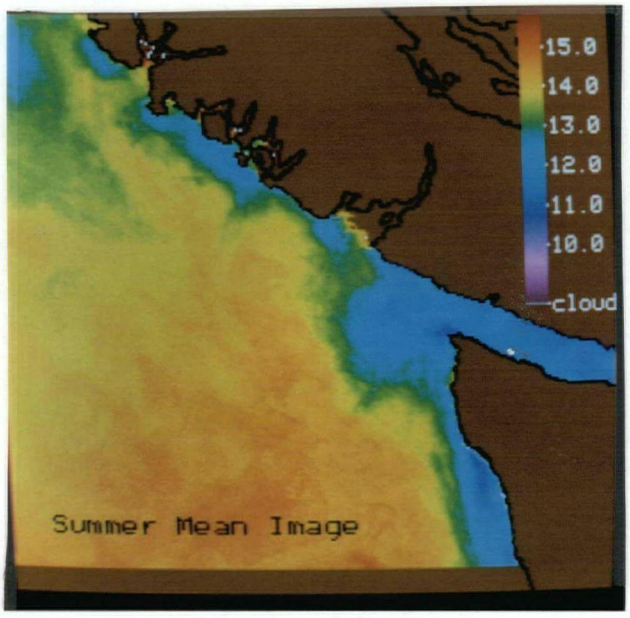

Figure 3.9: Summer mean sea surface temperature image, representing the period prior to the cooling event.

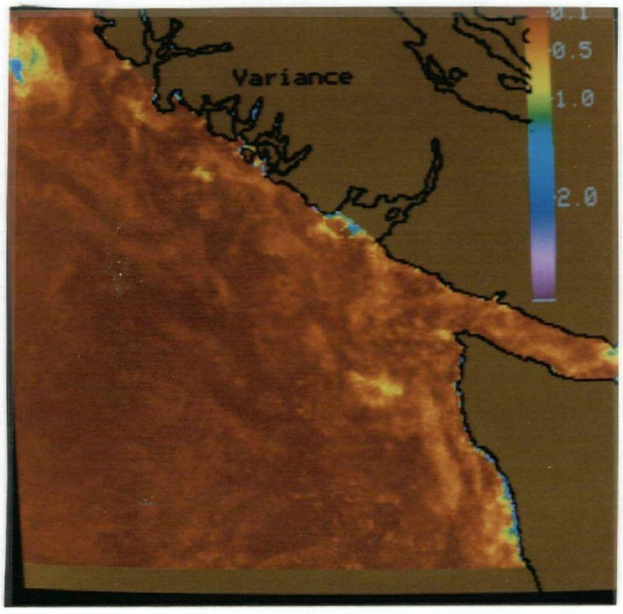

Figure 3.10: Spatial patterns of surface temperature variance associated with the summer mean sea surface temperature image.

Variance was low throughout the rest of the study area. This image is presented as evidence that temperature fluctuations within the zones identified in the mean image were minimal, and the mean image is a realistic representation of temperatures and thermal patterns prior to the cooling event.

3.2 In-situ Hydrographic Data

3.2.1 Winter

Examples of the four variables collected by the automated underway surface sampler during the winter cruises of SHOP8306, UBC8320 and UBCREP are shown in Figure 3.11a–f (UBC8320 Legs 1–6). Surface data from SHOP8306 is presented in a data report available from the Institute of Ocean Sciences, Sidney, B.C., prepared by Broccoli Oceanographic. Inc. (1983). All surface data is available as digitized values stored on magnetic tape at the U.B.C. Satellite Oceanography Laboratory.

Although this chapter deals specifically with physical measurements, surface chlorophyll concentration and zooplankton abundance are plotted parallel with temperature and salinity to introduce spatial relationships between the physical and biological regimes and for later comparison. Locations of each of the winter transects are given in Figure 2.5. The location of SHOP8306 and UBC8320 transects are superimposed on the mean winter temperature image in Figure 3.12.

The association of lower temperatures with lower salinities is immediately obvious in Figure 3.11. Contour plots of the spatial distribution of surface temperature and salinity from UBC8320 data (Figures 3.13 and 3.14) show that this low temperature, low salinity water was restricted to the inner shelf, and most pronounced near the mouth of Juan de Fuca Strait. Although the satellite image shows surface thermal patterns, contours of in-situ temperature are presented to give a spatial representation of surface temperature using the same data grid and temporal synopticity as salinity (and later, chlorophyll and zooplankton). Surface salinity distribution over the shelf

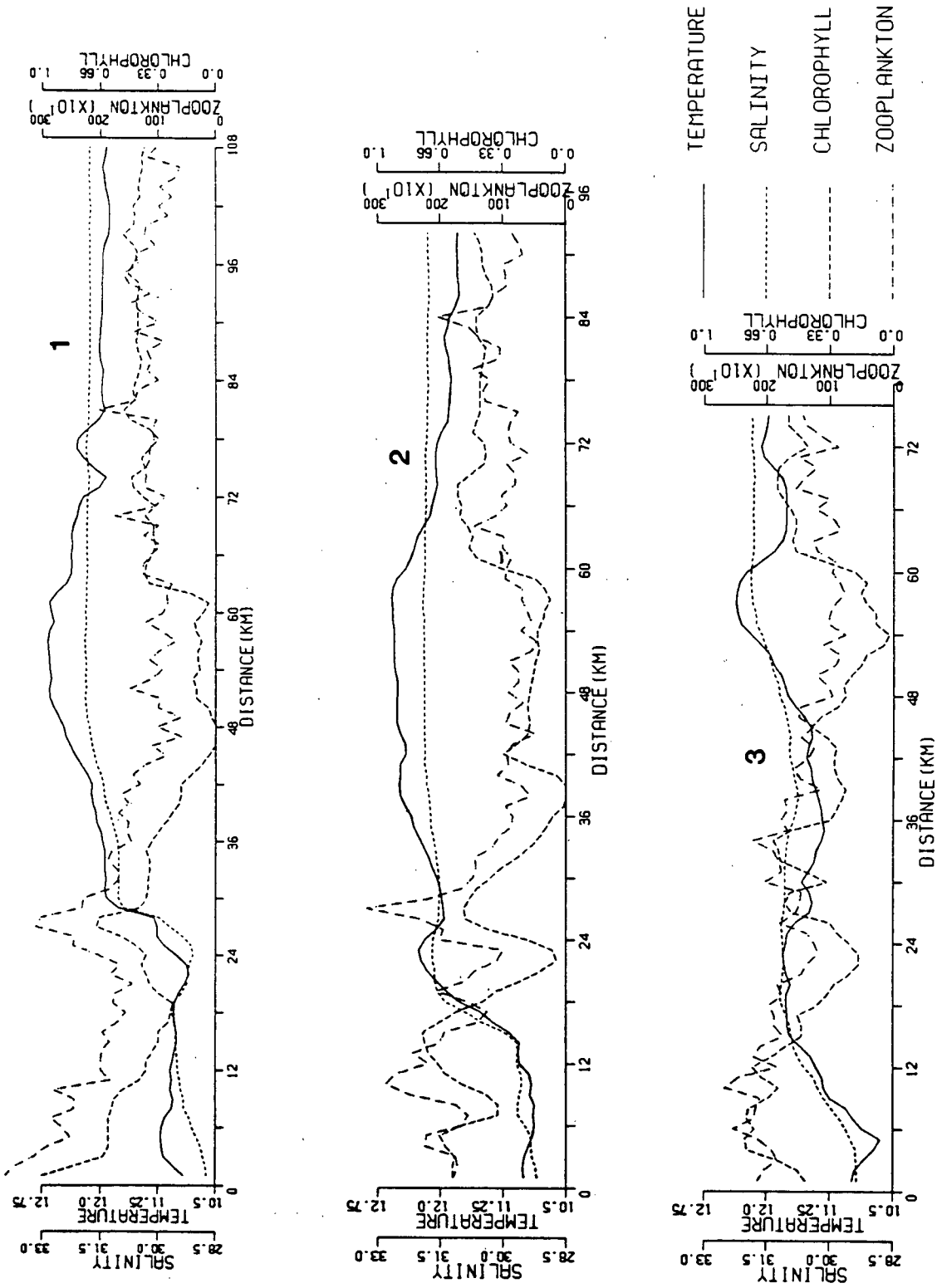

Figure 3.11: See next caption.

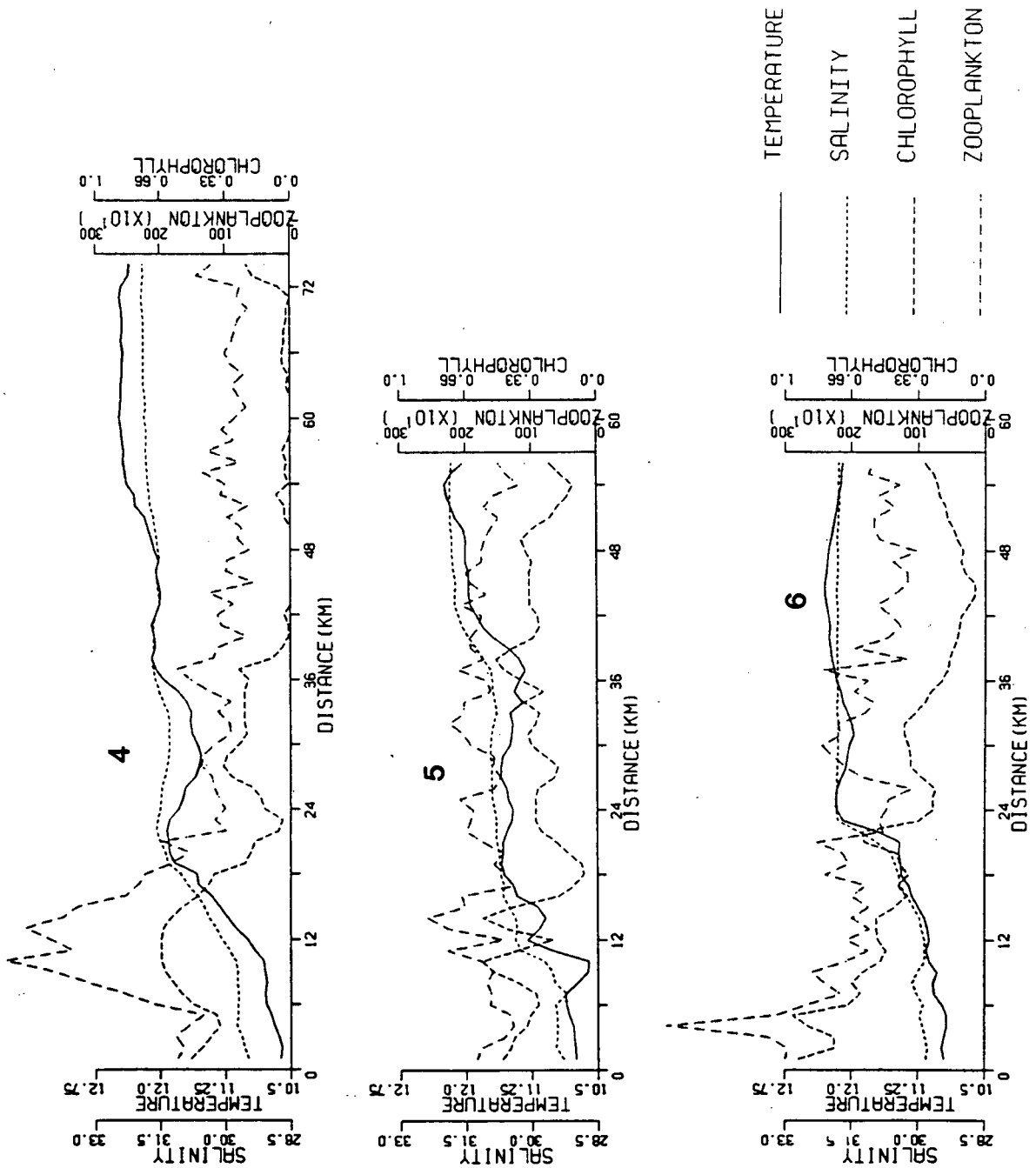

Figure 3.11: Winter surface temperature (°C), salinity, chlorophyll ($mg \cdot m^{-3}$) and zooplankton ($counts \cdot m^{-3}$) data from UBC8320 Legs 1–6.

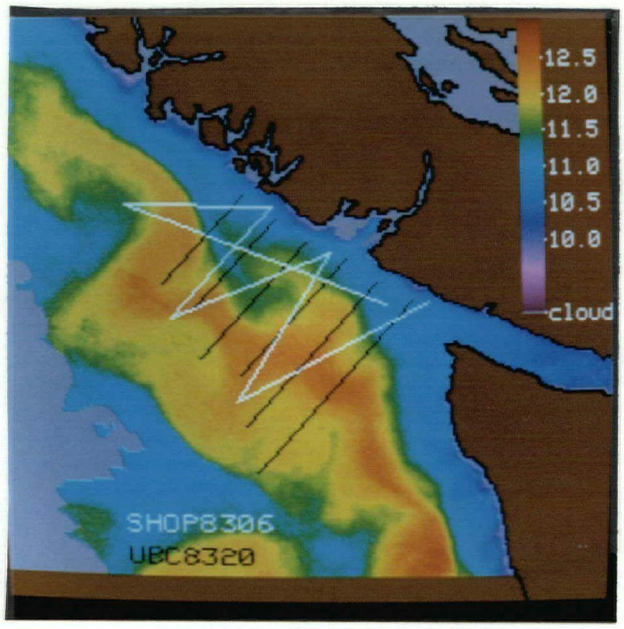

Figure 3.12: Winter ship sampling transects in relation to mean sea surface temperatures.

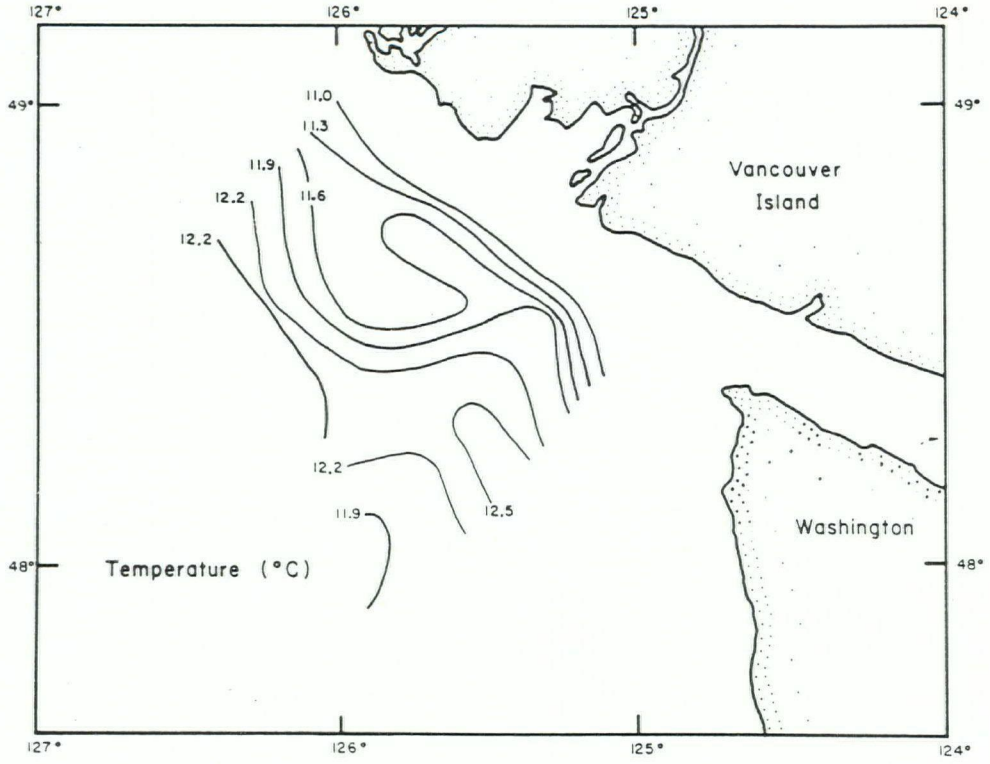

Figure 3.13: Contours of ship measured winter surface temperature (UBC8320 data.)

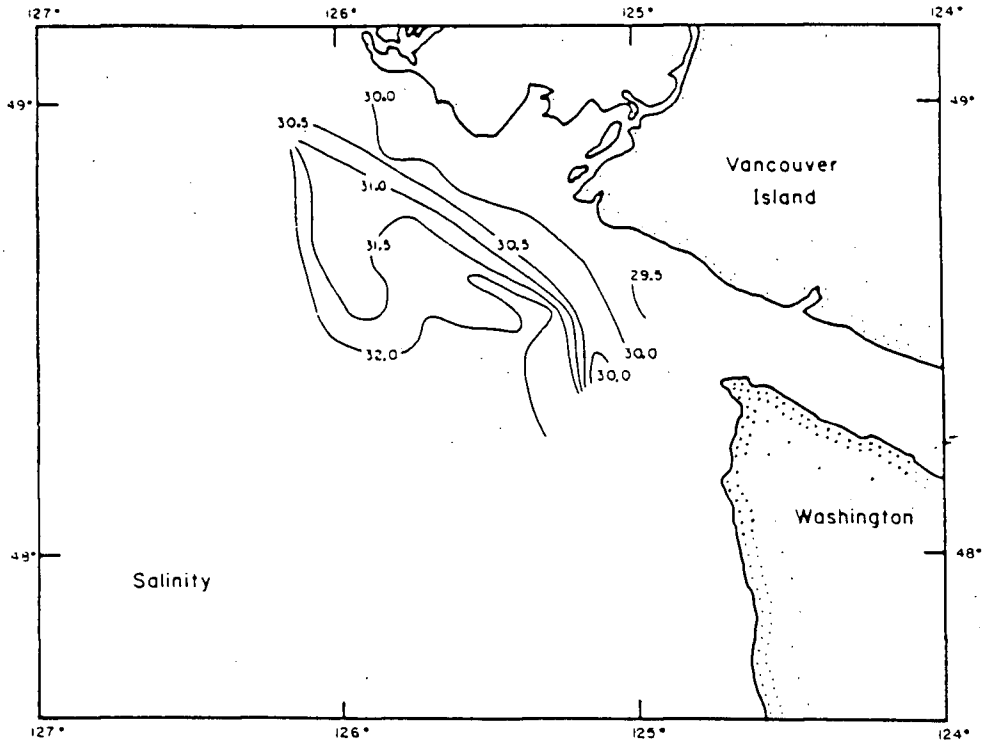

Figure 3.14: Contours of winter surface salinity (UBC8320 data).

increased from less than 30 in nearshore areas, to 32 over the outer shelf. A steep salinity gradient (1.0 in 4 km) was associated with the 30 isohaline and was most pronounced in the southern portion of the study area. The surface expression of the 31.5 isohaline extended furthest from shore in the northern portion of the study area over La Perouse Bank. Salinities greater than 31.5 showed their greatest on-shelf penetration in the vicinity of SHOP and UBC Legs 2, just south of La Perouse Bank. Salinity contours show that most of the spatial structure seen in the temperature distribution is reflected in the salinity distribution except that associated with the warmest water in the study area, over the outer shelf. The steep salinity gradient was coincident with the thermal front seen in both the imagery and in-situ data (Figures 3.2 and 3.11).

T/S plots of surface data from each winter sampling sequence (Figures 3.15, 3.16 and 3.17) show the hydrographic relationship of surface waters and support the surface zonation described from satellite imagery. Near-shore water had the lowest tempera-

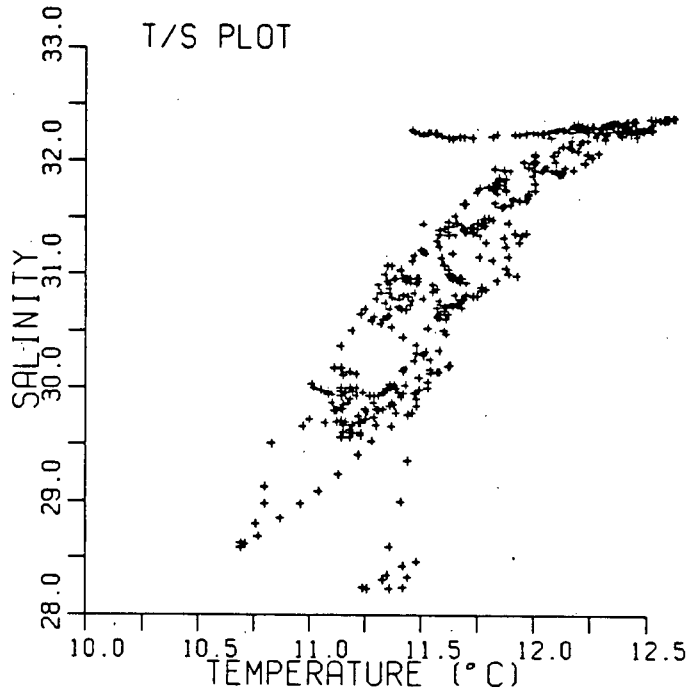

Figure 3.15: Surface temperature / salinity relationships of SHOP8306 data.

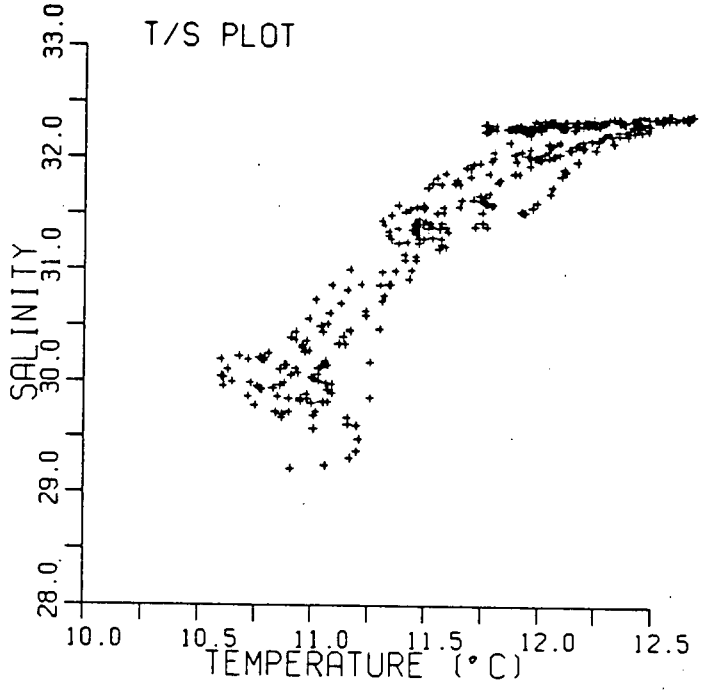

Figure 3.16: Surface temperature / salinity relationships of UBC8320 data.

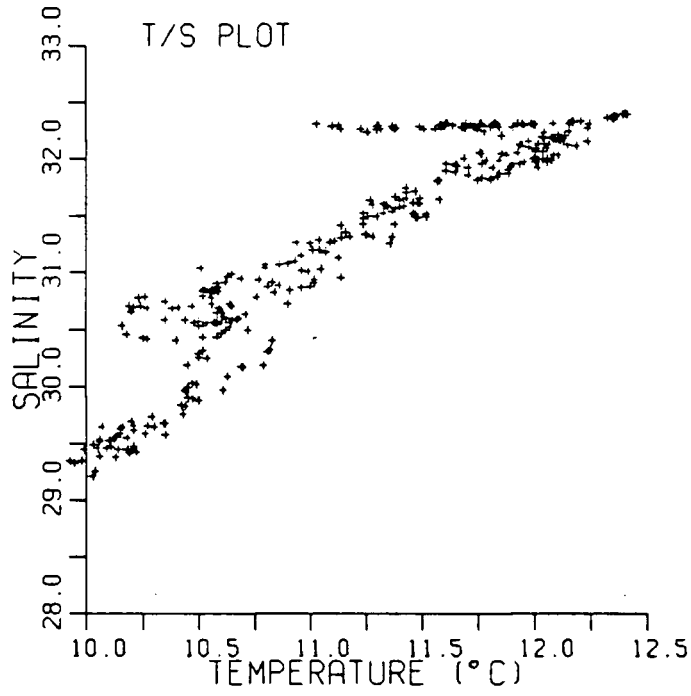

Figure 3.17: Surface temperature / salinity relationships of UBCREP data.

ture ($<$ 11.5°C), and lowest salinity ($<$ 31.5). Two types of surface water with higher salinities ($>$ 32.0) are differentiated by temperature in the plots. Warmest temperatures in the study area were above 12.20°C. A second high salinity water type had temperatures between 11.50°C and 12.20°C. Other data points form a line between the coastal water characteristics and the warmest, high salinity water indicating that mixing and interaction between colder coastal water and the warmest water formed a major portion of sampled surface water over the winter shelf.

Contours of subsurface temperature and salinity (Figures 3.18a-f and 3.19a-f) show the inner-shelf colder, low salinity water was a near surface feature (see Figure 2.5 for station locations). The warmest surface water identified in the image sequence and surface contours was a distinct core of warm water ($<$ 11.50°C) over the outer shelf at Leg 1. At Legs 2 and 3 this water intruded over much of the shelf and undercut colder near-surface water. The main core was visible again at Leg 4 over the outer shelf. Legs 5 and 6 showed warmer water at the surface over the outer shelf, but beneath coastal

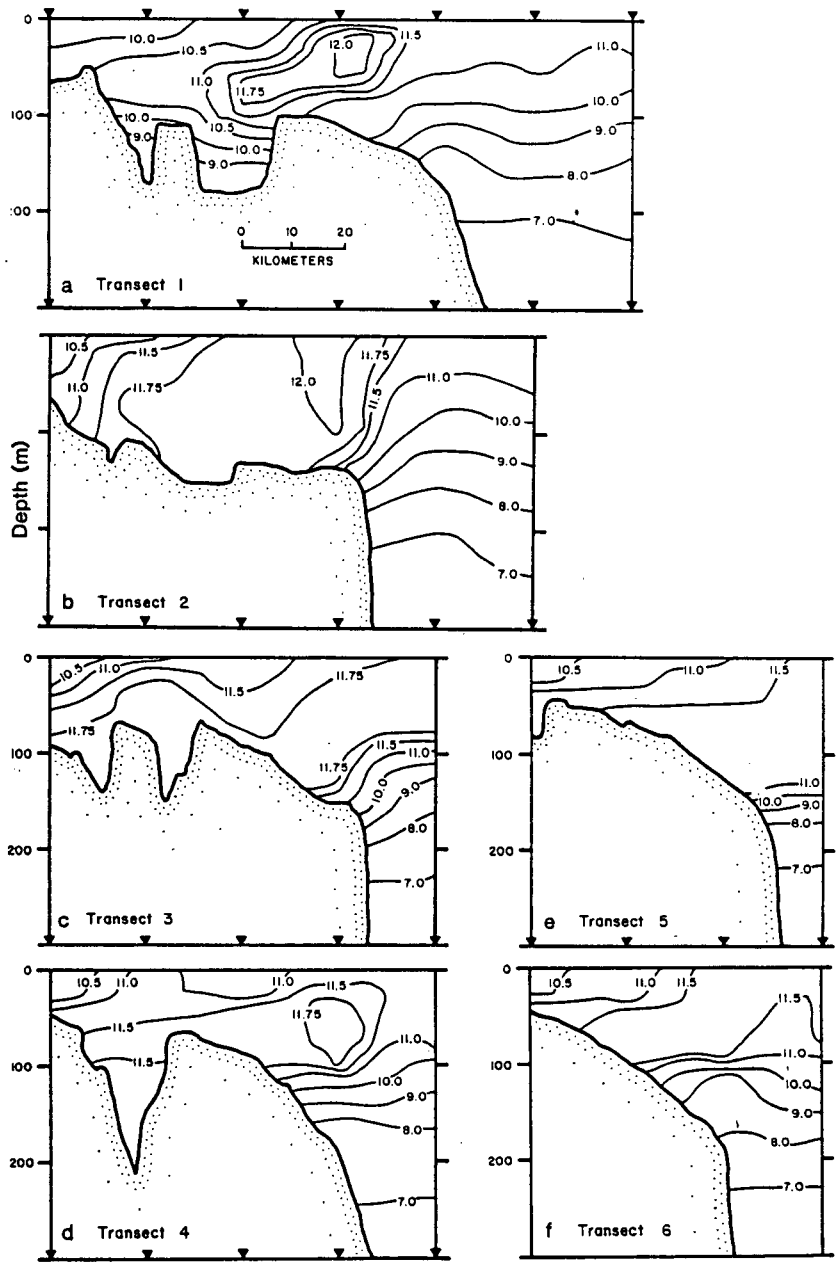

Figure 3.18: Contours of subsurface temperature along UBC8320 Legs 1–6. Triangles represent station locations.

water near the coast. At both Legs 5 and 6, a clearly defined core of warm water was not visible. Figure 3.12 shows these transects did not penetrate far enough from shore to cross the main core of warmest water.

At the temperatures and salinities present during winter sampling, density is primarily a function of salinity. Vertical salinity contours show the shelf was most strongly stratified near the coast where the low temperature, low salinity coastal water was present at the surface. Seaward of the frontal zone, vertical stratification was reduced, and was minimum in the warmest water (Figure 3.19).

3.2.2 Summer

Examples of the four surface variables collected by the automated sampler during the summer cruises of SHOP8402 and UBC8410 are given in Figure 3.20a-e (UBC8410 Legs 1–4, and 6). Surface data from SHOP8402 is presented in a data report available from the Institute of Ocean Sciences, Sidney, B.C., prepared by Broccoli Oceanographic. Inc. (1984). All surface data from these cruises is available as digitized values stored on magnetic tape at the U.B.C. Satellite Oceanography Laboratory. Details of the chlorophyll and zooplankton distribution will be discussed in Chapter 4. Locations of these summer transects are shown in Figure 2.6 and in relation to summer surface thermal patterns in Figures 3.21 and 3.6.

Temporal correlation of surface thermal patterns (Figure 3.8) indicates that data from SHOP8402, sampled within a 24 hour period, can be considered synoptic. The satellite data (Section 3.1.2), however, showed that all UBC8410 transects (July 11-18) were not synoptic. Surface data from this cruise is divided into two parts. Legs 1–4 were collected within a $3\frac{1}{2}$ day period before the cooling event and are considered synoptic. Leg 6 was sampled 78 hours later during the cooling event and will be discussed separately.

Ship sampled surface temperature (Figures 3.20) confirms the thermal patterns seen in the imagery. In general, surface temperatures were lowest near shore and highest

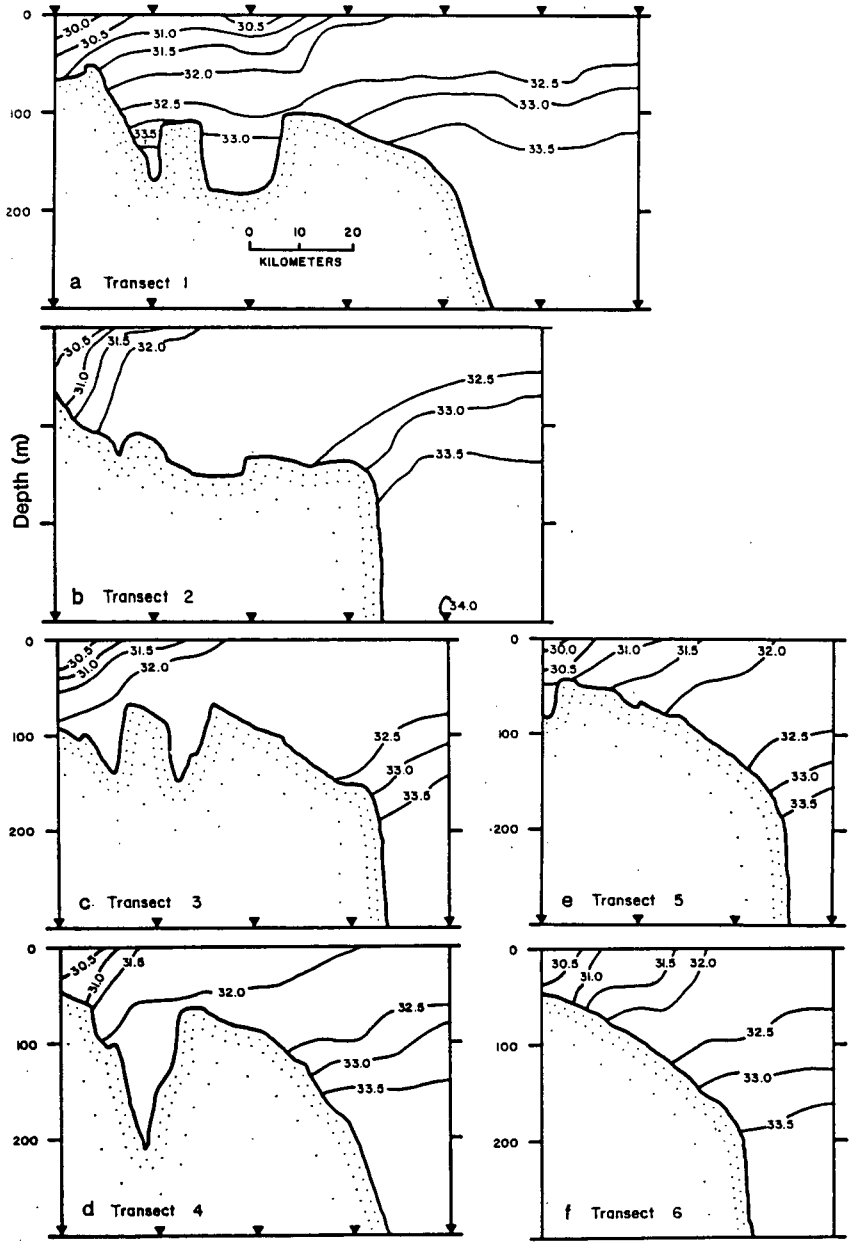

Figure 3.19: Contours of subsurface salinity along UBC8320 Legs 1–6. Triangles represent station locations.

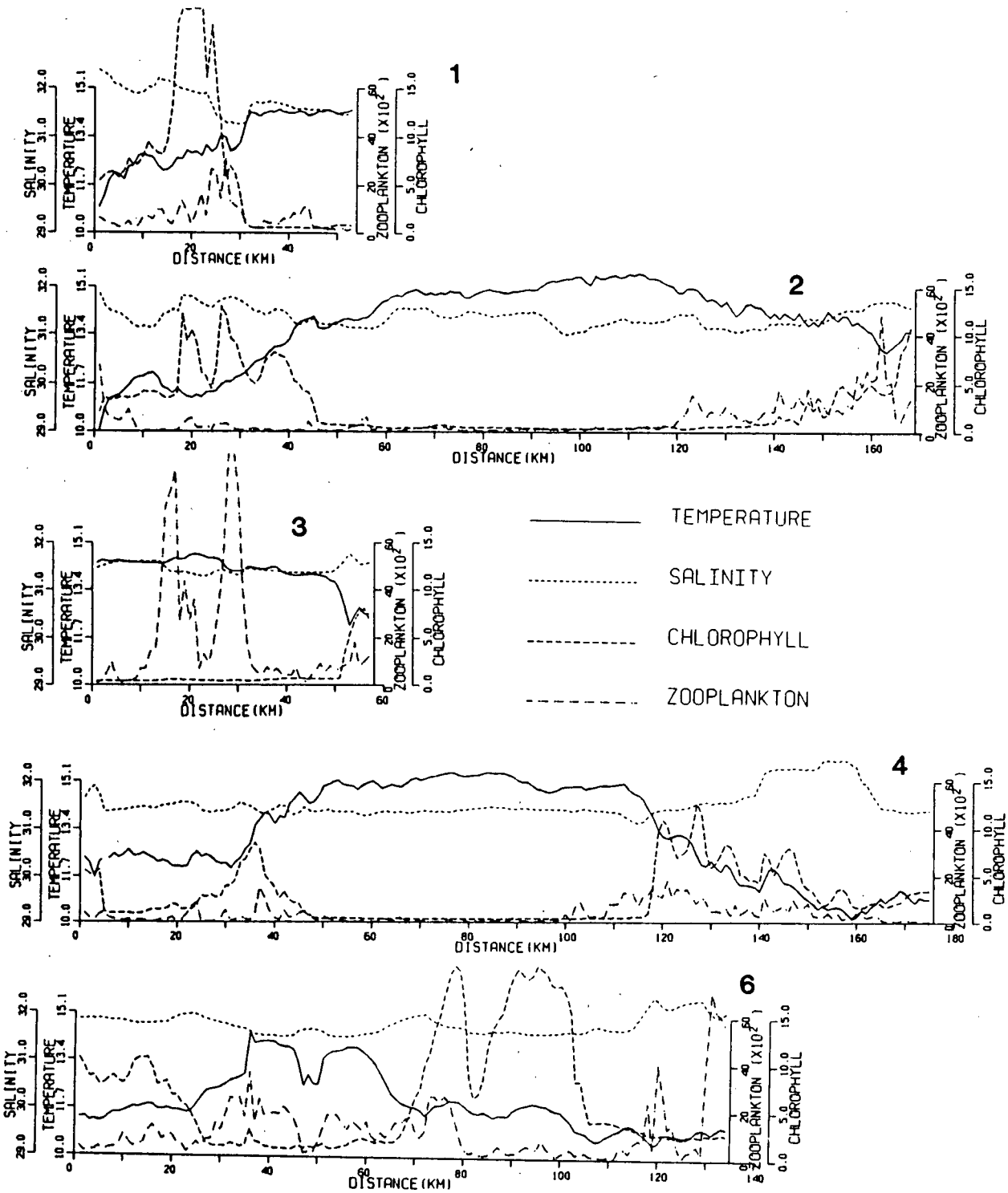

Figure 3.20: Summer surface temperature (°C), salinity, chlorophyll ($mg \cdot m^{-3}$) and zooplankton ($counts \cdot m^{-3}$) data from UBC8410 Legs 1–4, and 6.

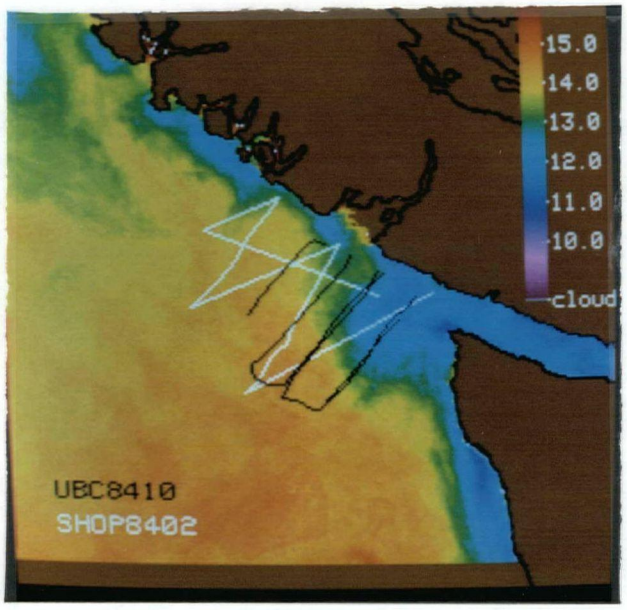

Figure 3.21: Summer ship sampling transects (SHOP8402 and UBC8410 legs 1-4) for the period prior to the cooling event, in relation to the mean sea surface temperature image.

over the outer shelf. Near-shore low temperatures were less than 11.5°C at Leg 1 and less than 13.5°C at the near-shore portions of legs further north (Legs 2 and 3). Temperatures offshore showed little variability and were greater than 14.0°C. Higher surface salinities along the sampling legs (Figure 3.20) were, in general, associated with lower temperatures.

Summer relationships between surface temperature and salinity were not as distinct as those observed during the winter. T/S plots of surface characteristics from both SHOP8402 (Figure 3.22) and UBC8410 (Figure 3.23 and 3.24) show a general trend of colder temperatures associated with higher salinities but do not give a clear definition of water masses and mixing trends. This is most likely due to strong solar heating of surface water which would change the relationship between surface temperature and salinity over time. Surface temperatures in this region are likely to be less conservative in the summer than in the winter when temperature differences between surface water and air temperature are not as great, and solar heating is minimal.

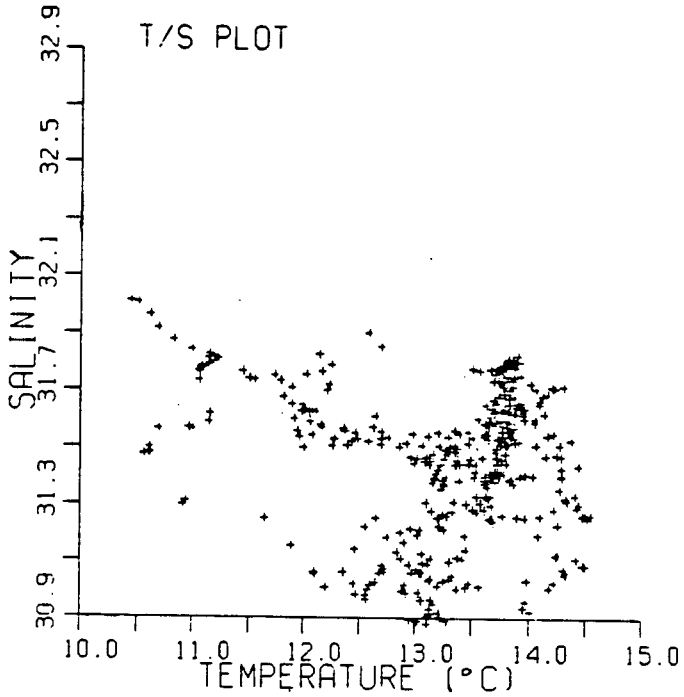

Figure 3.22: Surface temperature / salinity relationships of SHOP8402 data.

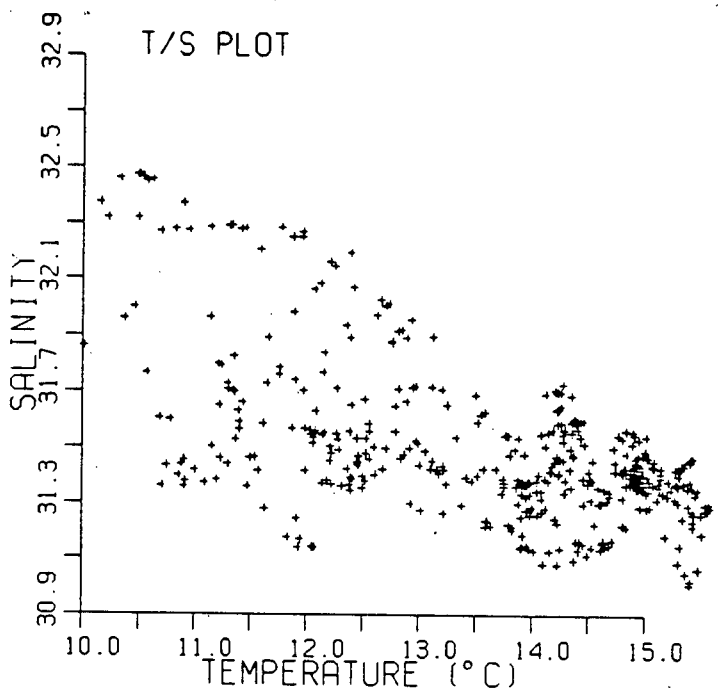

Figure 3.23: Surface temperature / salinity relationships of UBC8410 data from Legs 1–4.

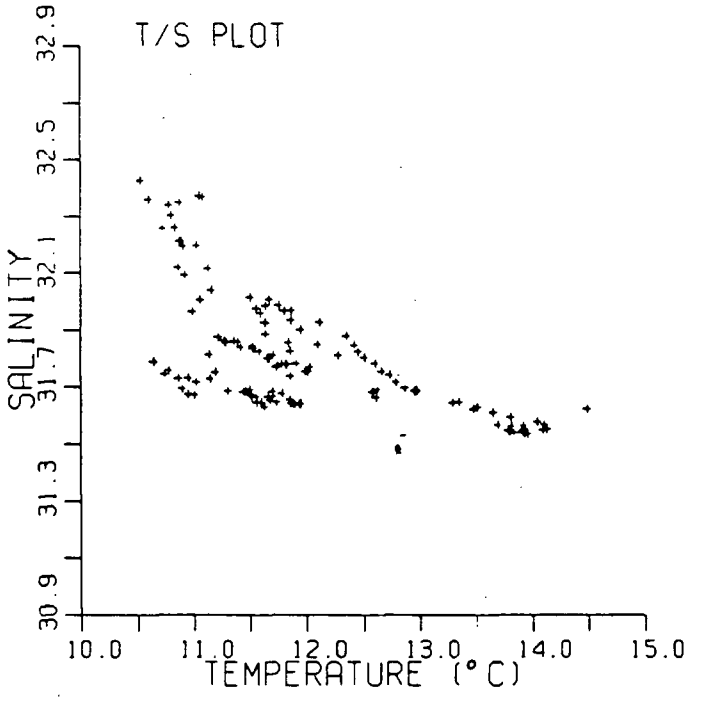

Figure 3.24: Surface temperature / salinity relationships of UBC8410 data from Leg 6.

Subsurface isopleths of both temperature and oxygen (Figures 3.25 and 3.26) sloped upward towards the shore. The location of stations sampled for these profiles in relation to surface thermal patterns is given in Figure 3.27. Vertical temperature profiles sampled along Leg 2 (south) (Figure 3.25) showed vertical stratification was least in the colder region centered over Juan de Fuca Canyon (Figure 3.25). Water temperatures in the top five meters were below 11.0°C. A frontal zone separated this vertically mixed water from offshore more stratified water with near-surface temperatures above 13.0°C. North of this transect (Leg 2 north) and over the shallow banks (Leg 4), no frontal zone existed and stratified offshore conditions extended across the entire shelf. The imagery shows these stations (Figure 3.27) to be entirely within the warm zone overlying the northern portion of the study area prior to the cooling event. Oxygen isopleths showed the penetration of low concentrations ($< 3.0 mg \cdot l^{-3}$) onto the shelf in the vicinity of the cold surface water.

Surface data from Leg 6 (Figure 3.20e) were collected after the cooling event iden-

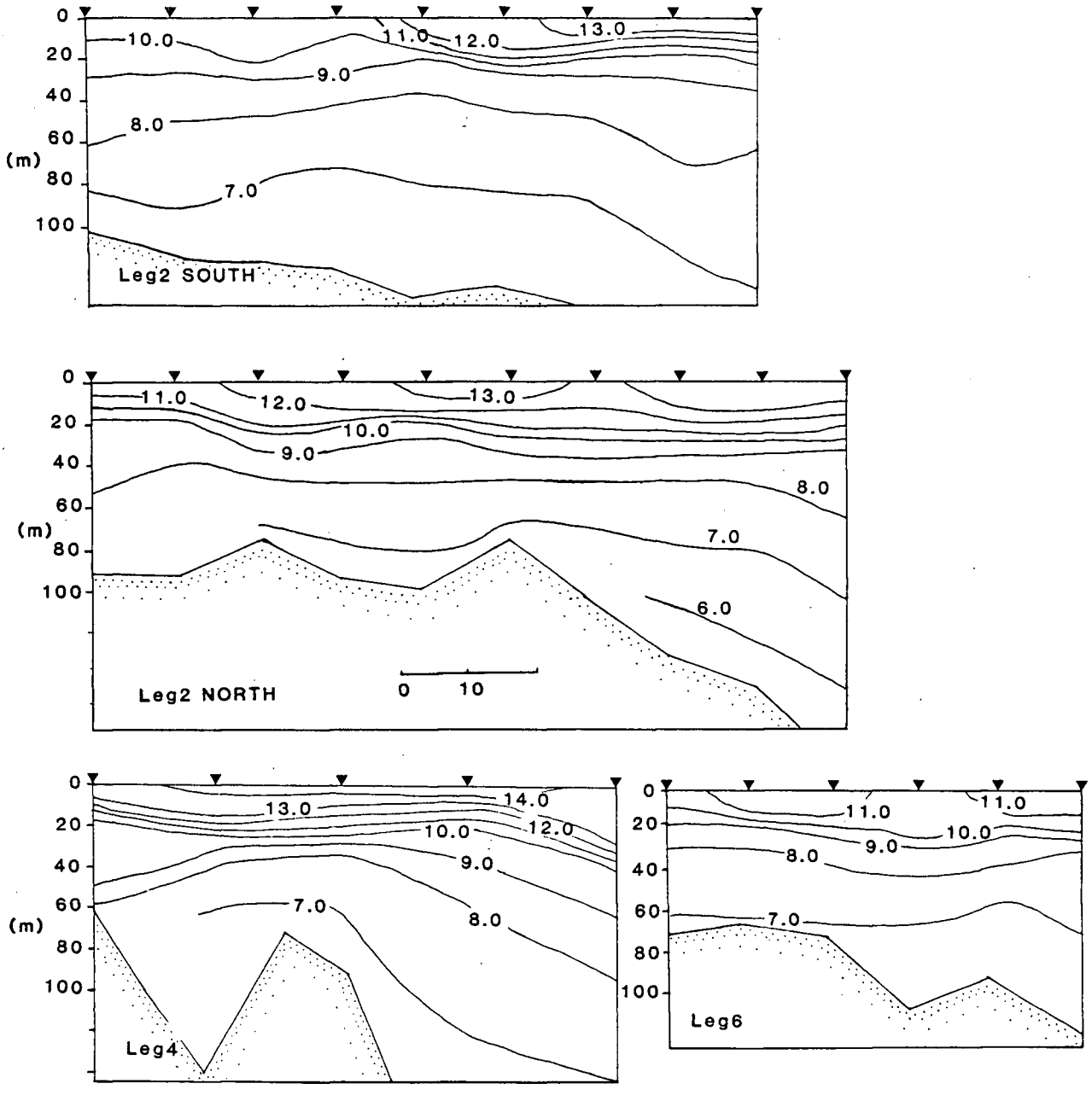

Figure 3.25: Summer subsurface contours of temperature sampled during UBC8410, Legs 2 (south), 2 (north), 4 and 6. Triangles represent station positions.

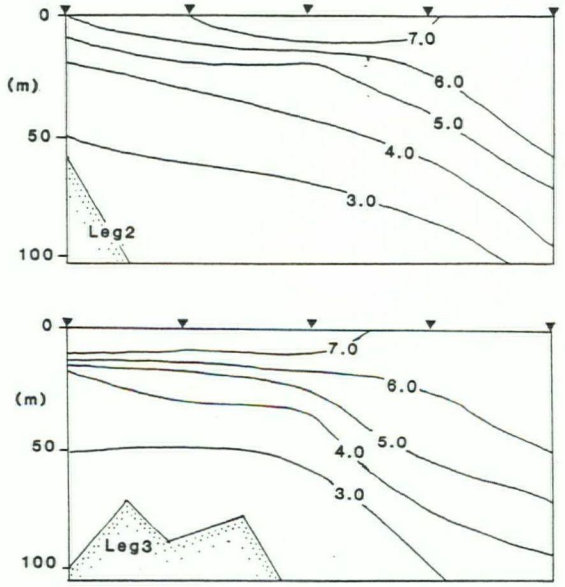

Figure 3.26: Subsurface contours of oxygen sampled during UBC8410, Legs 2 and 3.

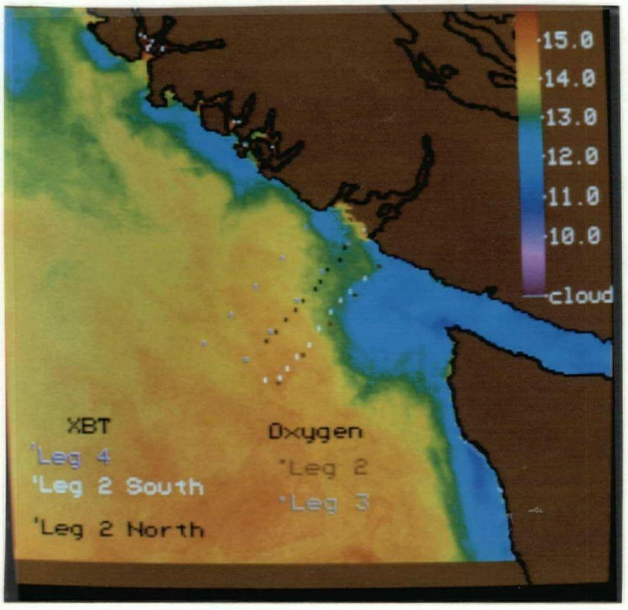

Figure 3.27: Location of stations sampled for subsurface temperature and oxygen in relation to mean sea surface temperature patterns.

tified in Figure 3.7. Examination of the T/S properties of surface water sampled along this leg (Figure 3.24) shows that most water was of high salinity and low temperature, similar to that previously seen in the colder upwelling region over Juan de Fuca Canyon. This water was present in the shelf region previously occupied by stratified warm surface water. Leg 6 passed through a warm tongue of water twice (Figure 3.6), explaining the double peak in surface temperature in Figure 3.20e. T/S characteristics of this warmer water (Figure 3.24) were most similar to those of the stratified warmer water which previously occupied this area of the shelf (Figure 3.23), the main body of which was now much further offshore.

Contours of vertical temperature sampled during Leg 6 (Figure 3.25) show that the water column in this region of the shelf was no longer as stratified. Temperatures in the top five meters (10.15–11.23°C) were more than 2°C cooler than those measured in the same location during Leg 4 and Leg 2(north) (3 days previously). The location of these vertical profiles in relation to surface temperature (Figure 3.6) shows that these contours did not include water from the warm tongue.

3.3 Discussion of Physical Processes

Winter shelf hydrography was dominated by a zone of relatively warm water over the outer shelf visible in both satellite imagery and in vertical profiles of temperature. This water is visible as the warmest water in each of the winter T/S plots. The high temperature suggests a southern origin, and the relatively low salinity a coastal association. This warm water is most likely the northward flowing Davidson Current which *Ikeda et al. (1984a)* identified in winter infrared imagery of the same area. The continuity of this water with warm water from as far south as central Oregon, as described by *Hickey (1981)* from current meter data, was visible in larger scale presentations (not shown) of the same images. Comparison of the T/S properties in this water with those given by *Hickey (1979)* for Davidson Current water off northern California, show those observed in this study to be both warmer and less saline. The influence of the Columbia River

on water properties near Vancouver Island has been noted by *Lewis (1978)* and it is not unreasonable to assume that dischange from this 'upstream' source might measurably reduce Davidson Current salinity. Higher temperatures could be due to the anomalous warming effects of the 1982-83 El Niño *(Emery and Hamilton, 1985)*. *Simpson (1983)* shows that 1983 temperatures in the upper 200 meters off California were as much as 4°C above the long term seasonal mean. Surface temperatures for the southern B.C. shelf given by *Douglas and Wickett (1978)* for March, 1978 are on average 2°C cooler than those measured in this study.

A relationship between the cross-shelf position of Davidson Current water and bathymetry is suggested by their spatial relationship in the satellite imagery (Figure 3.2). Vertical contours of temperature (Figure 3.18a–f) support this relationship and suggest a mechanism for the isolation of colder coastal water over the shallow La Perouse Bank area. South of La Perouse Bank, the shelf is relatively wide and deep and cut by Juan de Fuca Canyon. Davidson Current water flowing northward along the relatively straight Washington and Oregon shelf intruded onto the shelf in this region before being deflected west by the orientation of the B.C. shelf. The outer-shelf warm current core identified at Leg 1 (Figure 3.18a) intruded over most of the shelf at Leg 2 (Figure 3.18b). By Leg 3 (Figure 3.18c), the warm water intruded across the shelf undercutting colder less saline water close to shore. The relatively dense water occupied deeper areas on the east side of La Perouse Bank at Legs 3 and 4 (Figures 3.18c-d), bulging upward and reaching the surface at the second station of Legs 4, thereby isolating colder coastal water over the shallow part of La Perouse Bank. Surface T/S plots show water isolated over La Perouse Bank had characteristics intermediate between Coastal Current water and Davidson Current water. The main core of the current swung off the shelf in an anticyclonic manner around the bank and was visible again in Figure 3.18d. Satellite images confirm that sampling transects did not pass through the main portion of the current at Legs 5 and 6. This flow pattern is supported by contours of dynamic height calculated from CTD data (Figure 3.28) and has been documented

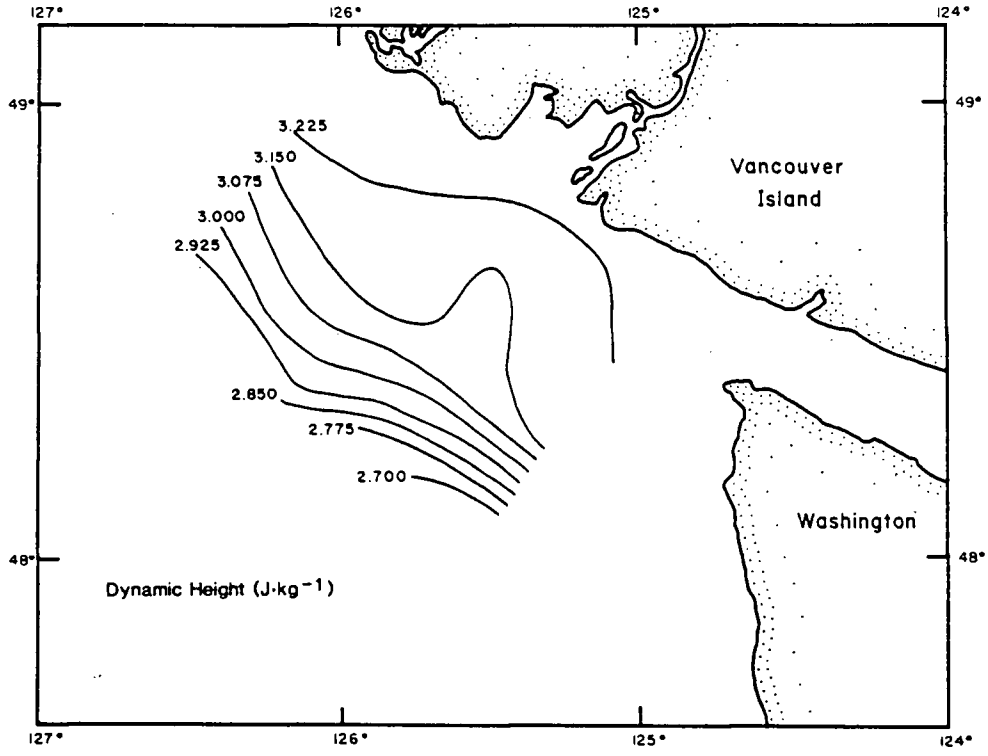

Figure 3.28: Winter dynamic height at 10 m relative to 100 m.

by *Freeland et al. (1984)* (see their Figures 5 and 6). *Sundby (1984)* presents evidence of a similar isolation of cold, relatively fresh coastal water on top of shallow banks by a northward flowing current off the Norwegian coast.

Subsurface profiles of temperature and salinity show a shallow, cold, relatively fresh water type near-shore which is indicative of estuarine influence from Juan de Fuca Strait and/or coastal rivers. Colder regions visible in the satellite imagery represent the buoyancy driven Vancouver Island Coastal Current *(Freeland et al. 1984; Hickey et al. in prep)*. Vertical profiles identify these regions as the most strongly stratified areas of the shelf during the winter. This water is visible as the coldest, and least saline in each of the winter T/S plots. Satellite imagery documents the extension and isolation of Coastal Current water over the winter shelf in the vicinity of La Perouse Bank.

Regions of large surface temperature gradient identified in the imagery (Figure 3.3) were coincident with large salinity gradients (Figure 3.14) and formed a frontal zone

separating Vancouver Island Coastal Current water from Davidson Current water. The exact subsurface shape of the frontal zone cannot be resolved by the 18.5 km separation of vertical stations, however, the undercutting of less dense Coastal Current water by more dense Davidson Current water indicates a retrograde shape. This shape is similar to that of frontal zones observed in areas of estuarine influence *(Garvine 1974)*. The seaward sloping free surface induces downwelling and convergence in the frontal region. The similarity in shape implies an estuarine influence on shelf hydrography and possible convergence at the frontal zone observed in both the surface temperature contours and the surface salinity contours.

Water seaward of the Davidson Current had a similar high salinity, but a lower temperature than Davidson water on the winter T/S plots. For the purposes of this study, this water is labelled North Pacific water. No implication of the actual relationship between this water, and water from the open North Pacific is intended. This water represents the most oceanic of the water types sampled during the winter study period.

The summer association of colder surface temperatures with higher salinities is opposite to that found in winter and indicates a subsurface origin of near-shore colder surface water. Cross-shelf contours of subsurface temperature and oxygen tilt upward toward the shore and the shape of the frontal zone is prograde, typical of upwelling systems and characteristic of the Pacific coast of North America during summer *(Pietrafesa 1983)*. Bakun wind calculations for July 1984 *(from Hickey et al. in prep.)* indicate northwest (upwelling favorable) winds prior to, and throughout the study period. Previous work indicates that the Vancouver Island Coastal Current is present throughout the summer *(Hickey et al. in prep.)*. Unfortunately, it s presence is difficult to discern as no subsurface salinity data is available for the summer cruises (due to the failure of the CTD). The association of higher surface salinities with colder temperatures at the nearshore ends of the transects is not indicative of buoyancy induced by a freshwater influence. It is possible that the summer transects were not close enough to shore to

sample any coastal current.

The persistent cold feature in the Juan de Fuca Canyon region identified in the image sequence is most likely the surface expression of topographically induced upwelling. This feature is the cyclonic eddy described by *Denman and Freeland (1982)* and analyzed in infrared imagery by *Emery et al. (1986)*. The upwelling induced by a cyclonic eddy on the continental shelf can be enhanced if the eddy is situated over a narrow canyon which is oriented perpendicular to the direction of flow. If the width of the canyon is relatively narrow, the flow above it will not adjust. The coriolis force, which balances the pressure gradient in the upper water column, will be negligible in the canyon, as there will be no cross-canyon motion. This leaves an unbalanced up-canyon pressure gradient, which induces the flow of relatively deep water onto the shelf in the center of the eddy. This upwelling of cold, nutrient-rich water obviously has important biological implications, as pointed out by *Denman and Freeland (1982)*. Subsurface data show that the upwelling of colder, low oxygen water onto the shelf was occurring even before the major cooling event of July 16–17, consistent with *Denman and Freeland's (1982)* interpretation of topographically enhanced upwelling in the Juan de Fuca Canyon region. Vertical temperature profiles show the eddy was weakly stratified and separated from stratified offshore conditions by a frontal zone which is clearly visible in the imagery. Vertical profiles of temperature and oxygen indicate that subsurface deeper water was upwelled onto the shelf in the vicinity of the eddy. Satellite data show the central portion of the eddy had the coldest temperatures, representing the most recently upwelled water.

Areas north of the cold eddy region, over La Perouse Bank, are strongly stratified during the early portion of the study period (Figure 3.25Leg 2north and 4) but lose this stratification (Figure 3.25Leg 6) after the cooling event shown in Figure 3.7. Bakun wind data presented by *Hickey et al. (in prep.)* (and Alex Herman, U. Washington, College of Oceanography, personal communication) show an increase in the upwelling favourable winds on the southern B.C. shelf in the July 14–15 period. These

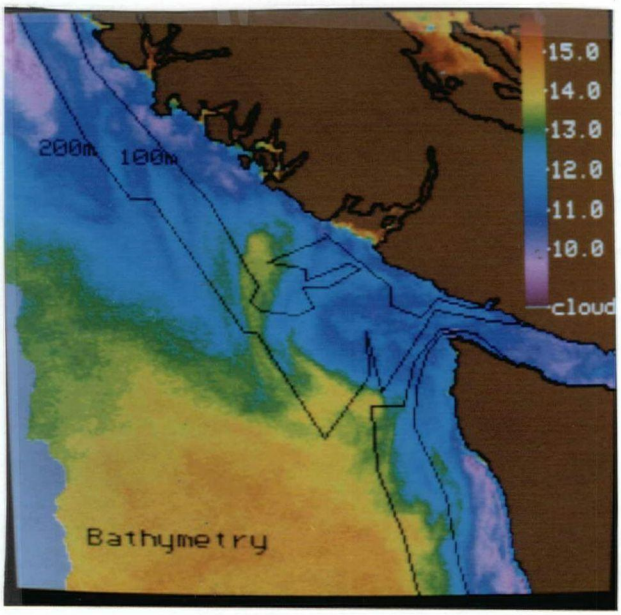

Figure 3.29: Relationship between surface thermal patterns (July 17, N6.26288) and bathymetry during the upwelling event of July 15–17.

are supported by unquantified but very obvious observations from the ship while at sea. Sampling had to be abandoned completely for 48 hours due to heavy seas and wind out of the northwest (see Figure 2.1). Two processes probably contribute to the surface cooling shown in Figure 3.7 and are responsible for the difference in surface temperature patterns between Figures 3.5 and 3.6. Increased wind mixing, and the subsequent breakdown of surface stratification would reduce the surface temperature over the study area. The largest proportion of the observed change in surface temperature is most likely due to an episodic wind-driven upwelling event. The dramatic change in thermal patterns visible in these satellite images was a result of the offshore advection of stratified, warm surface water. Visual analysis of the image sequence showed the frontal zone migrating offshore. The position of the frontal zone in relation to bottom topography is shown in Figure 3.29. This is consistent with previous satellite observations of an upwelling episode by *Ikeda and Emery (1984)* and changes in surface thermal patterns induced by similar episodic upwelling on the Oregon coast

B.C.) show a strong surface frontal zone over the outer shelf, with strongly stratified water to seaward and no well defined thermocline over the shelf. This is consistent with subsurface thermal patterns expected during or after an upwelling event.

Chapter 4

SHELF PLANKTON BIOMASS ZONATION

This chapter presents and discusses relationships between surface plankton distributions and surface hydrography during the winter and summer study periods. These relationships are shown first by demonstrating associations between hydrographic characteristics and specific chlorophyll and zooplankton concentrations. Repeated sampling of similar transects allow an estimate of the time periods over which observed relationships might be valid. Relationships with hydrography are then extended first qualitatively and then quantitatively to comparisons between plankton distributions and patterns of sea surface temperature measured by infrared satellite images.

4.1 Relationships between Plankton Concentrations and Surface Hydrography

4.1.1 General Qualitative Relationships

Winter regions of low temperature and salinity (Figure 3.11) were areas of highest chlorophyll and zooplankton concentration. Maximum biomass was therefore associated with Vancouver Island Coastal Current water and near-shore regions on the winter shelf. In southern portions of the study area (Legs 1, 2, and 3, Figure 3.11), frontal zones separating this water from warmer and more saline outer-shelf water were co-

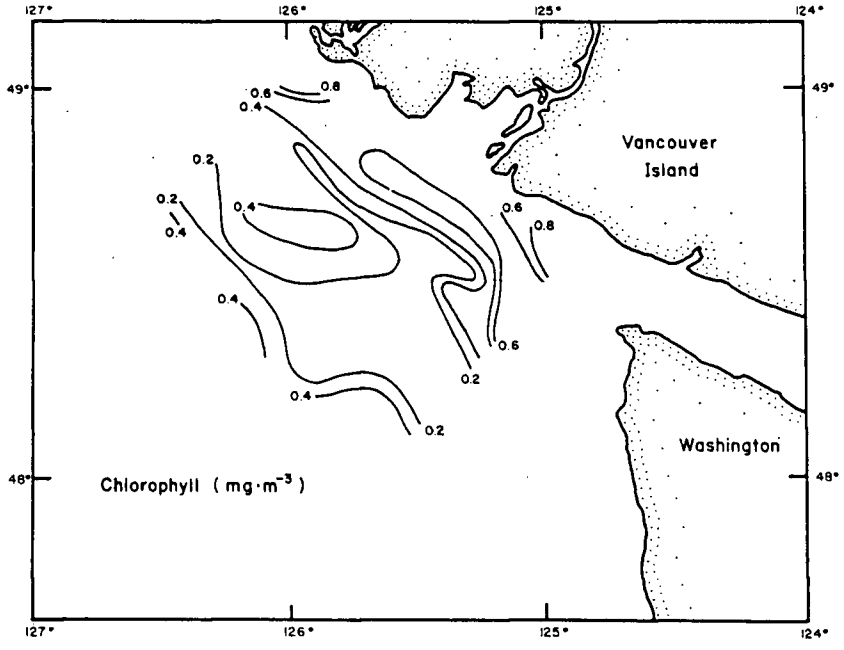

Figure 4.1: Contours of winter surface chlorophyll concentration ($mg \cdot m^{-3}$) (UBC8320 data).

incident with localized peaks in both chlorophyll and zooplankton concentration. In warmer water seaward of the frontal zones (Davidson Current and North Pacific water), zooplankton concentrations were consistently low. Chlorophyll concentrations were lowest in the warmest water over the middle shelf (Davidson Current), and increased again in cooler North Pacific water over the outer shelf.

Contours of winter chlorophyll and zooplankton concentration (Figures 4.1 and 4.2) (UBC8320 data) show that spatial patterns of distribution resembled the spatial patterns of surface hydrographic variables shown in Figures 3.13 and 3.14. An elongated peak in both chlorophyll and zooplankton concentration coincided with the position of hydrographic frontal zones identified in Figures 3.11 and 3.3. This peak did not extend beyond the La Perouse Bank area. Contours of low chlorophyll concentration matched those of Davidson Current water identified in the satellite imagery (Figure 3.2) and an increase in chlorophyll concentration was coincident with the transition from Davidson Current water to North Pacific water.

Summer regions of cold, higher salinity water were regions of highest chlorophyll

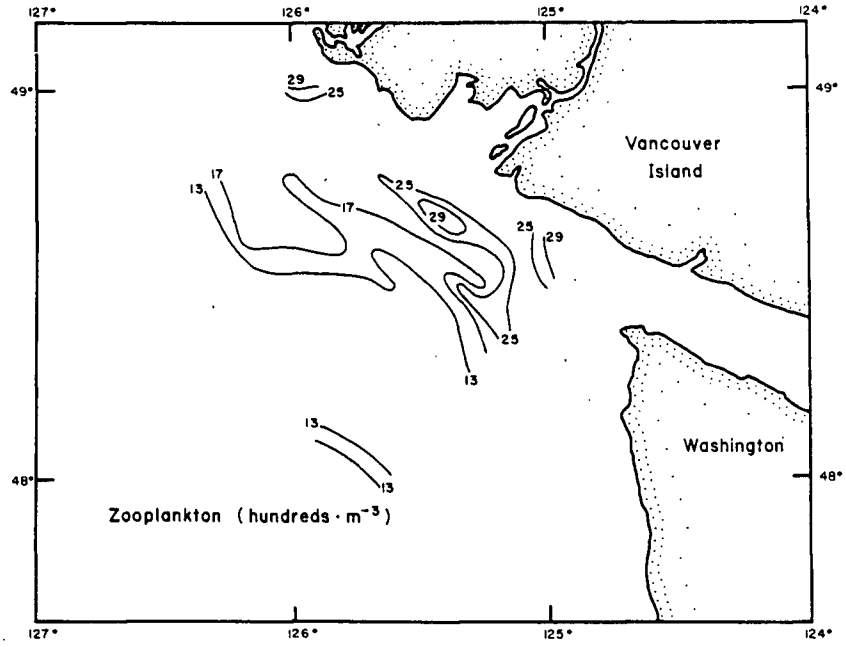

Figure 4.2: Contours of winter surface zooplankton concentration (counts $\cdot$ m^{-3}) (UBC8320 data).

concentration (Figure 3.20). These correspond to upwelling regions described in Chapter 3. Warmer water, associated with a more stratified water column, had the lowest concentrations of chlorophyll found during the summer. Maximum concentrations were seen on the cold side of the frontal zone separating upwelled water from stratified regions (UBC8410 Legs 1, 2, and 4). Summer zooplankton concentrations (Figure 3.20) did not show a constant relationship with surface temperature and salinity. Peaks were observed around the outer edge of cooler water in the southern portion of the study area and lower concentrations with warmer water. However, high zooplankton concentrations were also found in warmer and stratified regions of low chlorophyll concentration at the northern transect (ie. UBC8410 Leg 3).

The similarity of contours of summer chlorophyll concentration (UBC8410 Legs 1–4) (Figure 4.3) and sea surface temperature patterns (Figure 3.9) indicate a strong relationship between physical processes and biological distributions. Contours of chlorophyll followed contours of temperature in the vicinity of the upwelling region over the southern shelf and the distribution of lowest concentrations followed that of the

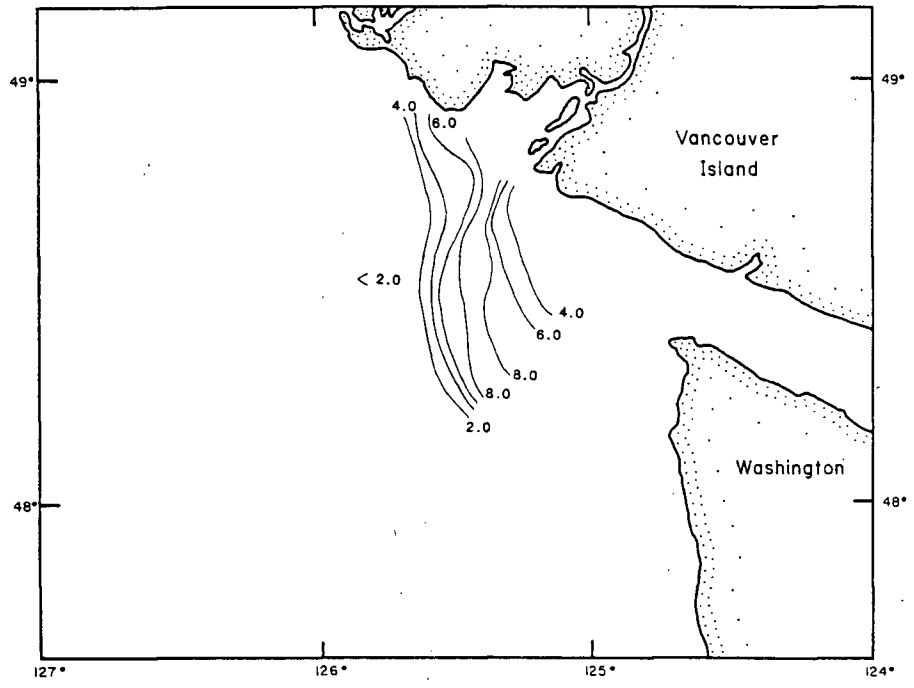

Figure 4.3: Contours of summer surface chlorophyll concentration ($mg \cdot m^{-3}$) (UBC8410 Legs 1–4).

warmest surface water. Contours of zooplankton distribution (Figure 4.4) show a more ambiguous pattern but suggest that increases were possibly associated with the outer areas of the eddy and the shelf area in the vicinity of La Perouse Bank.

Summary statistics (Table 4.1) of the winter and summer SHOP cruises provide a general comparison of the biological regimes between the two seasons. These cruises sampled virtually identical transects over the shelf (Figures 2.5 and 2.6). Summer maximum and mean chlorophyll concentrations were approximately an order of magnitude higher than winter values. Maximum zooplankton concentrations were an order of magnitude higher during the summer, but mean concentrations were actually lower. The variance associated with both chlorophyll and zooplankton concentrations was greater during summer indicating a greater intensity of spatial patchiness. Whether lower summer zooplankton concentrations are real or an artifact of the sampling procedure is unknown. The different particle counting instruments used during the two seasons could have differing gains and sensitivities and result in differing sampling efficiencies. Seasonal differences in particle size distribution might result in particle counts having a

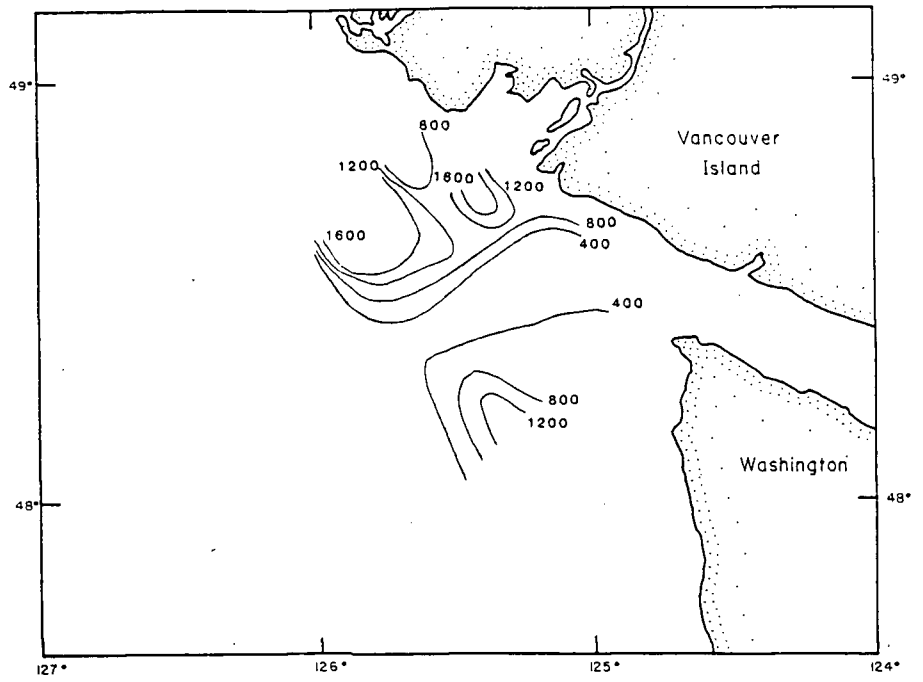

Figure 4.4: Contours of summer surface zooplankton concentration (counts $\cdot$ m^{-3}) (UBC8410 Legs 1–4).

	N	Mean	σ^2	σ	Maximum	Minimum
SHOP8306						
Temp	539	11.79	0.213	0.461	12.63	10.69
Sal	539	31.25	1.128	1.062	32.39	28.23
Chl	539	0.48	0.072	0.268	1.84	0.01
Zoop	539	2329.	1340083.	1158.	6756.	379.
SHOP8402						
Temp	437	13.25	0.796	0.892	14.55	10.44
Sal	437	31.46	0.066	0.258	32.01	30.88
Chl	437	3.05	14.759	3.842	26.31	0.80
Zoop	437	1997.	9715718.	3117.	41048.	48.

Table 4.1: Summary statistics of cruises SHOP8306 and SHOP8402. Chlorophyll concentrations are in mg $\cdot$ m^{-3}, and zooplankton concentrations in counts $\cdot$ m^{-3}.

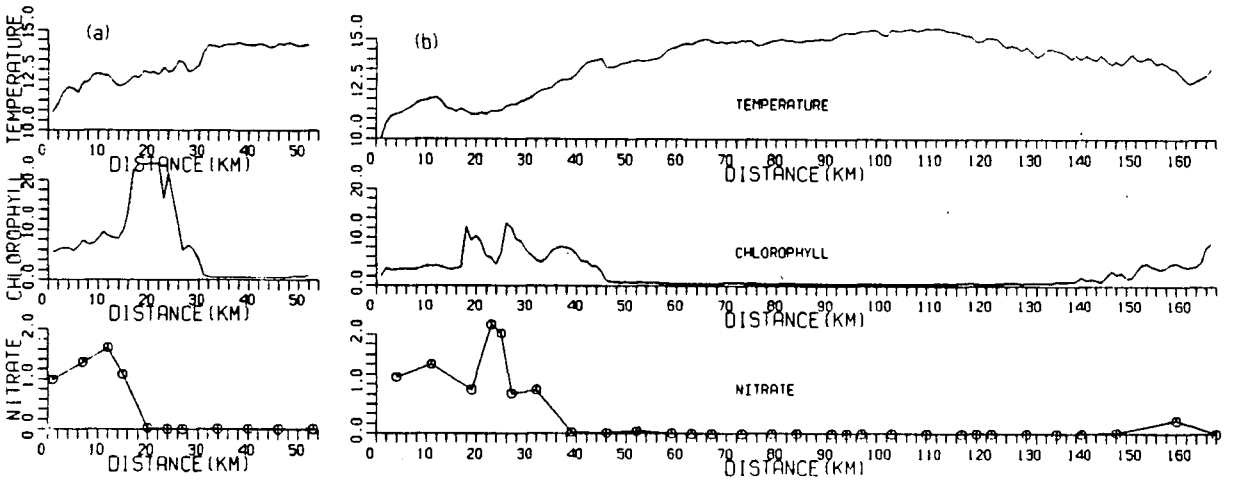

Figure 4.5: Summer surface nitrate concentrations ($\mu g\,at \cdot l^{-1}$) in the study area, shown in relation to surface temperature °C and chlorophyll concentrations ($mg \cdot m^{-3}$) for Leg 1 (a) and Leg 2 (b) (southern portion - offshore - northern portion).

differing relationship to biomass. Differences in the instrument plumbing might cause differing physical damage to the organisms, resulting in differing numbers of 'particles' arriving at the counter. Each of these effects would be consistent within a season making zooplankton concentrations within a cruise and also between cruises within a season intercomparable. These sampling differences do not affect patterns of relative concentration and comparisons of distributional patterns between seasons are still valid.

Nutrient concentrations in the study area probably played a negligible role in determining winter phytoplankton distributions and productivity. Winter nitrate concentrations (actually nitrate plus nitrite) averaged $\approx 5.0\mu g\,at \cdot l^{-1}$ and were never less than $1.4\mu g\,at \cdot l^{-1}$ in any of the hydrographic regimes. These concentrations are considerably above those which would result in any nutrient limitation *(MacIsaac and Dugdale 1969)*. Phosphate levels were never less than $1.0\mu g\,at \cdot l^{-1}$. Phosphate is rarely limiting in the marine environment and is not likely to be here.

Summer surface nutrient concentrations indicated a spatial relationship between physical processes, nutrient availability and chlorophyll distributions. Surface nitrate concentrations in the vicinity of the eddy, prior to the cooling event, are shown in relation to surface temperature and chlorophyll concentration in Figure 4.5. Highest

nutrient concentrations were found in colder water. Concentrations were always less than $0.1\mu g\,at \cdot l^{-1}$ in warmer stratified regions. Lower concentrations were also observed in cool regions of maximum chlorophyll concentration, implying utilization. Nutrient samples from Leg 6, during the wind event, showed that regions which had previously been stratified with surface concentrations below $0.1\mu g\,at \cdot l^{-1}$, not only had reduced temperatures, but also had increased nitrate concentrations with a mean (N=6) of $0.48\mu g\,at \cdot l^{-1}$. Within the warm tongue isolated in the vicinity of La Perouse Bank (see Figure 3.6), surface nitrate concentrations remained below $0.1\mu g\,at \cdot l^{-1}$.

Relationships between nutrient distribution and satellite measured thermal patterns in response to wind driven upwelling shown by *Conrad (1980)* are similar to those presented in Figure 4.5, although on a larger scale. Strong negative correlations between surface nutrient concentration and temperature were observed off California in recently upwelled water. This correlation broke down as both surface advection and spatial differences in phytoplankton growth (nutrient utilization) in 'older' upwelled water changed their relationship *(Conrad 1980)*. Utilization of surface nutrients is suggested in Figure 4.5. There was a general negative correlation between surface temperature and nitrate concentration, and a general positive correlation between nitrate concentration and chlorophyll concentration. These relationships broke down in the regions of highest chlorophyll concentration where associated low nutrient concentrations imply depletion by the phytoplankton population. Seaward of the frontal zone, in warmer and more stratified regions, both nutrient and chlorophyll concentrations were low.

4.1.2 Winter Quantitative Relationships

Winter surface hydrographic properties examined in Chapter 3 showed three distinct surface hydrographic zones distinguishable on T/S plots. Figure 4.6a and b show there is a quantitative relationship between winter plankton concentrations and these hydrographic zones. Water from the Davidson Current, Vancouver Island Coastal Current

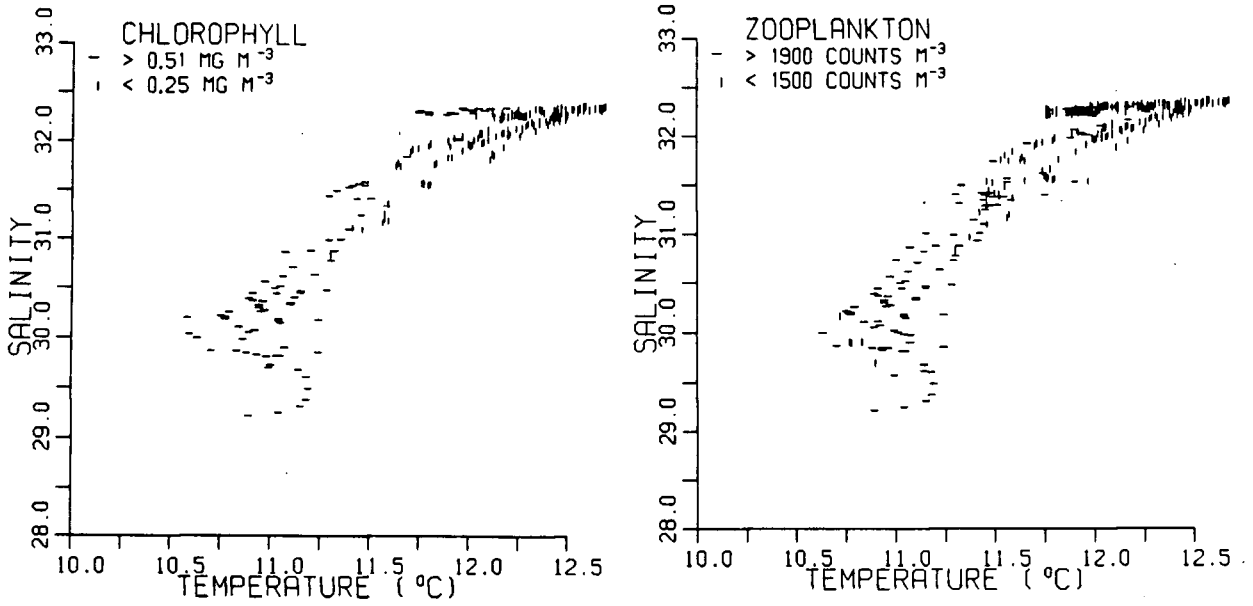

Figure 4.6: The association of a) winter chlorophyll concentrations and b) winter zooplankton concentrations with surface T/S properties (UBC8320 data).

and North Pacific were each associated with characteristic chlorophyll and zooplankton concentrations. Vancouver Island Coastal Current water and North Pacific water supported chlorophyll concentrations above $0.51 mg \cdot m^{-3}$. North Pacific water was never associated with concentrations below $0.25 mg \cdot m^{-3}$. Davidson Current water was associated with concentrations below $0.25 mg \cdot m^{-3}$ and never supported concentrations above $0.51 mg \cdot m^{-3}$. Sampling points along the line defining mixing between Davidson Current water and Vancouver Island Coastal Current water had both high and low concentrations. Points closer to Davidson Current characteristics most often had concentrations below $0.25 mg \cdot m^{-3}$. Zooplankton concentrations above $1900 counts \cdot m^{-3}$ were associated with Vancouver Island Coastal Current water. Both Davidson Current water and North Pacific water were characterized by zooplankton concentrations below $1500 counts \cdot m^{-3}$. While the hydrographic separation of zooplankton concentrations in Figure 4.6b is not as robust as that for chlorophyll concentrations (Figure 4.6a), a similar trend is seen in the sampling points representing mixing between Davidson Current water and Vancouver Island Coastal Current water. Points most similar to David-

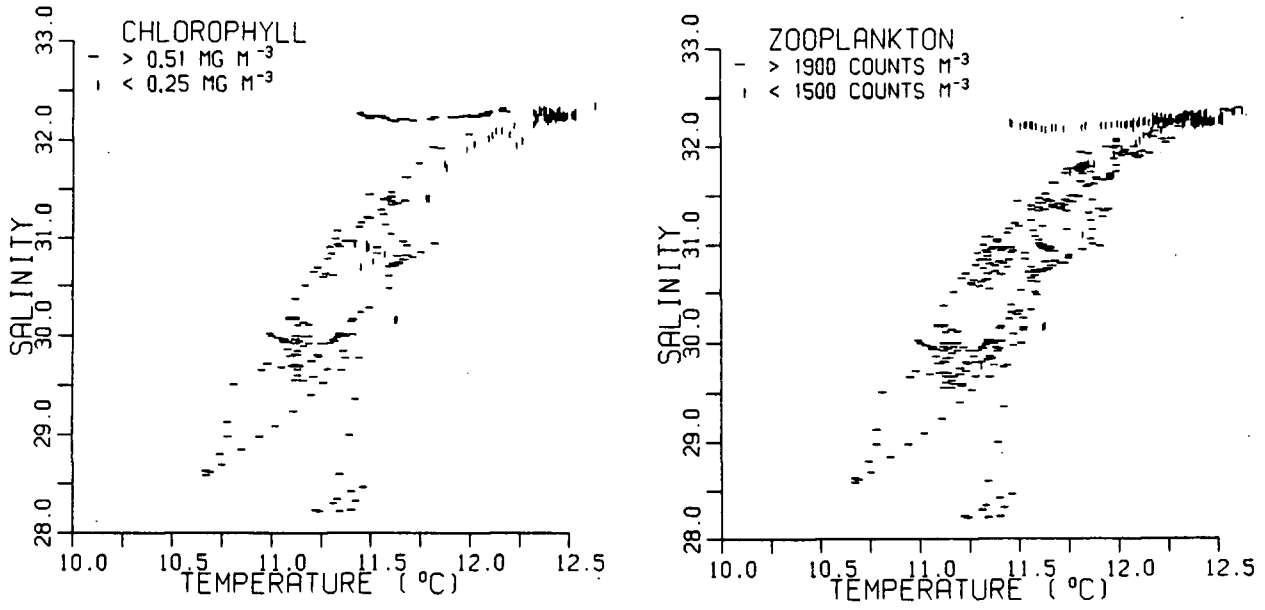

Figure 4.7: The association of a) winter chlorophyll concentrations and b) winter zooplankton concentrations with surface T/S properties (SHOP8306 data).

son Current hydrographic characteristics most often have zooplankton concentrations below 1500counts $\cdot$ m^{-3}.

A comparison of these relationships over the three winter sampling sequences (sampling times are shown in Figure 2.1) provides an indication of their stability in time. T/S plots of each sampling sequence (Chapter 3) show the same three hydrographic regimes were sampled by both SHOP8306 and UBCREP as well as UBC8320. Figures 4.7a and b and 4.8a and b show the relationship between hydrographic properties and plankton concentrations for these sequences. The association of specific chlorophyll concentrations with each hydrographic regime was stable over the first two sampling sequences (SHOP8306 and UBC8320). The exclusive association of chlorophyll concentrations below 0.25mg $\cdot$ m^{-3} with Davidson Current water was less obvious during UBCREP. Many sample points in this regime had increased concentrations. A more dramatic change is seen in the relationship between zooplankton concentrations and hydrographic properties over the winter sampling period. Vancouver Island Coastal Current water and mixed regions maintained higher zooplankton concentrations over

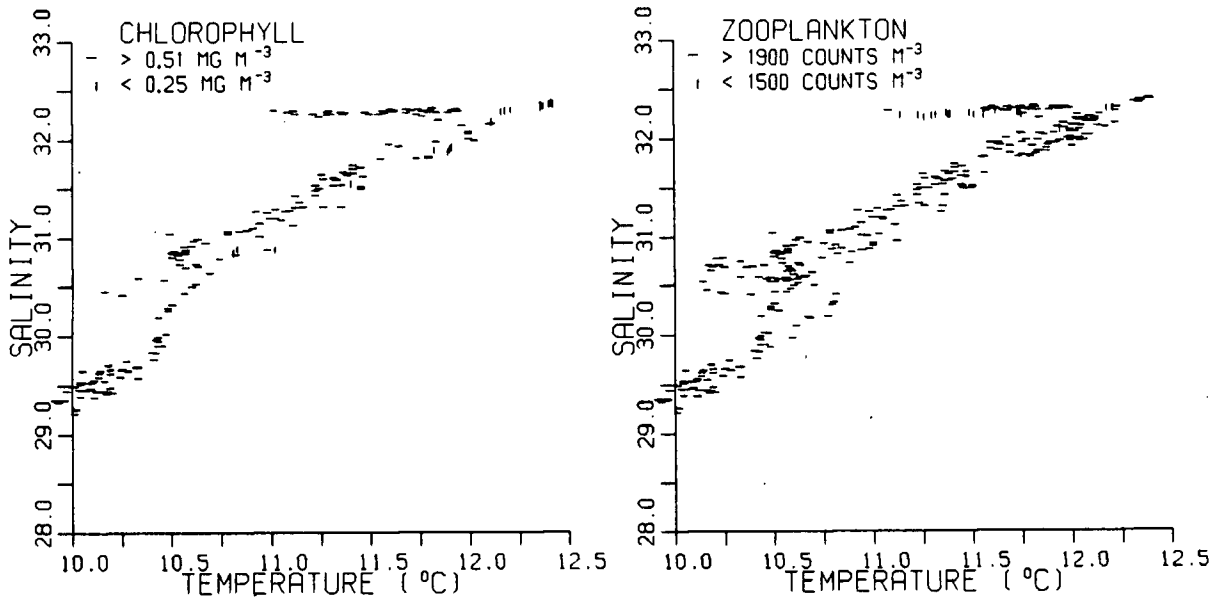

Figure 4.8: The association of a) winter chlorophyll concentrations and b) winter zooplankton concentrations with surface T/S properties (UBCREP data).

the three sampling sequences and most data points in North Pacific water maintained lower concentrations. Sample points within Davidson Current water, however, show increased concentrations during UBCREP ($> 1900 \text{counts} \cdot \text{m}^{-3}$). The exclusive association of lower zooplankton concentrations with Davidson Current water did not remain stable over the six day winter sampling period. As no satellite images coincided with the UBCREP portion of the cruise (see Figure 2.1), the associations present during the SHOP and UBC8320 portions of the cruise are applicable to the entire winter image sequence for comparative purposes.

The T/S/plankton plots indicate that surface water on the shelf in the winter was divided into identifiable hydrographic regimes, each of which was associated with a specific plankton concentration. Low plankton variability within each was a characteristic of these regimes.

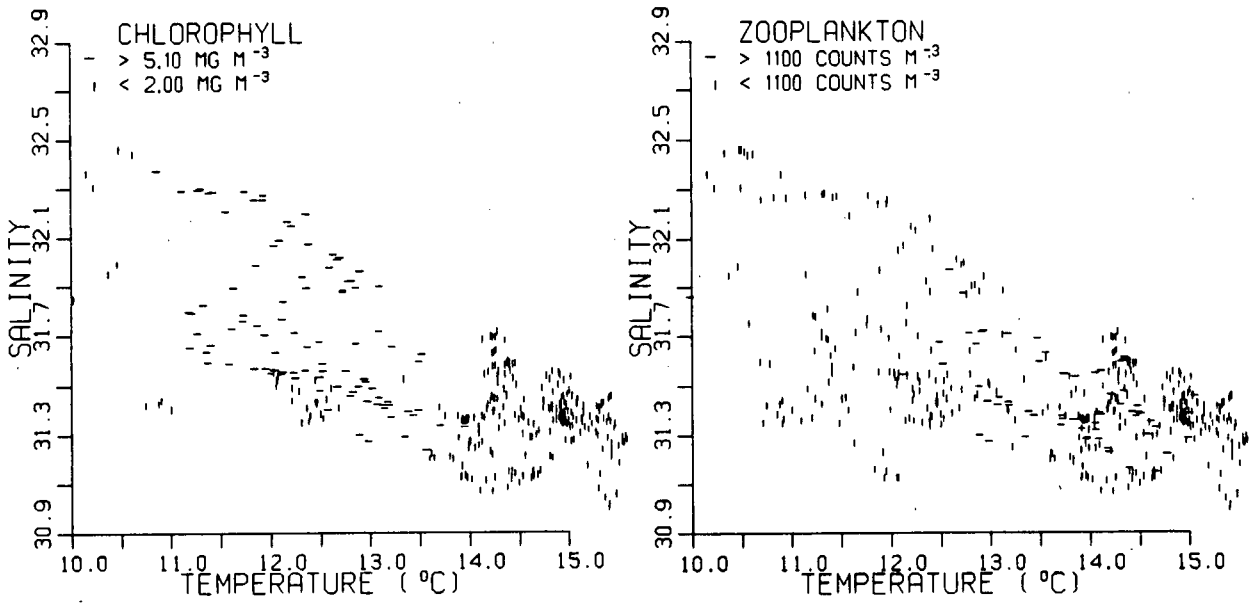

Figure 4.9: The association of a) summer chlorophyll concentrations and b) summer zooplankton concentrations with surface T/S properties (UBC8410 Legs 1-4 data).

4.1.3 Summer Quantitative Relationships

Quantitative comparisons of summer chlorophyll concentrations with surface hydrographic characteristics (Figure 4.9a) showed regions with surface temperatures above 13.5°C (stratified water) did not support chlorophyll concentrations above 5.10mg $\cdot$ m^{-3} and were generally associated with concentrations less than 2.00mg $\cdot$ m^{-3}. In contrast, regions near the upwelling center, with surface temperatures colder than 13.5°C rarely had concentrations below 5.1mg $\cdot$ m^{-3}. Exceptions to this pattern occurred at sample points with temperatures less than 11.0°C. Associated with these temperatures, were chlorophyll concentrations less than 2.0mg $\cdot$ m^{-3}. Similar relationships were observed during SHOP8402 (Figure 4.10a) although the temperature threshold separating high chlorophyll concentrations from low concentrations was 13.0°C. Data sampled during the wind event (UBC8410 Leg 6, Figure 4.11a) showed that water above 12.0°C was associated with chlorophyll concentrations below 2.00mg $\cdot$ m^{-3} and water below 12.0°C with concentrations above 5.10mg $\cdot$ m^{-3}. This implies that the warm tongue of water visible in the satellite data (Figure 3.6) maintained chlorophyll concentrations charac-

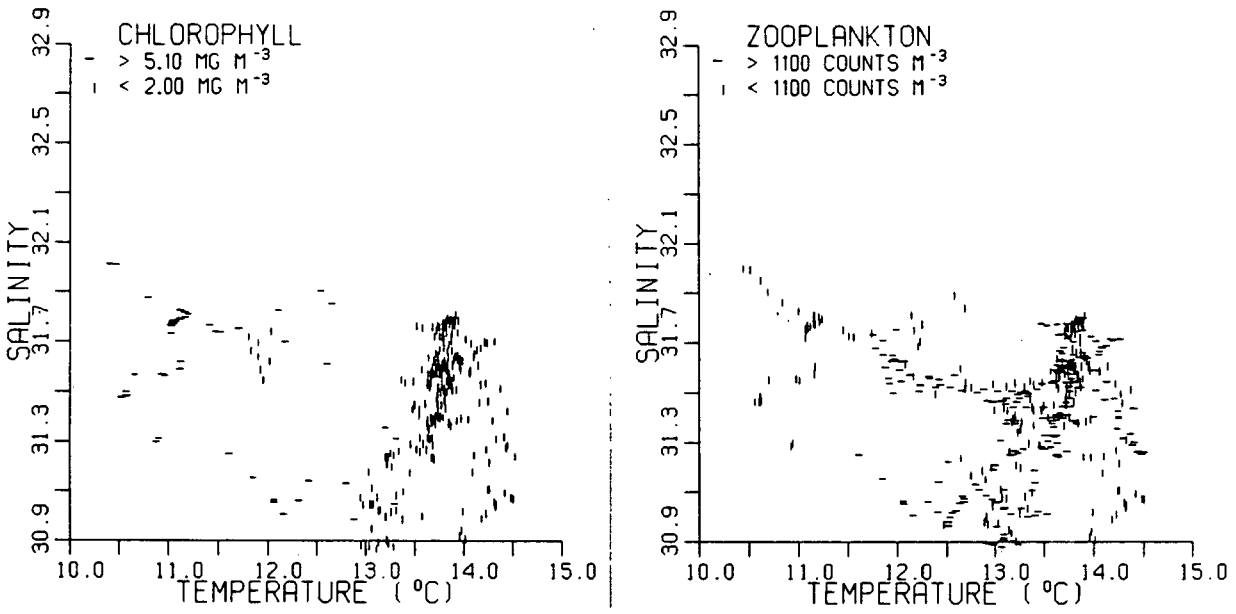

Figure 4.10: The association of a) summer chlorophyll concentrations and b) summer zooplankton concentrations with surface T/S properties (SHOP8402 data).

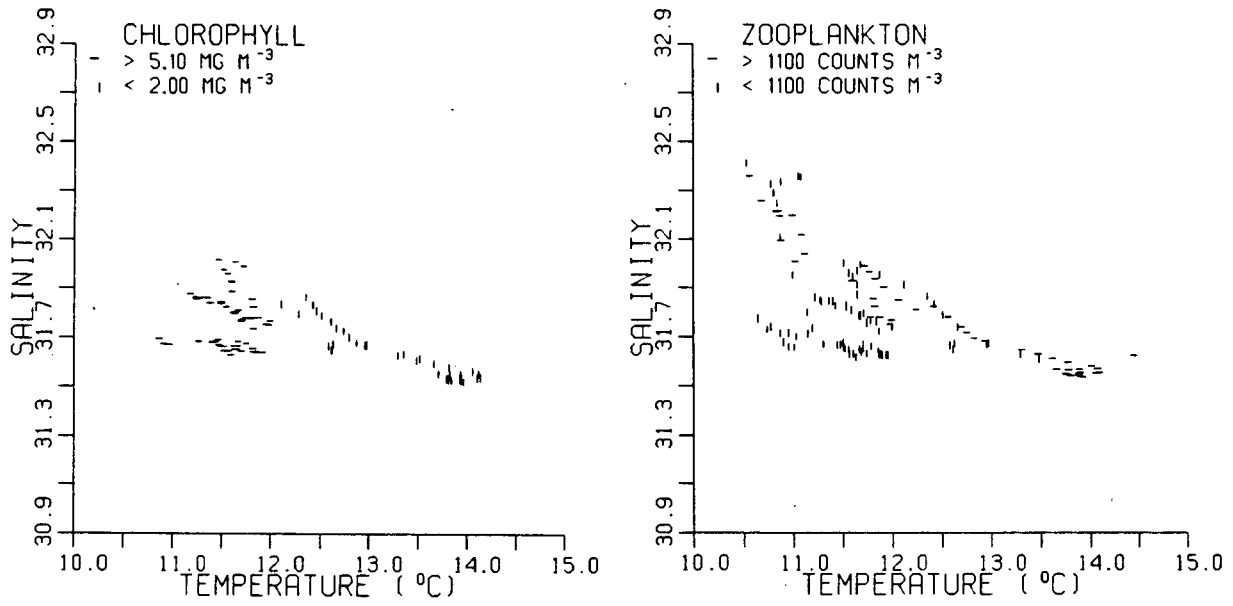

Figure 4.11: The association of a) summer chlorophyll concentrations and b) summer zooplankton concentrations with surface T/S properties (UBC8410 Leg 6 data).

teristic of the previous stratified conditions of the area. This is supported by the lack of nutrient input into this warm water during the wind event, discussed previously. Surrounding areas of the shelf, which before the wind event were warm and stratified with chlorophyll concentrations below 2.0mg $\cdot$ m^{-3}, changed to cooler surface temperatures and support concentrations above 5.10mg $\cdot$ m^{-3}.

These data indicate that the general form of association between surface hydrographic properties and chlorophyll concentration was maintained over the entire summer sampling period despite dramatic changes in surface temperature distribution associated with the wind event. The actual temperature threshold separating the two regimes, however, varied over this 9 day period. Figures 4.9, 4.10 and 4.11 suggest that while chlorophyll concentrations might vary in their association with specific surface temperatures, they maintained a constant relationship with surface thermal patterns.

Summer zooplankton concentrations did not show a consistent association with surface hydrographic characteristics (Figures 4.9b, 4.10b, and 4.11b). Concentrations above and below the 1100counts $\cdot$ m^{-3} threshold occurred in both the warmer and cooler hydrographic regimes. Highest concentrations ($<$ 1100counts $\cdot$ m^{-3}) especially during UBC8410 were primarily present at intermediate temperatures. The continuous plot of surface zooplankton concentration for UBC8410 Leg 3 (Figure 3.20) shows high concentrations in the warm and stratified northern portion of the study area. These peaks do not appear to be associated with any identifiable surface hydrographic feature. Samples taken from the same shelf area during the wind event (UBC8410 Leg 6, Figure 4.11b) showed that this warm water maintained these high zooplankton concentrations despite the advection and changes in sea surface temperature pattern.

4.2 Surface Plankton Concentrations and Satellite Temperature

The previous section demonstrates that the surface hydrographic zones identified in Chapter 3 are, to a varying degree, associated with specific plankton concentrations.

Comparisons of these plankton concentrations with surface temperatures mapped by the satellite images will show whether the associations demonstrated in in-situ T/S space are maintained when compared to satellite temperature and also whether these associations are maintained in space over the study area. Distributions of plankton are a result of both biological processes (for example trophic interactions such as nutrient availability and predator/prey relationships) and physical processes (for example both vertical and horizontal mixing, and advection). This spatial comparison addresses only the component of distribution correlated with physical processes. It is a tracer of these processes (temperature) which the satellite is able to measure. It is logical to assume that phytoplankton will be more closely related to their physical environment than zooplankton. For the phytoplankton, trophic considerations and physical processes overlap to a large degree. Nutrient and light availability are primarily determined by physical processes. Zooplankton, although still affected by mixing and advective processes, are at least one trophic level removed from physical processes. Resultant zooplankton distributions will be a more complex interaction of biological processes, such as prey availability, and physical processes. The extent to which zooplankton grazing affects the distribution of phytoplankton standing stock will be determined by the relationship between zooplankton abundance, grazing rates, and the growth rate of the phytoplankton population. As no rate processes were measured during this study, the magnitude of the component resulting from biological interactions can only be speculated. This study examines that component of the resultant distributions which were related to surface hydrography.

4.2.1 Winter

Winter plankton concentration thresholds used to examine relationships between concentration and surface hydrography are superimposed on the mean winter satellite image (Figure 4.12a and b) to show their spatial relationship with satellite measured sea surface temperature patterns. The association of the thermally defined regions dis-

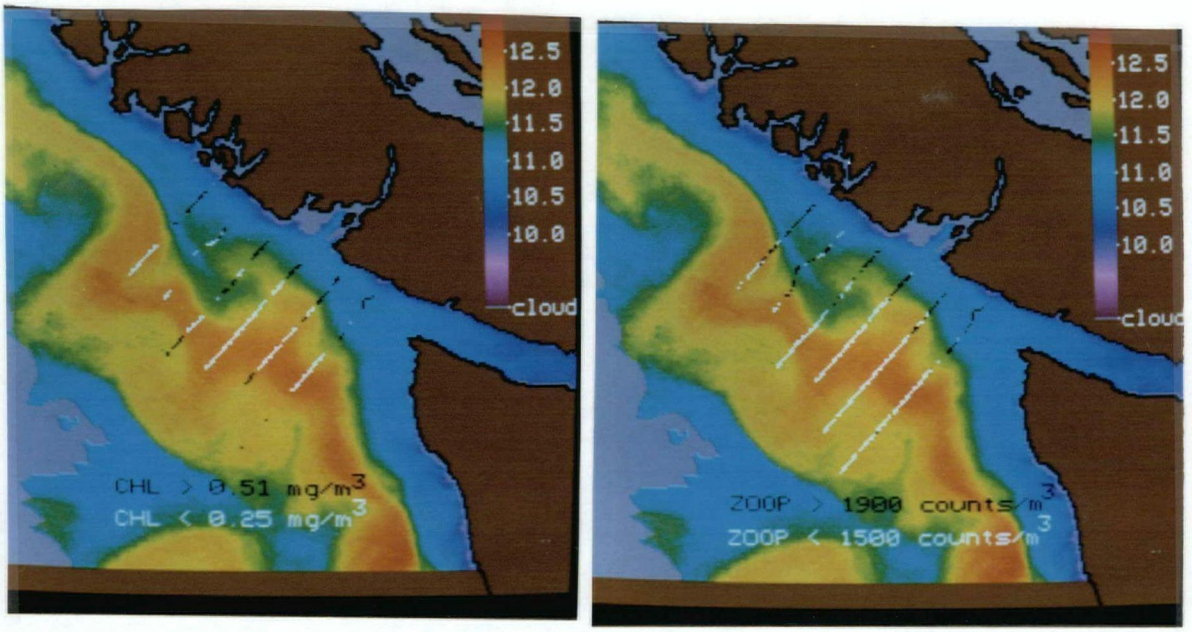

Figure 4.12: Winter mean sea surface temperature image showing a) surface chlorophyll concentrations and b) zooplankton concentrations along each UBC8320 leg.

cussed in Chapter 3 with specific plankton concentrations is evident. Surface thermal features visible in the imagery are coincident with boundaries in the plankton regime. These data show the association of colder regions occupied by Vancouver Island Coastal Current water with higher zooplankton and chlorophyll concentrations and the warmer Davidson Current water with low chlorophyll concentrations. Low zooplankton concentrations were associated with both thermal regimes seaward of the Coastal Current water.

Winter higher chlorophyll concentrations in Vancouver Island Coastal Current water could be due to advection from an upstream source or to increased production within the water column in these coastal regions. Winter chlorophyll concentrations in Juan de Fuca Strait observed by *Lewis (1978)* were similar to those found in Coastal Current water during this study. This suggests that either similar growth environments occur in both locations, or that Juan de Fuca Strait is a potential source of the phytoplankton biomass observed in Vancouver Island Coastal Current water. Higher chlorophyll concentrations within this hydrographic regime could also be due to increased primary

productivity resulting from the increased vertical stability of this region. Winter data show that nutrient concentrations were not limiting. In general, the temperate winter water column is characterized by a well mixed surface layer, with phytoplankton populations subjected to high nutrient concentrations and low light levels *(Parsons et al. 1966, Fournier et al. 1979, Fournier et al. 1984)*. Light is the principle factor limiting winter primary production. Unlike summer conditions, when vertical stratification results in abundant light but nutrient depletion, winter hydrographic conditions which increase the vertical stability of the water column will increase the light availability to cells in the upper water column at a time when nutrients are plentiful. This can result in increased primary production *(Fournier et al. 1979)*. Providing that horizontal advection is slower than the rate of production, localized increases in phytoplankton biomass can occur in areas of increased winter stratification *(Parsons and LeBrasseur 1968)*. Vertical hydrographic profiles (Chapter 3) show that the Vancouver Island Coastal Current was the most strongly stratified region of the winter shelf and could potentially have the highest rates of primary production on the winter shelf. *Pomeroy et al. (1983)* showed similar increases in chlorophyll concentration on the southeastern U.S. continental shelf in areas of stronger vertical stability induced by the influence of low salinity estuarine water. Vertical profiles in Chapter 3 show the shelf areas occupied by Davidson Current water were the least stratified. Increased vertical mixing in this region might explain the extremely low chlorophyll concentrations associated with this hydrographic zone.

The higher zooplankton concentrations in Vancouver Island Coastal Current water than in the other regimes resulted either from differences in reproduction, survival, or advection from upstream sources. Unfortunately, very little winter zooplankton data from the B.C. coast is available for comparison. Winter secondary production rates are known to be low in temperate regions *(Parsons et al. 1984)*, a result of both colder temperatures and reduced food availability. The increased phytoplankton concentrations in Vancouver Island Coastal Current water could result in both increased survival

and/or reproductive rates (for those species which are capable of year-round reproduction) within the zooplankton population in this regime. Zooplankton concentrations in Juan de Fuca Strait were not measured, making it difficult to determine the potential contribution from this upstream source. The coincidence of high zooplankton concentrations with high phytoplankton concentrations does imply, however, that grazing rates were not high enough to dominate phytoplankton distributional patterns. Additional evidence of relatively low grazing rates and the domination of both populations by similar physical processes, is the coincidence of localized peaks of chlorophyll and zooplankton at the frontal zone in the southern portion of the study area. These peaks are evident in both Figures 4.12a and b and more obviously in Figures 4.1 and 4.2 and Figure 3.11. The exact coincidence of these peaks would be unlikely if grazing was a dominant process. In addition, zooplankton reproductive rates in the winter are probably not rapid enough for the exploitation of a localized food source to be manifested as a localized increase in zooplankton concentration. Horizontal dispersion rates are most likely to be greater than growth rates, reducing the possibility of patch formation through biological processes *(Okubo 1978)*.

The similarity of winter plankton and hydrographic distributions, and the general positive correlation of phytoplankton and zooplankton concentrations indicate either a large degree of physical control over biological distributions or a rapid biological response to physical forcing. During winter, in temperate latitudes, low incident light and low temperature regimes will slow biological processes, reducing the biological component of any response. Winter plankton will act more as Lagrangian tracers of the physical regime. This implies that the similarity in distributions of hydrographic and biological variables on the winter shelf is primarily a function of physical advective processes. Lower winter spatial variance of both zooplankton and chlorophyll concentrations shown in Table 4.1 is additional evidence of this.

4.2.2 Summer

Summer chlorophyll concentrations superimposed on the mean satellite image (Figure 4.13a) show a consistent relationship between chlorophyll concentration and sea surface temperature. This figure shows highest concentrations were associated with the cold water around the outer edge of the eddy. Lowest concentrations were present in both the coldest water in the center of the eddy, and also throughout the warmest water. This supports the relationship shown in the T/S/plankton plots and demonstrates that this relationship was maintained spatially over the entire study area. Patterns of zooplankton distribution (Figure 4.13b) were less consistently related to features visible in the imagery. High concentrations of zooplankton along the northern transect (Leg 3) were in warm surface water, shown to be strongly stratified in Chapter 3. Increased concentrations in the vicinity of the eddy, however, were generally associated with the surface frontal zone at the outer edge of the eddy rather than any specific temperature. Although these increases in concentration were not consistent along the frontal region, they do suggest that higher zooplankton biomass was generally coincident with the regions of higher phytoplankton concentration seen in Figure 4.13a. The highest concentrations seen by *Mackas et al. (1980)* over the outer-shelf in the southern portion of the study area are similar to those seen in Figure 4.13, although these authors did not observe an associated peak in chlorophyll concentration. Comparison of Figure 4.13b with Figure 2.6 shows the peak in zooplankton concentration evident along Leg 3 (the northern transect) was in the vicinity of La Perouse Bank. A peak in this region was not observed by *Mackas et al. (1980)*. An explanation for this high zooplankton concentration in a stratified region of low surface chlorophyll concentration is difficult to determine from these data. It is possible that subsurface processes not sampled during the study result in this peak.

Both chlorophyll and zooplankton distributions were related to surface patterns during the wind event (Figure 4.14a and b). Changes in concentration coincided with the warm tongue isolated over the La Perouse Bank area. Comparisons between these data

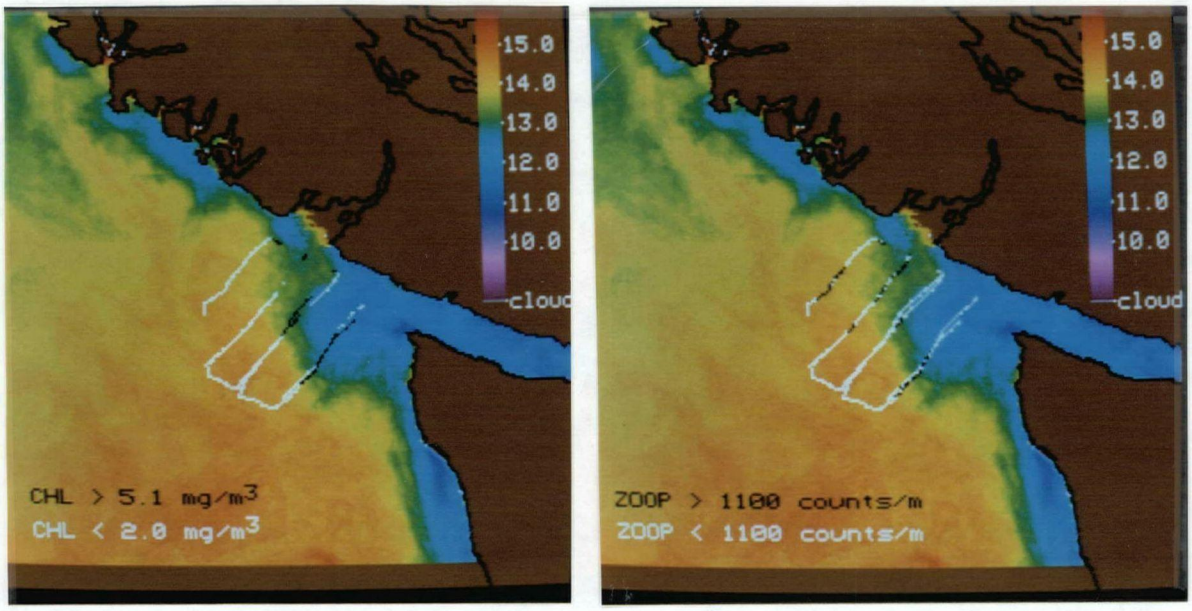

Figure 4.13: Summer mean sea surface temperature image showing a) surface chlorophyll and b) zooplankton concentrations along each UBC8410 leg (Legs 1–4).

and concentrations along Leg 3 (Figure 4.13) imply that the warm tongue maintained the same plankton concentrations that were present in the region before the wind event. The association of high zooplankton concentrations with low chlorophyll concentrations in warm surface water over La Perouse Bank was still present during the wind event. Chlorophyll concentrations in the surrounding colder water ($< 13.0°C$) were higher than those present in the warmer water previously located in this region. Maintenance of the zooplankton population over La Perouse Bank (Figure 4.14b), despite the offshore advection associated with the upwelling event, has important implications for this biologically productive region. The La Perouse Bank area is an important commercial fishing region (La Perouse Project, 1987) and a nursery area for the planktonic larvae and juveniles of many commercially important species. The success of this region as a nursery might be due, in part, to a reduced offshore advection during upwelling events.

Summer data indicate that upwelling, stratification and the resultant distribution of surface nutrients played a major role in determining the summer phytoplankton distri-

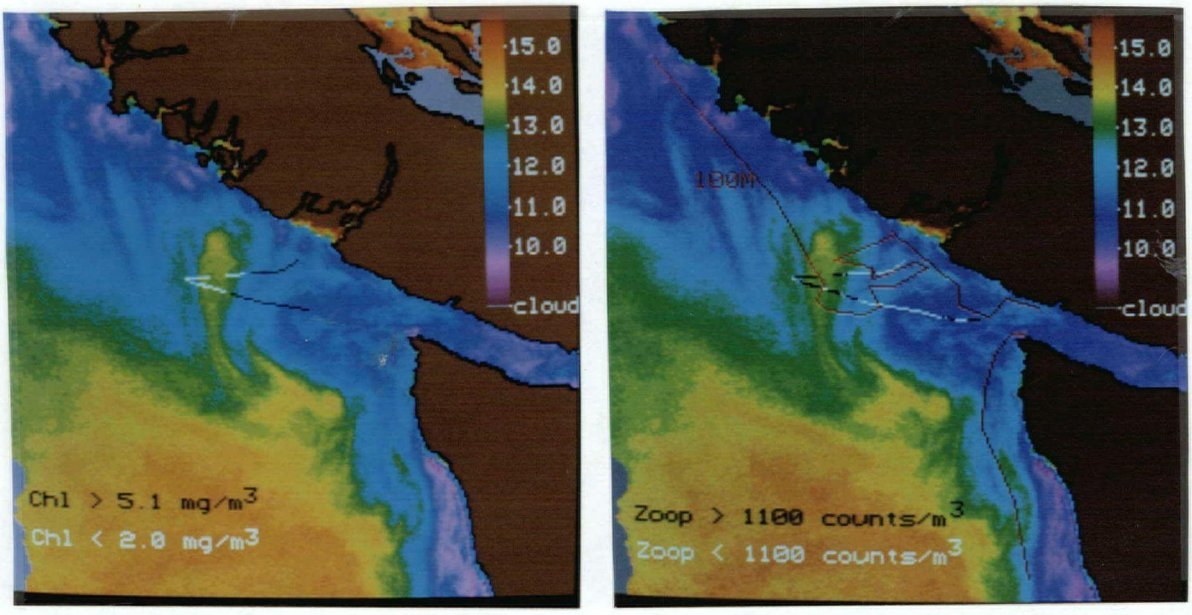

Figure 4.14: Summer sea surface temperature image during the wind event showing a) surface chlorophyll and b) zooplankton concentrations along UBC8410 Leg 6. The 100 m contour on b) shows the location of La Perouse Bank.

butional patterns seen in Figure 4.13a. These data conform to the generalized picture of the typical phytoplankton response to the upwelling of nutrient rich deep water in eastern boundary current systems *(Jones et al. 1983, Traganza et al. 1983, Brink et al. 1981)*. In the most recently upwelled and coldest water, primary production and biomass are relatively low with the initial 'seed' phytoplankton cells in a 'shifted-down' physiological state *(MacIsaac et al. 1985)*. As the cells become exposed to higher light intensities, they undergo a light-induced 'shift-up' in nutrient uptake rates. The rate of 'shift-up' is most likely related to irradiance, and hence the extent of vertical mixing, and the initial concentration of the limiting nutrient in the upwelled water *(Wilkerson and Dugdale 1987; Zimmerman et al. 1987)*. Seaward or downstream of this region, nutrient concentrations are rapidly reduced, and there is a rapid increase in the phytoplankton biomass. Evidence of this relationship is seen in Figure 4.5. Growth in this region occurs at maximum rates *(MacIsaac et al. 1985)*. As the upwelled water warms and ages at the surface, the water column becomes increasingly stratified

and nutrient depleted. In this region, the phytoplankton return to the 'shifted-down' physiological state, in which rates of photosynthesis and nutrient uptake are reduced. Biomass in this region is low and growth is most likely supported mainly by nitrogen regenerated within the water column *(Eppley and Peterson 1979; Cochlan 1986)*. The low chlorophyll concentrations in the warmer regions of the study area probably represent a nutrient limited phytoplankton population, typical of mid-summer stratified conditions at middle latitudes *(Parsons et al. 1984)*. There is thus both a spatial and a temporal component in the phytoplankton response to nutrient enrichment of surface water in the presence of advection *(Campbell and Esaias 1985)*. The resultant distribution has both a physical (upwelling and advection) component and a biological (nutrient uptake, cell division and biomass) component.

4.3 Distributional Similarities: a Statistical Estimation

Figures 4.12 – 4.14 present the associations identified in the T/S/plankton plots in a spatial context. They indicate that relationships between plankton concentrations and surface hydrography were not only maintained when compared to satellite measured sea surface temperature, but also formed coherent and relatively unambiguous spatial patterns similar to those in the imagery. This comparison shows that major features of both phytoplankton and zooplankton surface distribution might be represented by satellite images of surface thermal patterns. Statistical estimates of the association of chlorophyll and zooplankton with satellite temperature will quantify the ability of the images to model these distributional patterns. In addition, these statistics can be used to produce predicted 'plankton' images, providing a two-dimensional spatial representation of concentration. Errors associated with these 'plankton' images will highlight areas of the shelf where concentrations are well modelled by the overall statistical association and areas where satellite images do not predict biological patterns.

Two approaches were used to quantify similarities between satellite measured ther-

mal patterns and winter chlorophyll and zooplankton distributions, and summer chlorophyll distributions before and during the wind event. The first approach used a least squares approximation to define regression equations relating plankton concentrations with satellite temperature. These equations were then used to create a 'plankton' image from the mean satellite temperature image. The statistical relationship between image (modelled) concentrations and ship-measured concentrations was calculated and used as a measure of pattern similarity. The second approach expanded on the relationship between specific plankton concentrations and hydrographic zones which were identified in the T/S/plankton plots of the previous section. These data show that variability in plankton concentration within certain hydrographic zones was low. Specific zones within each image were isolated by density slicing the thermal image at subjectively chosen hydrographic thresholds. Each zone was then assigned the mean plankton concentration calculated from in-situ data points within the thresholds. A 'plankton' image was created from these regions, and the statistical relationship between modelled and measured concentrations calculated.

Three statistics were used to quantify the relationship between modelled plankton and measured plankton concentrations. A root mean square difference between the two quantities provided a dimensional estimate of the model success in the same units as the treated data. RMS difference is defined as

$$RMSDIF = \sqrt{\frac{1}{N}\sum_{i=1}^{N}(x_i - \hat{x}_i)^2}$$

where x_i are the actual measured concentrations, $\hat{x}_i$ are the modelled values from the same locations in the 'plankton' image and N is the number of data points. This statistic is equal to the standard deviation when the modelled value is the mean of the measured values (as it will be within specific hydrographic regimes following the second modelling approach). Comparisons of model success between the different units of chlorophyll and zooplankton concentration, and also between various normalizing transformations of the plankton data, were made with a dimensionless 'error' term

defined by normalizing the mean square difference by the original variance. Total model error was defined as

$$\varepsilon^2 = \frac{\sum(x_i - \hat{x}_i)^2}{\sum(x_i - \bar{x})^2}$$

where $\bar{x}$ is the mean of the measured plankton values and other terms are as previously defined. This term is the proportion of the original variance unexplained by the model and the term r^2, where

$$r^2 = \frac{\sum(\hat{x}_i - \bar{x})^2}{\sum(x_i - \bar{x})^2}$$

is the proportion of the variance explained by the model. Both of these terms are non-dimensional and it can be seen that

$$\varepsilon^2 + r^2 = 1.$$

Any attempt to estimate the statistical significance of these terms relies on the number of degrees of freedom in the calculation. The number of data points used in these calculations was 461 and 453 respectively for the winter and summer cruises, and 130 for the summer cruise portion during the wind event. Each of these data points, however, cannot be considered independent *(Mackas 1984; Millard et al. 1985)*, and the effective number of degrees of freedom associated with the calculations is less than N. The lack of independence of individual data points is a function of the short distance between them (high rate of sampling) in relation to the length scales of oceanographic processes. The spatial scale of the automated sampler data was 1 km, considerably less than the $\approx$ 30 km length scales observed to dominate this region of the continental shelf by *Freeland and Denman (1985)*. For temperature and salinity, this autocorrelation is a result of mixing associated with eddies, tidal advection and other processes with length scales larger than 1 km. For chlorophyll and zooplankton concentrations, the autocorrelation is a result of interaction with these physical processes as well as biological processes, both of which induce spatial patchiness.

An estimate was made of the proportion of the chlorophyll and zooplankton variance associated with large scale variability and the large scale temperature field. Both

Winter	Raw Data			Detrended		
	T	C	Z	T	C	Z
T	0.246			0.099		
C	-0.070	0.036		-0.034	0.024	
Z	-119.3	83.4	377005.4	-60.0	46.8	210439.4

Table 4.2: Winter mean covariance matrix of temperature, chlorophyll, and zooplankton for the six winter UBC8320 transects before and after removal of least squares fit straight line representing the large scale variability.

modelling approaches utilized the relationship between the whole temperature field and the plankton concentrations to produce a 'plankton' image. That proportion of the biological variance associated with large scale structure will not have been adequately sampled by the cruise transects and will be associated with very few degrees of freedom. Only that proportion of the variance associated with structures considerably smaller than the transects will have enough realizations within the cruise data set to give a statistically reasonable number of degrees of freedom. During both winter and summer, the large scale structure was a general cross-shelf gradient from colder temperatures and higher plankton concentrations nearer shore to higher temperatures and lower plankton concentrations offshore. The dependence of chlorophyll and zooplankton on the large scale temperature field was estimated by first examining the covariance matrix of these variables for each transect of the cruises used to form models (UBC8320 and UBC8410). The cross-shelf gradient of each variable along each transect was then removed by subtracting a least squares fit straight line. A second covariance matrix formed from the residuals was then calculated. A mean covariance matrix for winter and summer was made by averaging the covariances from each of the transects together. Approximately 50% of the winter covariance (Table 4.2) remained after removal of the large scale trend. This implies that approximately equal proportions of the winter covariance of temperature and both chlorophyll and zooplankton were associated with large scale features and with smaller scale features. The two mean summer covariance

Summer		Raw Data	Detrended	
	T	C	T	C
T	1.372		0.181	
C	-1.944	14.888	-0.457	10.996

Table 4.3: Summer mean covariance matrix of temperature and chlorophyll for the six summer UBC8410 transects before and after removal of least squares fit straight line representing the large scale variability. (Legs 2 and 4 were each divided into a northern and a southern transect and treated separately.)

matricies (Figure 4.3) show that although a large proportion of the chlorophyll variance is associated with small scale features, only $\approx$ 25% of the chlorophyll - temperature covariance is associated with features smaller than the length of transects.

Although statistically, the larger scale structure has not been adequately sampled in this study, the cross-shelf gradient making up this structure is an expected and commonly observed feature of coastal regions, especially along the North American west coast *(e.g. Mackas et al. 1980; Traganza et al. 1983; Ikeda et al. 1984b; Abbott and Zion 1985)*. This implies that although there is no statistical confidence that can be attached to variance associated with the large scale trend, it is reasonable to assume it to be a real and recurring feature. The small scale temperature - plankton variability is both more variable in time and space, and less well studied. The satellite data is especially suited for studying these smaller scale features. The number of independent realizations associated with the smaller scale structure can be estimated from detrended structure functions of the cross-shelf transects.

For smaller scale structure, to determine what proportion of the data points can be considered independent, a dominant length scale of variability must be calculated. It can be assumed that on average, data points separated by more than this length scale will be independent, and those closer than this separation are spatially autocorrelated and dependent. Previous authors have used the spatial structure function to investigate length scales in the marine environment *(Lutjeharms 1981; Deschamps et al. 1981;*

Denman and Freeland 1985). The spatial structure function, defined as

$$D^2(h) = \frac{1}{n}\sum_{i=1}^{n}(f_{(i)} - f_{(i+h)})^2$$

where f is the variable being investigated and h is a spatial distance or lag, represents as a mean square difference the statistical influence of a point upon other points at distance h. Dominant features of a specific spatial scale will produce a distinct peak in the function at that spatial lag and scales at which little spatial structure exists will be represented by flat portions of the function *(Lutjeharms 1981).*

Structure functions of surface temperature, salinity, chlorophyll and zooplankton from each leg of each cruise (see Figures 2.1, 2.5 and 2.6a and b) were calculated from data detrended by a least squares fit straight line. Summer chlorophyll and zooplankton data were first $\log_e$ transformed as recommended by *Denman and Freeland (1985)* to increase the normality of their distributions. This transformation was not applied to the winter biological data as rates of biological processes which tend to cause these variables to depart from a normal distribution, such as grazing and growth, are minimal during winter. Structure functions from each cross-shelf transect within a season were averaged to produce a mean function for each variable for the winter and summer sampling periods. The magnitude of the structure function for each variable was then scaled to fit between 0 and 1, to facilitate comparison. These structure functions (Figure 4.15) show that during both winter and summer, a length scale is apparent in the hydrographic and the planktonic data. The winter functions show that chlorophyll and zooplankton reach a peak at a separation of $\approx$ 15 km, and that both hydrographic variables (temperature and salinity) reach maximum dissimilarity at $\approx$ 18 km. The summer functions show that chlorophyll reaches a peak at $\approx$ 16 km, and temperature at $\approx$ 20 km.

Using the longer of the observed length scales for each season, and assuming that individual transects are themselves independent (separated by 18.5 km), an approximation of the number of independent realizations of the smaller scale structure can be calculated by dividing the number of data points in a cruise (separated by 1 km) by this

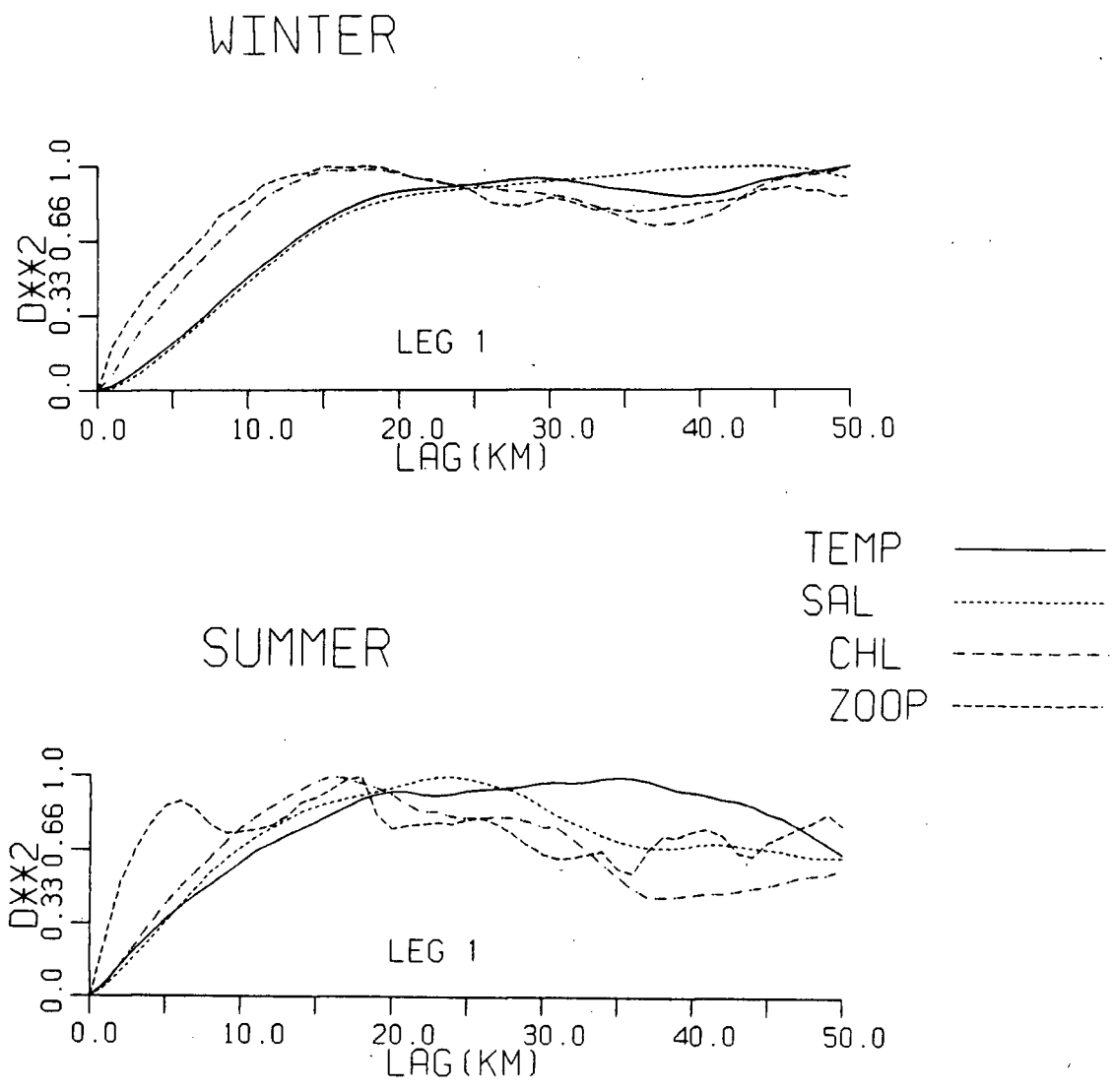

Figure 4.15: Mean structure functions of temperature, salinity, chlorophyll concentration, and zooplankton counts for a) winter and b) summer, scaled between 0 and 1. Mean functions for each variable were formed from the average of 11 winter and summer cross-shelf transects derived from both SHOP and UBC cruises.

length scale. The winter data set of 461 samples yields $\approx$ 26 independent realizations and the summer data set of 453 samples yields $\approx$ 23 independent realizations. These values are applicable only to that portion of the covariance associated with smaller scale structure. As the statistics (ε^2 and r^2) used in the models are derived from the whole cross-shelf field, an accurate estimate of their actual degrees of freedom is not possible from the data analyzed in this study. While these statistics are an effective representation of the relationship between the satellite data and the plankton concentrations, it is difficult to estimate their statistical applicability outside the time and space scales of the data itself.

4.3.1 Winter

Winter surface chlorophyll and zooplankton concentrations from UBC8320 were regressed against mean satellite temperatures using both untransformed and $\log_e$ transformed values. The success of these four regressions is presented in Table 4.4. Biological processes within plankton communities result in an 'over-dispersed' or patchy distribution of both organisms and other non-conservative properties, such as nutrients. This is a result of both the logarithmic relationship between biological rate processes and variables controlling them and the exponential nature of population growth itself. Relationships between population variables primarily controlled by these biological processes and any more conservative variable are therefore likely to be most closely described by some form of logarithmic function. Previous authors *(Cassie 1962, Denman and Freeland 1985, Abbott and Zion 1985)* have shown that a log transformation of plankton data is required to produce a normal distribution. This will linearize the relationship between plankton concentrations and a more conservative variable. The error (ε^2) associated with the winter regression of chlorophyll concentration ($[chl]$) with satellite temperature was approximately 22% less than that associated with the regression of $\log_e[chl]$. Not only does this mean that the $[chl]$ regression produced a better model of the chlorophyll data, but it also supports the previously presented hypothe-

Variable	RMSDIF	r^2	ε^2	α	β
$[chl]$	0.162	0.366	0.635	-0.290	3.782
$\log_e[chl]$	1.500	0.192	0.808	-1.727	18.879
$[zoop]$	490.29	0.441	0.560	-1028.5	13700.2
$\log_e[zoop]$	0.297	0.485	0.516	-0.679	15.29

Table 4.4: Winter regression model statistics for chlorophyll and zooplankton concentration and mean satellite temperature. Least squares regression coefficients are given as α and β, RMSDIF is in the same units as the variable. N = 461 for each regression.

sis that the biological component of processes controlling distribution are reduced in winter. A linear relationship between a relatively conservative tracer of the physical regime (temperature) and a biological variable such as chlorophyll implies that the phytoplankton cells were acting as Lagrangian tracers of the physical regime and their distribution was more likely a result of linear mixing of biomass than active growth. The magnitude of the errors associated with the regression of $\log_e[zoop]$ and $[zoop]$ was similar, suggesting that, similar to the phytoplankton community, biological processes within the zooplankton community do not play a dominant role in determining resultant distributions during the winter. Regressions representing the least statistical error ($[chl]$ and $\log_e[zoop]$) are shown in Figure 4.16a and b.

'Plankton' images of $[chl]$ and $\log_e[zoop]$ constructed from these regression equations are shown in Figures 4.17a and b. These images reproduce the general patterns of distribution shown by the contour plots (Figures 4.1 and 4.2) of the previous section, including mesoscale patterns associated with the isolation of coastal water over La Perouse Bank. However, they fail to show smaller scale peaks in concentration associated with the hydrographic frontal zone in the southern portion of the study area. In this region, peaks in both chlorophyll and zooplankton concentration were more closely associated with surface thermal gradient than surface temperature and will only contribute to the error of a simple regression. The strong surface thermal gradient in the northern portion of the study area (see Figure 3.3) was not associated with a peak in

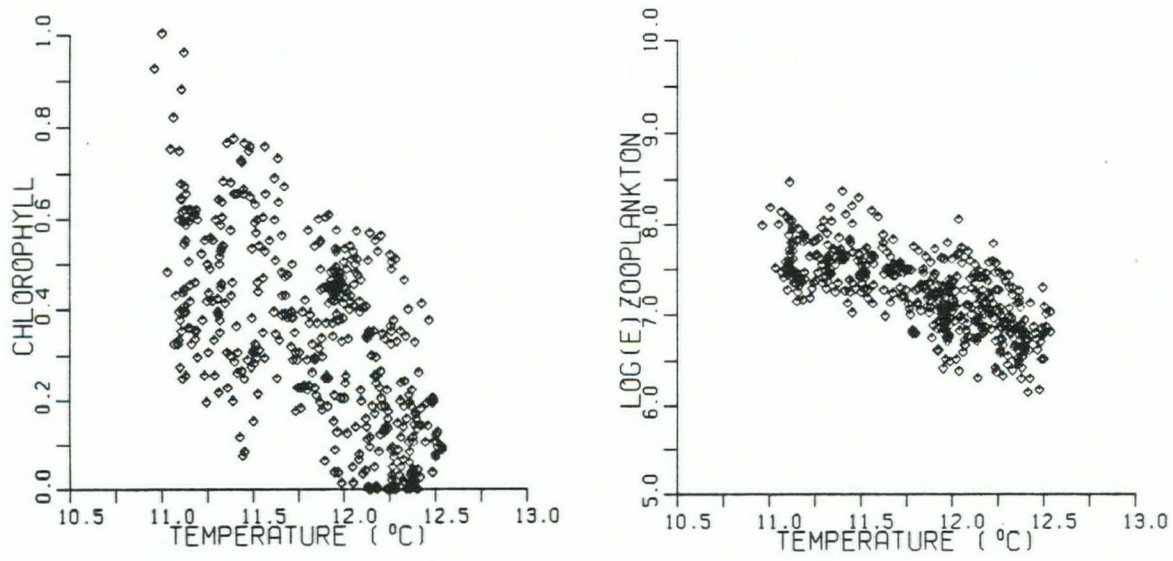

Figure 4.16: Winter (UBC8320 data) a) chlorophyll concentration and b) $\log_e$ zooplankton concentration plotted against mean satellite temperature.

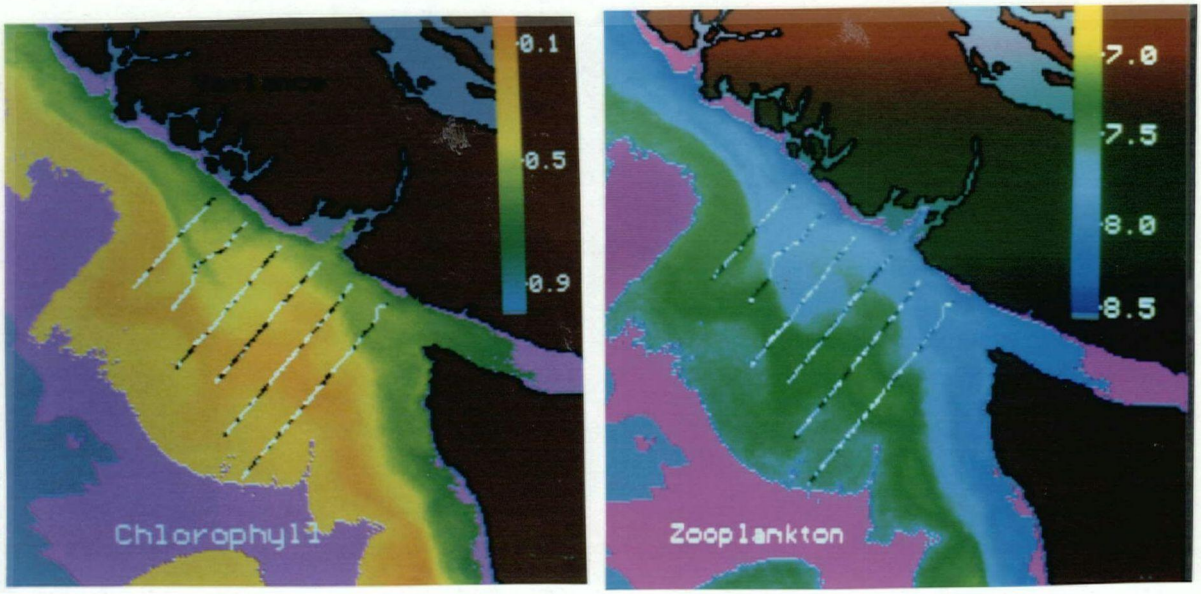

Figure 4.17: 'Plankton' image of winter surface a) chlorophyll distributions and b) $\log_e$ zooplankton distributions constructed from the regression equation of plankton concentration and satellite temperature. UBC8320 sampling transects are coded to indicate areas where the model differed from sampled concentration by more than the overall RMSDIF (BLACK) and by less than this RMSDIF (WHITE). A pink mask was applied to hydrographic regimes not sampled.

chlorophyll or zooplankton concentration. This inconsistency prevented a regression of concentration with surface temperature gradient being used to model concentrations along the frontal zone.

Superimposed on each image are the sampled transects coded to show regions where the model fits the actual data closely, and where departures from the overall regression equation occur (see figure caption). This code emphasizes the smaller overall error of the $\log_e[zoop]$ regression compared to the $[chl]$ data. Consistent patterns in this error indicate regions where failure might be due to systematic changes in the functional relationship between hydrography and plankton concentration. Both images show an expected lack of fit in frontal regions, especially at the front crossed by Legs 1, 2 and 3. The zooplankton image also indicates larger errors at the seaward portions of Legs 5 and 6. It is possible that lack of synopticity is contributing to the error in these regions. Figure 2.1 shows the satellite data used to calculate the mean temperature image were recorded between 24 and 84 hours prior to the in-situ sampling of these legs.

Temperature thresholds used to density slice the mean image into plankton zones were identified from redrawn T/S/plankton plots (Section 4.1) in which the ship measured temperature at each location was substituted by mean satellite temperature. Although some extreme temperature values were lost due to the smoothing involved in the mean calculation, overall relationships between both zooplankton and chlorophyll concentrations and hydrographic properties (Figures 4.6a and b) were maintained. Thresholds were subjectively chosen to produce thermal regions within which the plankton variability was minimized. These thresholds, and the mean plankton concentrations and RMS differences associated with them are given in Table 4.5. Temperature thresholds for chlorophyll distribution produced three regions approximating Vancouver Island Coastal Current water, Davidson Current water, and North Pacific water. Zooplankton temperature thresholds reflected the general decrease in concentration with increasing temperature and distance from shore. Thresholds corresponded roughly

Figure	Zone	T	$\bar{x}$	RMSDIF	r^2	ε^2
Chlorophyll			$(mg \cdot m^{-3})$	$(mg \cdot m^{-3})$		
4.18a	Total			0.162	0.336	0.639
	VICC	< 11.75	0.47	0.175		
	DC	> 12.25	0.15	0.136		
	NP	11.75–12.25	0.33	0.163		
Zooplankton			$(counts \cdot m^{-3})$	$(counts \cdot m^{-3})$		
4.18b	Total			503.2	0.413	0.590
	VICC	< 11.67	2327.5	645.1		
	Trans.	11.67–11.87	1664.1	409.6		
	Offshore	> 11.87	1119.7	387.0		

Table 4.5: Winter density slice model statistics for chlorophyll and zooplankton concentration using temperature (T) thresholds. Zones are named such that Total refers to all sampled data points or total image statistics, VICC refers to Vancouver Island Coastal Current water, DC refers to Davidson Current water, NP refers to North Pacific water, and Trans. are transitional zones.

to Vancouver Island Coastal Current water, a transitional zone, and offshore water. 'Plankton' images of chlorophyll and zooplankton concentration, created by assigning each pixel of the mean winter image a mean plankton concentration from Table 4.5, are presented in Figure 4.18a and b. Statistics comparing the whole images (Total) with ship measured values are given in Table 4.5. The error incurred by subdividing the image into three chlorophyll zones on the basis of surface temperature was similar to that of the regression model. Approximately 34% of the original chlorophyll variance was explained and the RMS difference is $0.162 mg \cdot m^{-3}$. Table 4.5 shows chlorophyll concentrations within Davidson Current water were the most effectively modelled. The error incurred by subdividing the image into three zooplankton zones was higher than that of the regression model primarily due to the large RMSDIF in Vancouver Island Coastal Current water. Both chlorophyll and zooplankton temperature threshold models showed maximum RMS differences in Coastal Current water. Statistics for this zone included the errors induced by the unmodelled frontal zone.

Spatial patterns of the RMSDIF in this image (Figure 4.18 indicate that errors in

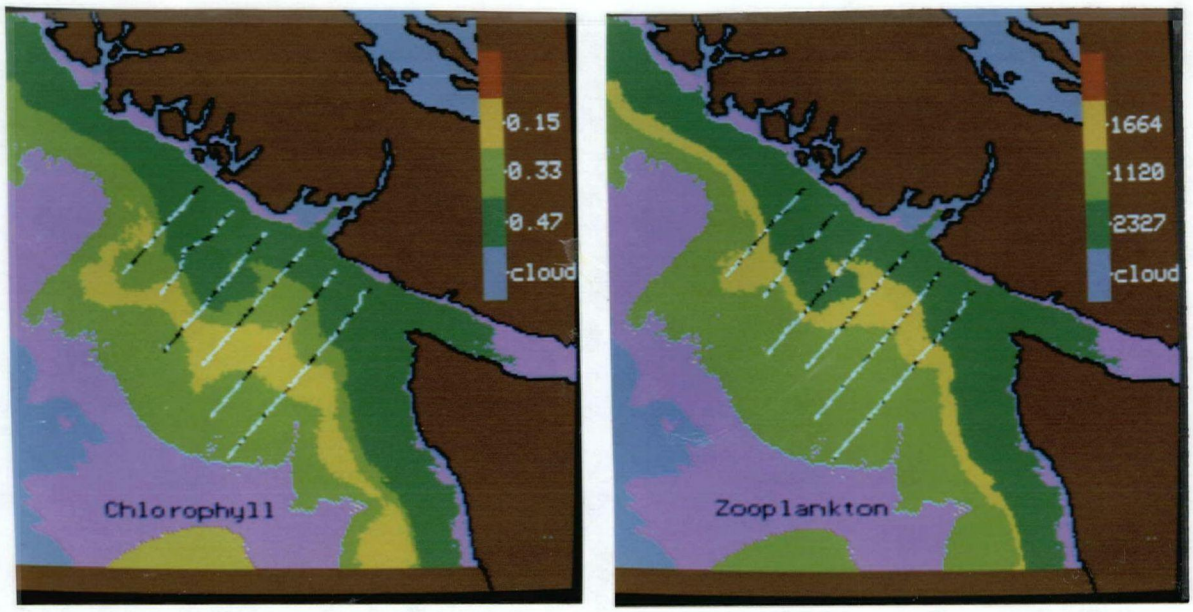

Figure 4.18: 'Plankton' image of winter surface a) chlorophyll distributions and b) zooplankton distributions constructed by density slicing at temperature thresholds and assigning mean concentrations to each pixel. UBC8320 sampling transects are shown, coded to indicate areas where the model differed from sampled concentration by more than the overall RMSDIF (BLACK) and by less than this RMSDIF (WHITE). A pink mask was applied to hydrographic regimes not sampled.

the chlorophyll concentration occurred primarily at the boundaries of the thresholded zones. This systematic spatial error was due both to changes in concentration not being as instantaneous as the change in hydrographic zone created by the model, and also due to lack of synopticity oof the mean image with each sampling transect. Fewer errors appear within the zones.

Each of these temperature-defined threshold models failed to distinguish between North Pacific water southwest of the Davidson Current regime and water resulting from the mixing of Davidson Current water and Coastal Current water. The T/S/plankton plots in Section 4.1 show that both Davidson Current and North Pacific water were best defined in terms of both temperature and salinity. A model was developed whereby surface salinity distributions were predicted by the satellite temperature image to produce a 'salinity' image. Using these two image products, every pixel of the study area could be assigned coordinates in T/S space to mimic the T/S/plankton diagrams. Figures 3.16 and 3.15 show that this will also allow considerable accuracy in predicting associated winter plankton concentrations.

The 'salinity' model was possible due to the consistent relationship between winter surface temperature and salinity evident in winter T/S plots (Figure 3.16). Surface water was assumed to be a result of mixing between three water regimes as described in Chapter 3. Salinity variations within both the Davidson Current and North Pacific regimes were small. This entire surface area was assigned the mean salinity calculated from all points within the region (32.25). The key to the model was that the separation between this region and less saline regimes could be unambiguously identified in the satellite imagery by the distinct surface thermal signature of Davidson Current water. All pixels in the image seaward of the main (warmest) core of this water were assigned this mean salinity. Salinity variation in Coastal Current water and in the region between this and the main core of Davidson Current water was modeled as a line of mixing between the warmest Davidson Current water present in the study area (12.65°C, 32.25) and the center of the cluster of points defining Coastal Current water (10.88°C,

Figure 4.19: 'Salinity' image of surface salinity distributions constructed from the model relating surface temperature and salinity.

30.00) (see Figure 3.16). All pixels shoreward of the main core of Davidson Current water were then assigned the salinity predicted by temperature, assuming mixing along the straight line joining these two water types in T/S space.

The 'salinity' image produced from this model (Figure 4.19) shows the same features as the contours of measured salinity (Figure 3.14). Redrawn T/S/plankton plots using modelled salinity, mean satellite temperatures and sampled plankton concentrations (Figures 4.20a and b) show the same separation of water types and plankton concentrations as that seen in the original T/S/plankton plots (Figure 4.6a and b). In fact, comparisons of the original T/S plots with Figure 4.20a and b show the salinity model actually underestimated the true salinity in the mixing region between Davidson Current and Coastal Current water, indicating an influence of North Pacific water (higher salinity, lower temperature) on the mixing regime. This underestimation, however, had no effect on the isolation of regions of similar biomass.

Thresholds used to define regions of similar plankton concentration in satellite derived T/S space are given in Table 4.6 along with means calculated for the resultant

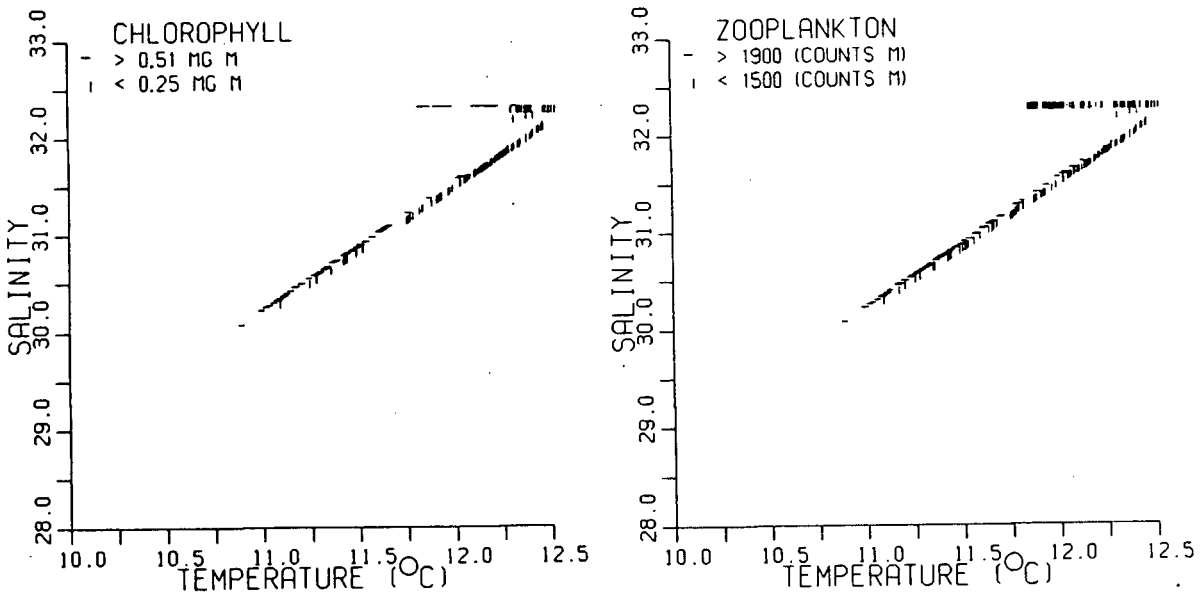

Figure 4.20: The association of winter (UBC8320 data) a) chlorophyll concentrations and b) zooplankton concentrations with mean satellite temperature and modelled salinity.

regions. 'Plankton' images constructed from these means are given in Figures 4.21a and b. Statistics of these images (Table 4.6) show that Figure 4.21a reduced the error of the chlorophyll estimation to 0.454, approximately 30% less than the simple temperature threshold model. This model explained approximately 55% of the sampled chlorophyll variance with an overall RMS difference of $0.137 \text{mg} \cdot \text{m}^{-3}$. The majority of the unexplained variance was still associated with the colder Coastal Current water. Chlorophyll concentrations in both Davidson Current and North Pacific water are more effectively modelled with RMS differences of 0.119 and $0.059 \text{mg} \cdot \text{m}^{-3}$ respectively. The error associated with the zooplankton image (Figure 4.21b) was approximately 10% less than that of Figure 4.18b (Table 4.6), but was still higher than the error associated with the $\log_e$ regression model. Table 4.6 shows the North Pacific water had the lowest RMS difference, indicating that chlorophyll concentrations within this hydrographic regime were the most precisely modelled. Coastal Current water was the least precisely modelled.

Figure	Zone	T	S	$\bar{x}$	RMSDIF	r^2	ε^2
Chlorophyll							
4.21a	Total				0.137	0.534	0.454
	VICC	< 11.75		0.47	0.175		
	DC	> 12.06	< 32.0	0.14	0.119		
		> 12.30	$= 32.25$				
	NP	> 12.30	> 32.0	0.46	0.059		
	Trans1	11.75–12.06	< 32.0	0.27	0.131		
Chlorophyll							
(not shown)	Total				0.139	0.526	0.471
	VICC	< 11.60		0.48	0.182		
	DC	> 12.20	< 32.25	0.13	0.113		
		> 12.30	$= 32.25$				
	NP	> 12.30	> 32.0	0.46	0.059		
	Trans1	11.60–11.90	< 32.0	0.20	0.146		
	Trans2	11.90–12.20	< 32.0	0.36	0.139		
Zooplankton							
4.21b	Total				481.5	0.459	0.540
	VICC	< 11.80		2088.7	634.6		
	Trans	> 11.80	< 31.85	1495.3	431.4		
	Offshore		> 31.85	1070.7	333.5		

Table 4.6: Winter density slice model statistics for chlorophyll and zooplankton concentration using both temperature (T) and modelled salinity (S) thresholds. For Zone names, Total refers to all data points in the study area or statistics for the total image, VICC refers to Vancouver Island Coastal Current water, DC refers to Davidson Current water, NP refers to North Pacific water, and Trans are transitional zones.

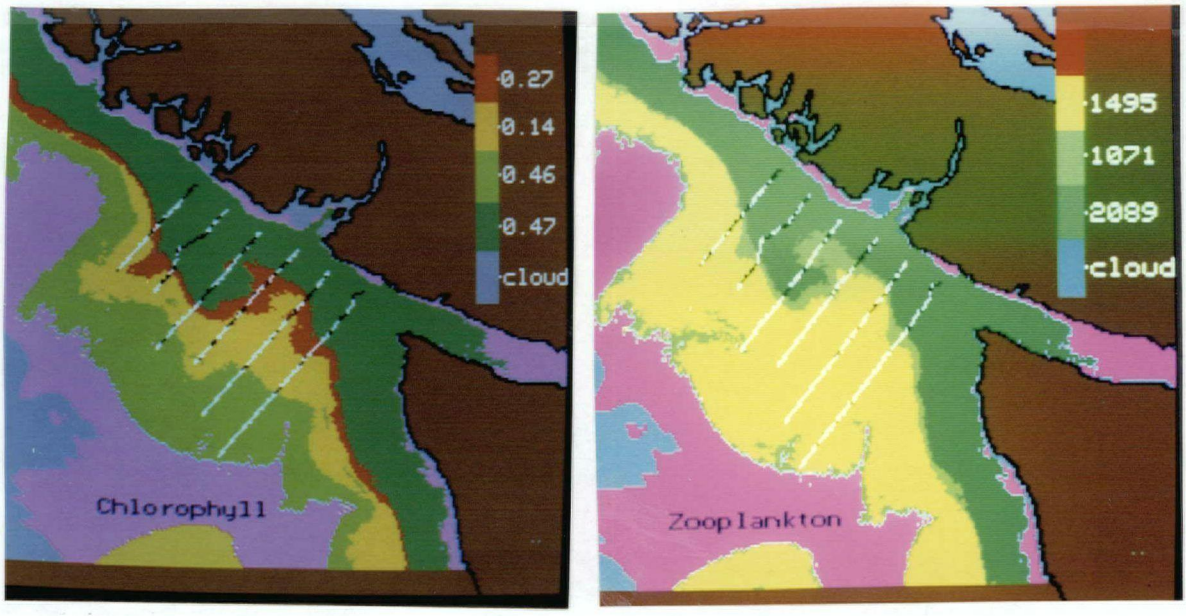

Figure 4.21: 'Plankton' image of winter a) chlorophyll concentration and b) zooplankton concentration constructed by density slicing in T/S space at both temperature and salinity thresholds and assigning mean concentrations to each pixel. UBC8320 sampling transects are coded to indicate areas where the model differed from sampled concentration by more than the RMSDIF (BLACK) and by less than the RMSDIF (WHITE). Pink mask denotes hydrographic regimes not sampled.

A further effort was made to reduce the error of the threshold chlorophyll model by subdividing the image into another T/S region, and narrowing the threshold limits of previously defined hydrographic regions. Redefined thresholds for these five regions are given in Table 4.6. No attempt was made to improve the extremely low RMS difference in North Pacific water. Statistics of this model (Table 4.6) show a slight improvement in the modelling of Davidson Current water concentrations, but both Coastal Current and undefined mixed water retain similar RMS differences. The image overall has an RMS difference of $0.139 \text{mg} \cdot \text{m}^{-3}$, which is slightly greater than that of the 4 zone model (Figure 4.21a). These results indicate that continued subdivision of the surface T/S regime into an increasing number of zones does not improve the prediction of plankton concentrations. There was a limit to the amount of plankton variance directly associated with T/S properties.

4.3.2 Summer

Summer chlorophyll 'plankton' images were produced from models of the relationship between in-situ sampled chlorophyll concentration and satellite measured temperature. T/S/plankton plots (Figures 4.9 and 4.10) show the majority of chlorophyll variation was explained by temperature, and salinity need not be considered. These figures also show no consistent relationship between zooplankton concentration and surface hydrography. Attempts to derive quantitative models of surface zooplankton distribution from surface temperature were not successful. Summer data were divided into two periods, with UBC8410 Legs 1–4 representing pre-wind event conditions, and UBC8410 Leg 6 representing conditions during the wind event.

Regressions of pre-wind event chlorophyll concentrations and mean satellite temperature (Table 4.7) showed that $\log_e$ transformed concentrations produced 40% less error than untransformed concentrations and explained approximately 60% of the sampled variance. The 'plankton' images produced by the $\log_e[chl]$ regression equations are shown in Figure 4.22a and b. The increased success of the $\log_e$ transformed regression

Variable	RMSDIF	r^2	ε^2	α	β
Legs 1–4					
$[chl]$	3.238	0.324	0.676	-2.587	37.965
$\log_e[chl]$	0.747	0.607	0.392	-1.070	14.883
$[zoop]$	1174.8	0.0003	0.9997	23.2	335.3
$\log_e[zoop]$	0.994	0.022	0.978	-0.231	8.764
Leg 6					
$[chl]$	5.596	0.141	0.859	-2.828	40.405
$\log_e[chl]$	0.833	0.310	0.689	-0.699	9.778
$[zoop]$	1222.6	0.020	0.980	179.4	-1042.5
$\log_e[zoop]$	0.975	0.145	0.855	0.414	1.522

Table 4.7: Summer regression model statistics for chlorophyll and zooplankton concentration and satellite temperature for pre-wind event and wind event data. Least squares regression coefficients for slope and intercept are given as α and β, RMSDIF is in the same units as the variable. N = 453 and temperature was from the mean satellite image for the pre-wind event data regression (UBC8410 Legs 1–4). N = 134 and temperature was from the single satellite image for wind event data (UBC8410 Leg 6).

is indicative of a significant biological control of patterns of chlorophyll concentration on the summer shelf. It implies a linear mixing of exponentially changing population variables such as growth rate, rather than a simple linear mixing of biomass as was observed in winter. This was probably largely due to rapid (exponential) population growth associated with the nutrient-rich upwelling zone. Figure 4.22 shows the association of highest chlorophyll concentrations with colder water within the upwelling regions. Low concentrations were present in the warmer regions, shown to be vertically stratified in Chapter 3. The lack of correlation between zooplankton concentration and satellite temperature is shown in Table 4.7.

Although the regression equation explains 60% of the variance, a significant failure is the prediction of the highest chlorophyll concentrations in the coldest and most recently upwelled water in the center of the eddy. This does not follow the theoretical association of chlorophyll and surface temperature in an upwelling area discussed in

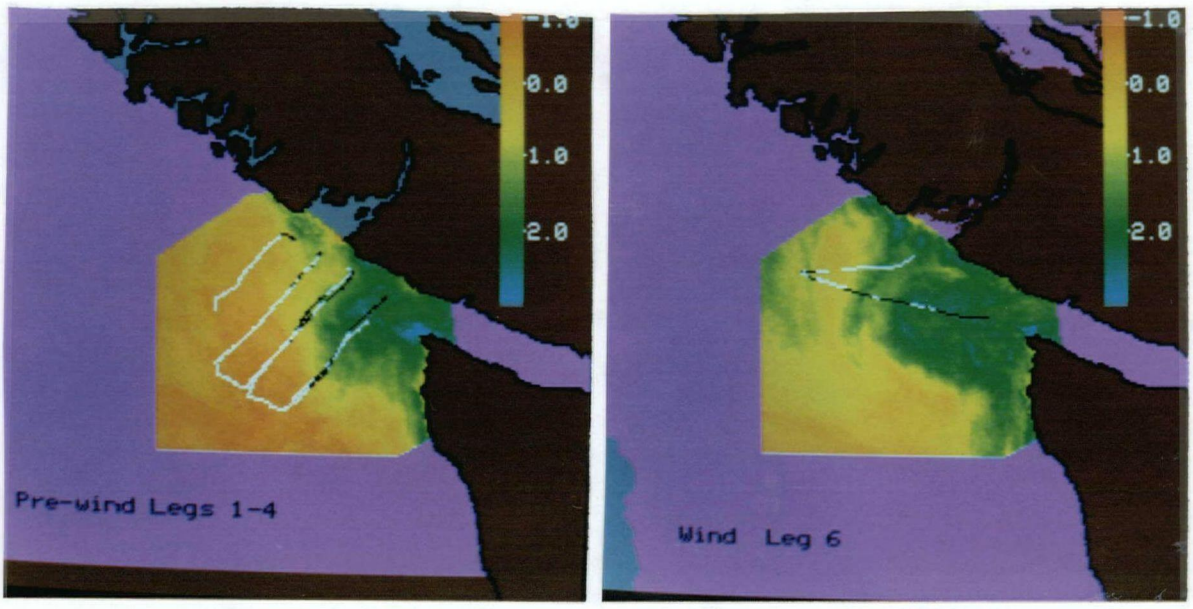

Figure 4.22: 'Plankton' image of $\log_e$ summer chlorophyll concentrations constructed from the regression equations of a) pre-wind event data, and b) wind event data. UBC8410 sampling transects are shown, coded to indicate areas where the model differed from sampled concentration by more than the RMSDIF (BLACK) and by less than the RMSDIF (WHITE). The pink mask denotes areas outside the study area.

Figure	Zone	T	$\bar{x}$	RMSDIF	r^2	ε^2
Pre-wind						
4.23a	Total			3.112	0.391	0.625
	Stratified	> 13.8	0.57	0.689		
	Coldest	< 12.0	2.24	0.594		
	Eddy	12.0–13.8	5.53	4.470		
Wind						
4.23b	Total			4.811	0.365	0.635
	Stratified	> 12.4	2.77	3.141		
	Coldest	< 11.0	5.69	5.082		
	Eddy	11.0 – 12.4	10.88	5.984		

Table 4.8: Summer density slice model statistics for chlorophyll concentration using temperature (T) thresholds. Zones are named such that Total refers to all sampled data points, Stratified refers to offshore warmest water, Coldest refers to most recently upwelled water, and eddy refers to upwelled water of intermediate temperature around the upwelling frontal zone.

the previous section. Lower concentrations are expected in most recently upwelled water and maximum values at some intermediate temperature on the outer edge of the upwelling zone.

A T/S/plankton plot constructed from satellite temperature values was used to identify temperature thresholds which would partition the shelf into three zones of chlorophyll concentration (see Figure 4.9a). Temperatures > 13.8°C represented warm regions (stratified water) with low concentrations; temperatures < 12.0°C represented cold regions (most recently upwelled water) also with low concentrations; intermediate temperatures (older upwelled water) represent highest concentrations. These thresholds changed to 12.4°C and 11.0°C respectively for application to the wind event image (see Figure 4.11a). Mean chlorophyll concentrations within these thresholds are given in Table 4.8, and the 'plankton' images created using these means given in Figure 4.23a and b. The RMS differences for each region (Table 4.8) show that the warm region and the newly upwelled water were most effectively modelled. Both images show the lower concentrations of chlorophyll expected in coldest water. A surprising characteristic of

the two images is the similarity in chlorophyll distributions in the southern portion of the study area shown in both. The images imply that chlorophyll distributions in the vicinity of the eddy were not greatly affected by the wind event. In this region, the input of additional nutrients to an already nutrient-rich surface regime probably did not affect phytoplankton growth rates and hence biomass, significantly. The greatest change in concentration is seen in the northern portion of the study area. In this region, changes in chlorophyll concentration probably lagged behind (temporally, and thus spatially) changes in patterns of sea surface temperature *(Campbell and Esaias 1985)*. This is supported by the fact that smallest ε^2 values relating chlorophyll concentration and satellite temperature were found for the image recorded $\approx$ 24 hours prior to the chlorophyll sampling (N6.26288) (see Figure 2.1) rather than the most concurrently recorded image. What changed during the wind event was the relationship between chlorophyll concentrations and specific temperatures, as exemplified by the T/S/plankton plots (Figures 4.9, 4.10 and 4.11) and the change in threshold values used to define regions of different chlorophyll concentration (Table 4.8).

Although the density slice model produced the three regions of chlorophyll concentration predicted from theoretical considerations, the total errors associated with the resultant 'plankton' images were larger than that of the regression model (Table 4.7). The threshold models explained only $\approx$ 40% of the sampled variance. Table 4.8 shows the majority of this error is associated with the high, but variable concentrations within the eddy.

The association of lower chlorophyll concentrations with both the coldest water and the warmest water, and maximum concentrations with an intermediate temperature suggested that the data might best be modelled by a non-linear equation. A gaussian equation would reproduce this relationship, predicting decreasing concentrations with both increasing and decreasing temperatures away from a chlorophyll maximum and also allow the stipulation of a minimum concentration (there was a measurable chlorophyll concentration in both the most newly upwelled water and in offshore stratified

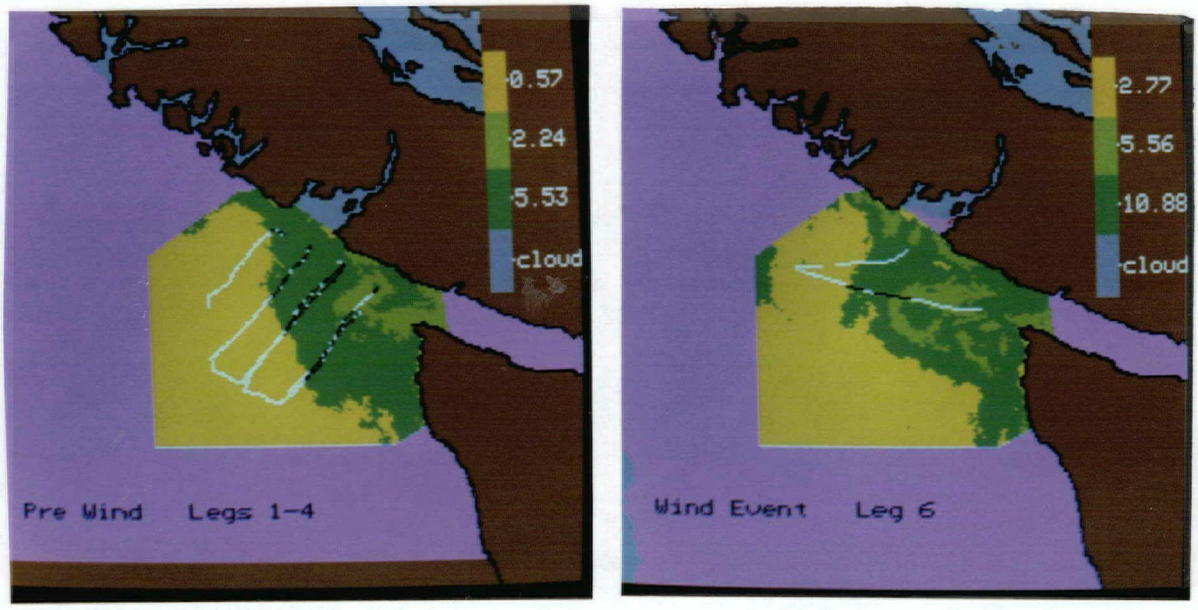

Figure 4.23: 'Plankton' image of summer chlorophyll concentrations constructed by density slicing the thermal images at temperature thresholds to give three chlorophyll concentration zones for a) pre-wind event data, and b) wind event data. UBC8410 sampling transects are shown, coded to indicate areas where the model differed from sampled concentration by more than the RMSDIF (BLACK) and by less than the RMSDIF (WHITE). The pink mask denotes areas outside the study area.

water). This form of response is not new to the study of plankton dynamics, and reoccurs in numerous rate responses to environmental stimuli. The biological reason behind this form of relationship is that many physiological processes function optimally at some specific level of a rate determining environmental factor, and function at a reduced rate at either higher or lower levels of this factor. This has been observed for example, in the effect of a required, but potentially toxic material on growth (e.g. copper concentration *(Lewis and Cave 1982)*), and the response of photosynthesis to light intensity *(Platt and Jassby 1976)*. The trophic relationship which might produce this type of response was originally proposed by *Riley (1946)* as a model of phytoplankton variation in the upper ocean. In modified form, he proposed the equation $dN/dt = N(P_h - R) - G$ where dN/dt was the change of the phytoplankton population (N), P_h the photosynthetic rate, R the respiration rate, and G the rate of grazing. The rate of photosynthesis is an exponential function of light intensity, nutrient concentration, and temperature. In the context of the upwelling area studied here, dN/dt has both a temporal and a spatial component due to advection, and changes in light intensity and nutrient concentration are probably the dominant terms. It is also possible that grazing was important at the outer edge of the upwelling area, where Figure 4.13b shows generally higher zooplankton concentrations. This equation emphasizes that the observed spatial variation in chlorophyll concentration in the vicinity of the eddy was most likely not a direct function of temperature. Trophic dynamics of the phytoplankton, and possibly the zooplankton, in response to the upwelling of nutrient rich deep water result in a consistent relationship between surface temperature and chlorophyll concentration which can be exploited by the satellite imagery to model the chlorophyll distribution.

A gaussian curve of the form

$$\log_e[chl] = a\exp(-b(T-c)^2) + d$$

where T is the satellite temperature in °C, was fitted to the pre-wind event data using a least-squares approximation. These data and the resultant curve are shown in

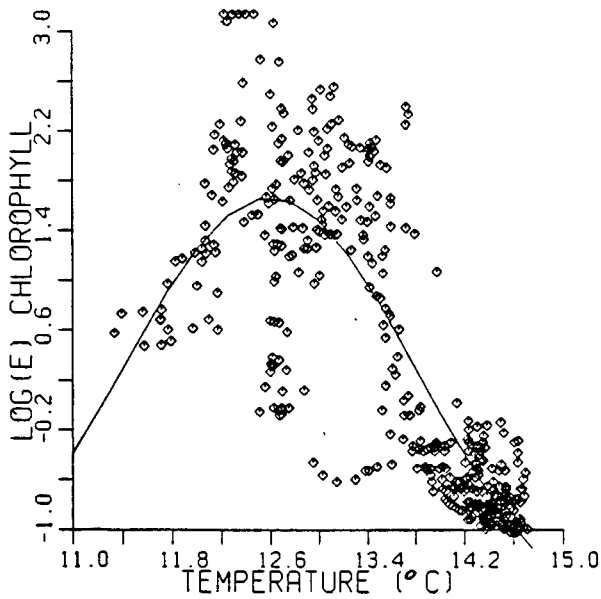

Figure 4.24: Relationship between $\log_e$ transformed summer pre-wind event chlorophyll concentrations (UBC8410 LEGS 1–4) and satellite temperatures, showing the least squares fit non-linear equation.

Variable	RMSDIF	r^2	ε^2
Legs 1–4 $\log_e[chl]$	0.628	0.719	0.277

Table 4.9: Summer non-linear regression model statistics for $\log_e$ chlorophyll concentration and satellite temperature for pre-wind event data, N = 453.

Figure 4.24. The least-squares approximation of the regression coefficients was

$$a = 3.5645,\ b = 0.3379,\ c = 12.5992,\ d = -1.8949$$

with c representing the temperature at which maximum chlorophyll concentrations were present. The 'plankton' image created from this regression equation is shown in Figure 4.25 and the statistics of its relationship with sampled data given in Table 4.9. This model reduced the $\log_e$ RMS difference between actual and modelled data to $0.628\text{mg} \cdot \text{m}^{-3}$, 16% less than the linear regression model. Figure 4.25 explains approximately 72% of the sampled chlorophyll variance. The error associated with this model is approximately 30% less than that of the linear regression.

Figure 4.25 shows a frontal zone with maximum chlorophyll concentrations along

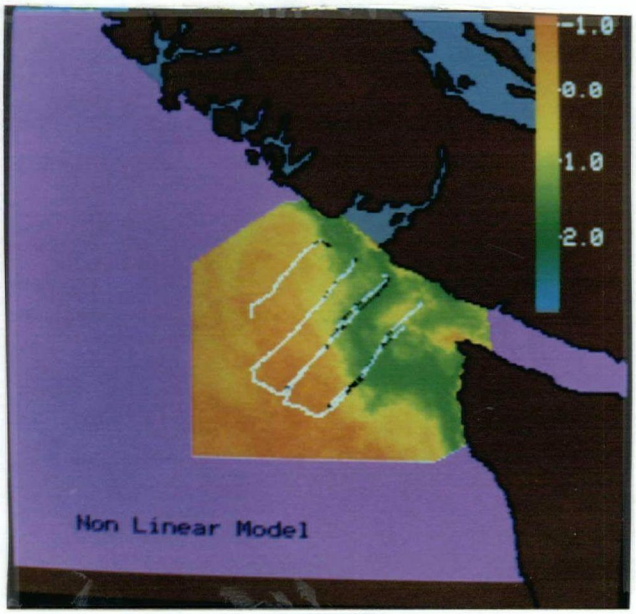

Figure 4.25: 'Plankton' image of summer $\log_e$ chlorophyll concentrations constructed from the non-linear regression equation. UBC8410 sampling transects are shown, coded to indicate areas where the model differed from sampled concentration by more than the RMSDIF (BLACK) and by less than the RMSDIF (WHITE). The pink mask denotes areas outside the study area.

the inside edge of the eddy, with lower concentrations in the center. A relatively sharp gradient coinciding with the thermal front (Figure 3.9) separates this zone of high concentrations from low concentrations found in warmer, stratified water outside the upwelling region.

The spatial relationship between temperature and chlorophyll measured in this study is supported by *Abbott and Zion (1985)* using data from the upwelling region of California. These authors reported similar correlation coefficients for linear regressions relating satellite measured $\log_e$ chlorophyll concentrations to satellite temperature and showed that a non-linear model improves the predictive capability of the regression (they do not give the mathematical form of their equation). *Shannon et al. (1985)* showed that peaks in chlorophyll concentration coincided with thermal frontal zones in the South African upwelling region. Although higher concentrations coincided with cooler surface temperatures, these authors showed maximum concentrations occurred downstream of the most recently upwelled water. Upwelling along both the California and South African coasts is induced by episodic wind events. Data reported in this chapter indicate that similar spatial relationships between surface chlorophyll concentration and surface temperature occur in the topographically induced upwelling zone on the southern British Columbia coast.

Summer chlorophyll distributions shown in Figure 4.25 differ from those reported by *Mackas et al. (1980)* and *Denman et al. (1981)*. These authors showed high concentrations over the outer edge of La Perouse Bank, immediately seaward of a region of mixing over the shallow banks. Figures 4.13a and 4.25 show this region has low chlorophyll concentrations and Figure 3.25 shows it to be stratified. In addition, both surface temperature or chlorophyll distributions shown by these authors did not indicate the presence of an upwelling eddy. Highest surface salinities shown by *Mackas et al. (1980)* were associated with offshore zones of maximum temperature. This is not indicative of active upwelling. Physical processes during these studies seem to be quite different from those reported here. *Denman and Freeland (1982)* stated that the

location of the eddy was related to bottom topography. Previous studies, and the results discussed here, emphasize a close relationship between bathymetry and physical processes and the link to resultant surface distributions of biological properties on the southern British Columbia shelf. This relationship was also present during the winter. Data presented here shows that the ability of satellite images to monitor these physical processes has important implications for the monitoring and mapping of resultant biological distributions. Statistical relationships between the spatial distribution of surface temperature and surface plankton, measured and quantified here, demonstrate both an interpolatory and a predictive role for infrared imagery when used in conjunction with concurrent in-situ sampling.

Chapter 5

ZOOPLANKTON COMMUNITY ZONATION

Mackas and Sefton (1982) suggest that summer spatial patterns of zooplankton community composition on the B.C. continental shelf reflect the general physical circulation and bathymetry. If such is the case, a more detailed analysis of relationships between community composition and hydrography is warranted. Synoptic maps of sea surface temperature derived from satellite images might provide both spatial and temporal information about the continental shelf community pattern.

This chapter examines relationships between the zooplankton community composition and the surface thermal regime of the B.C. continental shelf. The hypothesis is that in both winter and summer, satellite images of sea surface temperature reflect patterns of zooplankton community composition. Specific objectives are

1. to determine if winter and summer stations similar in zooplankton community characteristics form unambiguous patterns in geographic space,
2. to compare patterns of zooplankton community composition with patterns of circulation and hydrography described in Chapter 3,
3. to determine the extent to which patterns of zooplankton community composition are associated with satellite measured surface thermal patterns, and
4. to examine taxonomic differences in the identified communities and relate

them to the source of the water with which they are associated.

5.1 Data Preparation

The positions and names of stations sampled during the winter and summer cruises are shown in Figure 5.1a and b. The field sampling procedure is described in Chapter 2. Satellite data concurrent with zooplankton sample collection were reduced to a single image for each cruise representing the mean sea surface temperature at each pixel. Winter sampling took place over a 60 hour period during which 8 images were recorded. Sea surface temperature data used here are the mean of these 8 images. Summer sampling took place over a 48 hour period. The mean image presented here was calculated from the 4 images closest in time to this period (see Figure 2.1).

Previous statistical analysis of the zooplankton community in the study area using a detailed taxonomic enumeration (38 taxonomic categories, *Mackas and Sefton 1982*) showed that approximately 95% of the between station covariance structure would be preserved using only 10 to 12 categories. For the winter samples, a set of 15 taxonomic categories were chosen, identified and enumerated. A set of 17 taxonomic categories were enumerated from the summer samples. *Stone (1980)* and *Gardner (1982)* identify specific copepod taxa which are indicative of the large scale circulation off the B.C. west coast. *Mackas and Sefton (1982)* identify those taxa which form dominant members of the plankton community. Taxonomic categories for this study were chosen on the basis of potential value as an indicator species, numerical dominance within the sample, ease and accuracy of identification and suspected importance to the overall plankton ecology of the shelf. The level of taxonomic identification varied between categories. Copepods were both keyed to species (the last 3 developmental stages were counted) and also grouped into more general headings. Other less numerous but ecologically important invertebrates were also combined under general headings. Tables 5.1 and 5.2 list the taxonomic categories enumerated from the winter and summer samples respectively. For the numerically rare taxonomic categories (< 100 individuals in a sample), the

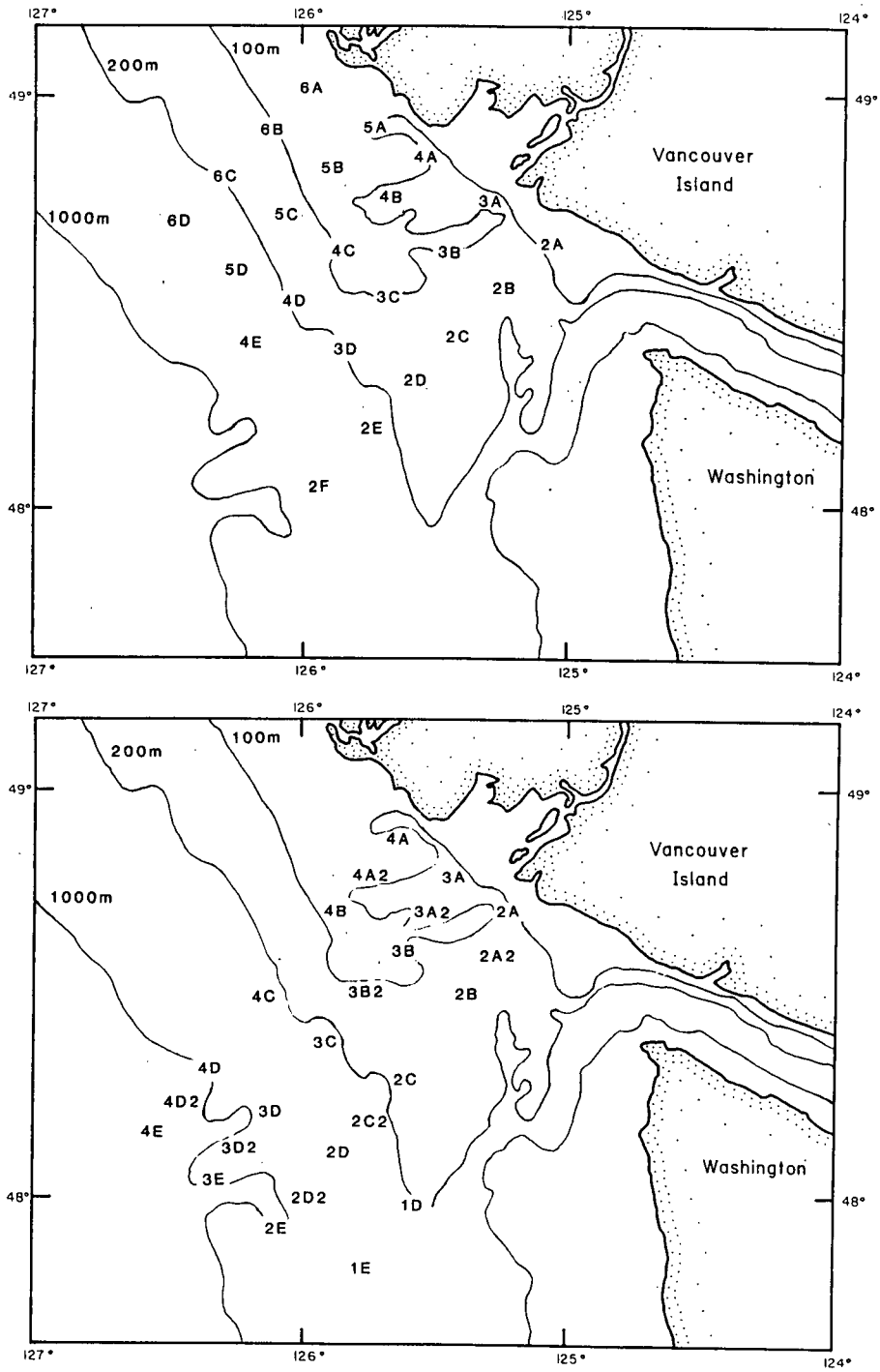

Figure 5.1: Locations and names of a) winter and b) summer stations sampled for community analysis.

Taxonomic category	Abbreviation
Total chaetognaths	CH
Total Small Copepods (< 2mm)	SC
Total Large Copepods (> 2mm)	LC
Total euphausiids	EUP
Tomopteris spp.	TOM
Metridia pacifica	Mp
Corycaeus anglicus	Ca
Euchaeta elongata	Ee
Eucalanus bungii	Eb
Heterorhabdus tanneri	Ht
Candacia bipinnata	Cb
Rhincalanus nasutus	Rn
Gaetanus intermedius	Gi
Euchirella curticauda	Ec
Epilabidocera longipeda	El

Table 5.1: Winter taxonomic categories enumerated.

entire sample was counted. To enumerate the more abundant categories, samples were sequentially split with a Folsom plankton splitter until the number of individuals was less than 300. The species enumeration data from both cruises is stored on the same magnetic tape as the four variable surface data (as stated in Chapter 3). This tape is stored at the U.B.C. Satellite Oceanography Laboratory.

During both winter and summer, a proportion of the enumerated categories were completely absent at some stations. A second data matrix for each cruise was created using those taxonomic categories which were missing entirely from any of the stations during a cruise. These categories were recombined into a presence/absence format and the resultant binary data matrices also used for community analysis. Taxonomic categories missing from more than 75% of the stations within a cruise were deleted from the original data matrices. This provided two data sets (there remained some overlap) with which to approach the objectives; one, bias towards more ubiquitous shelf taxa, and a second, bias towards spatially rarer or more patchy taxa. I distinguish here

Taxonomic category	Abbreviation
Total chaetognaths	CH
Total Small Copepods (< 2mm)	SC
Total Large Copepods (> 2mm)	LC
Total euphausiids	EUP
Total amphipods	AMP
Tomopteris spp.	TOM
Metridia pacifica	Mp
Euchaeta elongata	Ej
Eucalanus bungii	Eb
Heterorhabdus tanneri	Ht
Gaidius minutus	Gm
Calanus pacificus	Cp
Epilabidocera longipeda	El
Candacia bipinnata	Cb
Lucicutia ovalis	Lo
Neocalanus cristatus	Nc
Neocalanus plumchrus	Np

Table 5.2: Summer taxonomic categories enumerated.

between numerical rarity (biomass differences), which will be discussed below and rarity of occurence, which has no numerical connotations but implies patterns of distribution as might be expected of an indicator species.

Relationships between stations were determined by multivariate cluster analysis of the taxonomic composition of stations sampled during each cruise. This classification technique groups stations into clusters based on some measure of between-site correlation or similarity measured as a distance in multi-dimensional species space. Spatial patterns of zooplankton community composition were then identified as patterns formed in geographic space by stations classified as being close in species space.

Matrices defining between-station resemblances based on presence/absence characteristics for both cruises were calculated directly from the binary data. Resemblance was measured as a distance defined as

$$c(i,j) = \sqrt{2(1 - \cos \alpha_{i,j})}$$

where $\cos \alpha_{i,j}$ is the cosine separation of the two binary element station vectors i and j given by

$$\cos \alpha_{i,j} = \frac{a}{\sqrt{(a+b)(a+c)}}$$

and a, b, and c are the first three elements of a 2×2 contingency table defining the two stations *(Orloci 1978)*.

Classification of stations using the more ubiquitous taxonomic categories was based on between-station resemblance measured as a Euclidean distance in multi-dimensional species space. This is defined, for any two stations j and k as

$$e(j,k) = \sqrt{\sum_{h=1}^{t} (x_{hj} - x_{hk})^2}$$

where x is the count of taxonomic category h at the two stations and summation is over all species t being analysed *(Orloci 1978)*. To prevent domination of the resultant Euclidean distance by the numerically more abundant taxonomic categories, numbers per sample in the original data matrices were first normalized to relative frequency.

The necessity of this normalization was exacerbated by the use of such wide taxonomic categories as 'Total Small Copepods' in addition to actual species counts (see Tables 5.1 and 5.2). The number of each taxonomic category at each station was redefined as a relative frequency by

$$F(h,k) = \frac{x_{h,k}}{\sum_{k=1}^{n} x_h}$$

where x is the count of taxonomic category h at station k and summation is over all stations n. This normalization gives each axis defining a multi-dimensional hypervolume in species space an equal length (=1.0).

Each station vector has both a directional component, determined by the ratios of species frequencies, and a length component, determined (after the previously given normalization) by the magnitude of frequencies among those species present. Stations with identical species compositional ratios will actually be separated in multi-dimensional species space by differing magnitudes of relative frequency. In order to classify stations solely on the basis of relative species composition, the effect of differing magnitudes of relative frequency was removed from each station vector by normalizing such that

$$\sum_{h=1}^{t} F_k^2 = 1.0$$

where summation is over all species at station k. This maps each station vector onto a hyperspherical surface of radius 1.0, and the Euclidean distance between any two stations becomes a 'chord length' between two points on this surface. In practice, the matrix of between-station chord lengths was calculated directly from the frequency-normalized matrix by

$$c(j,k) = [2(1 - q_{jk}/\sqrt{q_{jj} \cdot q_{kk}})]^{1/2}$$

where $q_{jk} = \sum F_{hj}F_{hk}$, $q_{jj} = \sum F_{hj}^2$, $q_{kk} = \sum F_{hk}^2$ and summation is over all species h for two stations j and k *(Orloci 1978)*.

It is useful to discuss the effects of these data transformations to the raw data counts in less geometric terms. The frequency normalization weights each taxonomic category

equally in its potential contribution to the angular separation of station vectors defined in species space. This places increased weight or emphasis on the numerically less abundant categories and also on those categories with a more patchy distribution. The exclusion of spatially rare categories from this data matrix ensured that this emphasis did not unduly bias the contribution of such ecologically important categories as Total Small Copepods. The second transformation obviated the need to normalize the raw species counts by the volume of water filtered by each sample. This normalization means that stations with similar relative species compositional ratios will be interpreted as being close in species space, regardless of the actual magnitude of their relative frequencies.

The matrices of between-station resemblance were used as input to a complete linkage, agglomerative, hierarchic clustering algorithm. This algorithm forms groups or clusters by sequentially joining stations which are closest in species space. Distances between multi-station clusters are defined by the maximum of all possible pair-wise distances between members of one cluster and the other. While other, more complex algorithms exist, this one was chosen for its ease of implementation and its ability to form tight and separate initial clusters of most closely related stations. A potential disadvantage of the algorithm is the possibility of forming loose clusters, late in the hierarchy, with members whose main resemblance to one another is their non-association with the initial tighter clusters *(Pielou 1977)*. This disadvantage is suppressed, however, by avoiding over-interpretation of the details of inter-cluster distances for late formed clusters.

5.2 Community Identification and Description

Multivariate classifications of the stations sampled during winter and summer are presented as dendrograms showing between-cluster distance (Figures 5.2a and b and 5.3a and b). The dendrograms show that clusters formed by both the binary and frequency normalized data matrices are similar in station composition for both the winter

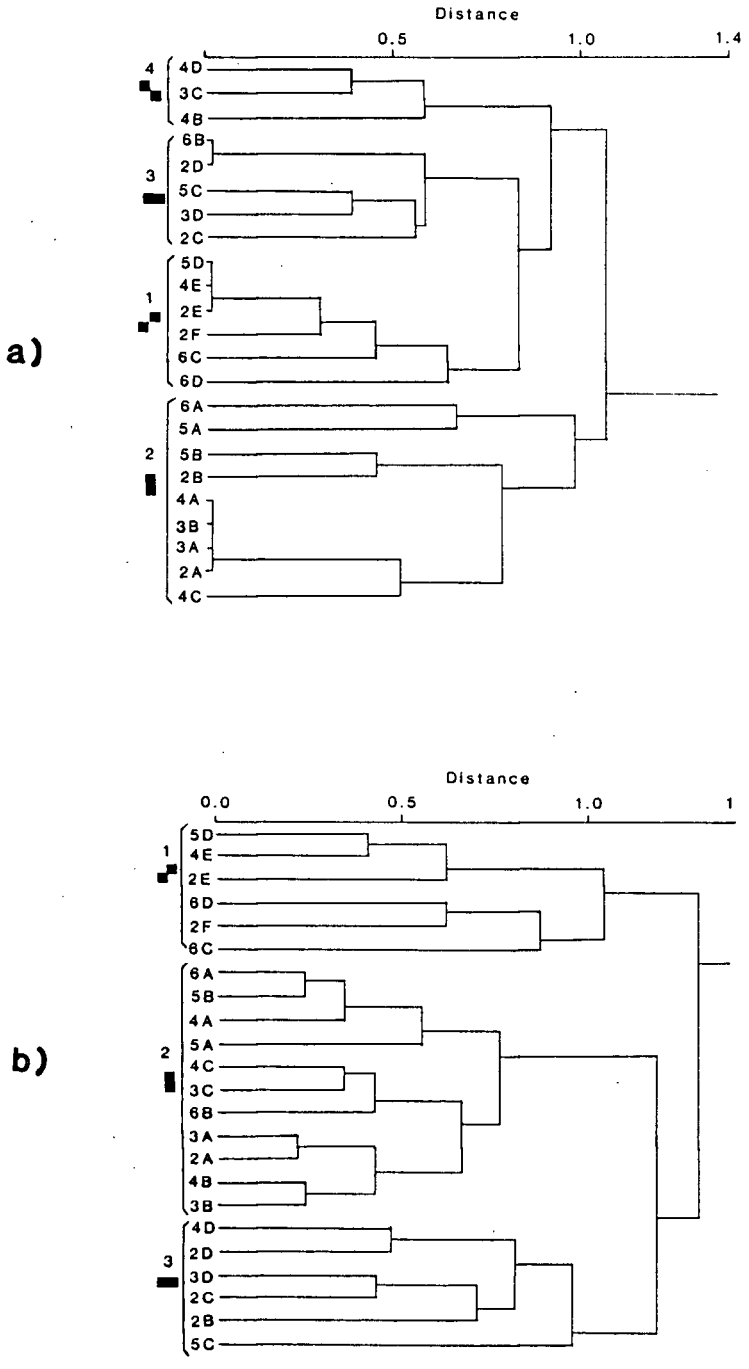

Figure 5.2: Dendrograms of winter station classification showing cluster similarity for a) the binary data and b) the frequency normalized data. Brackets indicate the interpreted dominant cluster groups and associated symbols will be used to show the spatial position of these clusters.

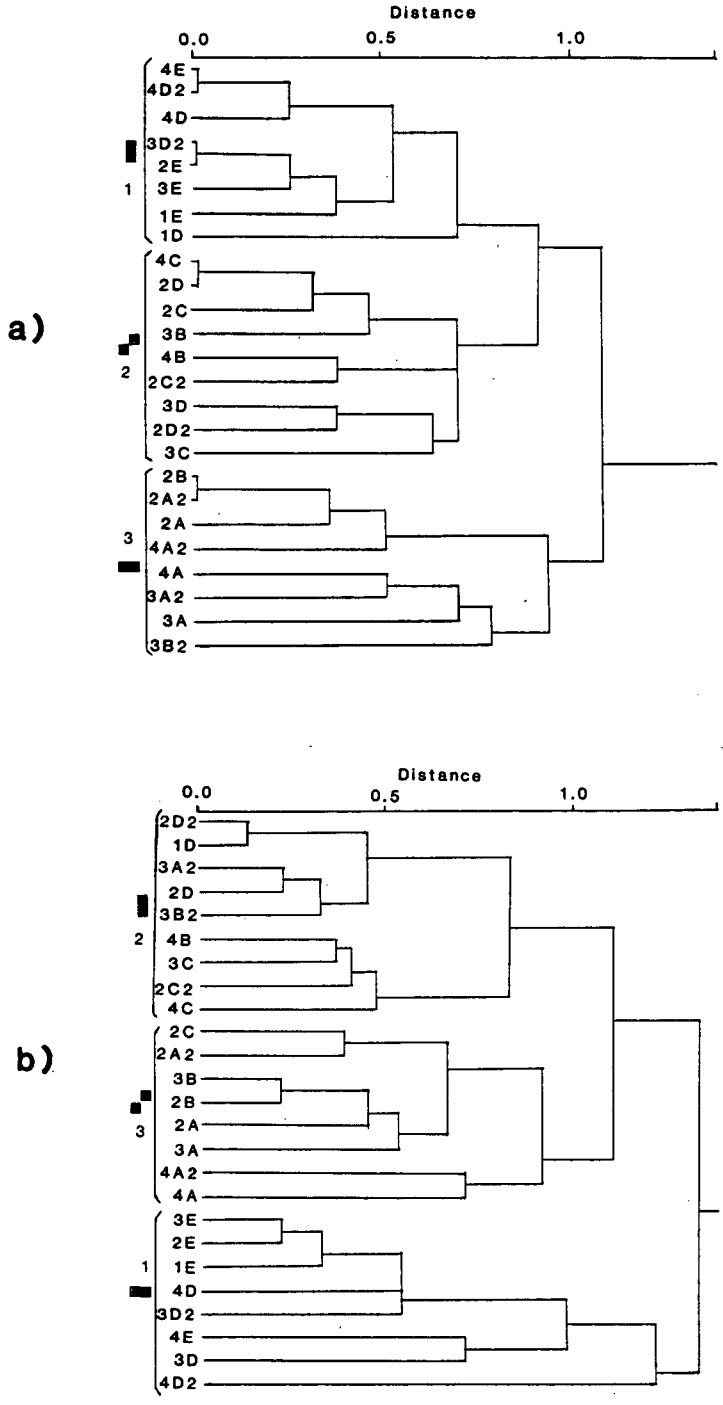

Figure 5.3: Dendrograms of summer station classification showing cluster similarity for a) the binary data and b) the frequency normalized data. Brackets indicate the interpreted dominant cluster groups and associated symbols will be used to show the spatial position of these clusters.

and summer cruises. This indicates a relatively stable zooplankton community pattern with regard to both the relative dominance among ubiquitous taxonomic groups and the occurrence of spatially rarer groups.

The spatial distribution of stations making up these clusters (Figures 5.1a and b) shows that stations closely related by community characteristics are also close in geographic space. This indicates first, that the taxonomic groups used for cluster analysis were effective in identifying community composition, and second that the spatial separation of sampling sites was small enough to resolve horizontal patchiness in both winter and summer zooplankton community composition.

Geographic positioning of the winter stations (Figure 5.1a) shows that Cluster 1 from both analyses represents an outer shelf zooplankton community. Taxonomic characteristics of these stations, based on the binary data are shown in Table 5.3. This cluster has the highest winter relative diversity, with all enumerated taxonomic groups represented. In addition, *Euchaeta elongata*, *Eucalanus bungii*, *Tomopteris spp.* and *Euchirella curticauda* were present at every station within the cluster. The term diversity should be interpreted with caution. It need not reflect the true diversity of the zooplankton community at these stations. Diversity is used here in relation to the enumerated taxonomic groups and the number of stations at which they are present and is relative to other clusters only.

Taxonomic characteristics of clusters formed from frequency normalized data are summarized in Table 5.4 as the mean taxonomic group frequency vector for each cluster. These characteristics are necessarily qualitative as the normalization procedures allow the clustering algorithm to classify only by the relative proportions of each taxonomic group. These data show that Cluster 1 from the outer-shelf had the highest proportion of most of the taxonomic groups enumerated but the lowest proportion of *Candacia bipinnata* and *Corycaeus anglicus*.

Cluster 2 from both winter analyses is made up of stations from the inner shelf (Figure 5.1a). The frequency data dendrogram (Figure 5.2b) includes more stations

	Station	Ee	Eb	TOM	Ec	Ht	Gi	Rn	El
Cluster 1	2E	1	1	1	1	1	1	0	0
	2F	1	1	1	1	1	1	1	0
	4E	1	1	1	1	1	1	0	0
	5D	1	1	1	1	1	1	0	0
	6C	1	1	1	1	1	0	0	0
	6D	1	1	1	1	0	1	1	1
Cluster 2	2A	0	1	0	0	0	0	0	0
	2B	0	1	0	1	0	0	0	1
	3A	0	1	0	0	0	0	0	0
	3B	0	1	0	0	0	0	0	0
	4A	0	1	0	0	0	0	0	0
	4C	0	1	0	0	0	0	1	0
	5A	0	0	0	0	1	0	0	0
	5B	0	1	0	0	0	0	0	1
	6A	0	0	0	0	0	0	0	0
Cluster 3	2C	0	1	1	0	1	0	1	0
	2D	0	1	1	0	0	0	0	0
	3D	0	1	1	0	1	0	0	1
	5C	0	1	1	0	1	0	0	0
	6B	0	1	1	0	0	0	0	0
Cluster 4	3C	0	1	1	0	0	0	1	0
	4B	0	0	1	0	0	0	1	0
	4D	1	1	1	0	0	0	1	0

Table 5.3: Winter station binary data, grouped by cluster membership. Species abbreviations show presence (1) or absence (0).

	CH	SC	LC	Mp	Ca	EUP	El	Eb	TOM	Ec	Ht	Cb	Gi
Cluster 1	.033	.049	.051	.102	.011	.071	.159	.115	.141	.160	.146	.027	.164
Cluster 2	.052	.042	.044	.021	.075	.021	.001	.011	.003	.000	.002	.038	.000
Cluster 3	.038	.041	.035	.026	.018	.056	.007	.033	.022	.007	.016	.070	.003

Table 5.4: Winter mean frequency vector for each cluster showing the component along each species axis.

in this cluster than the binary data dendrogram (Figure 5.2a). This cluster has the lowest relative diversity (Table 5.3) with *E.elongata, Tomopteris spp.*, and *Gaetanus intermedius* absent at all stations. With the exception of *E.bungii*, which is present at most stations in all clusters, the rest of the taxonomic groups are present in Cluster 2 at only one station each. The mean frequency vector (Table 5.4) shows Cluster 2 stations had the highest proportions of chaetognaths and *C.anglicus* but the lowest proportions of most other taxonomic groups.

Geographic positions of the remaining winter stations indicate a mid-shelf community separating the inner-shelf and the outer-shelf communities. The binary data dendrogram (Figure 5.2a) classifies these stations into two clusters (Clusters 3 and 4), with both more closely related to the outer-shelf community (Cluster 1) than the inner-shelf community (Cluster 2). Table 5.3 shows that Clusters 3 and 4 have an intermediate relative diversity with *E. curticauda* and *G.intermedius* missing entirely from both. The frequency dendrogram (Figure 5.2b) classifies the mid-shelf stations as a single cluster (Cluster 3) more closely related to the inner-shelf than the outer-shelf community in terms of the more ubiquitous taxonomic categories. The mean frequency vector of these stations (Table 5.4) shows characteristics intermediate between that of Cluster 1 and Cluster 2. Cluster 3 has the highest proportion of *C. bipinnata* but relatively low proportions of most other taxonomic groups.

A test was made to determine how robust cluster membership was when formed by a different clustering algorithm. The winter frequency normalized data matrix of between-station similarity (euclidean distance) was clustered using a single linkage, agglomerative, hierarchic algorithm. Distances between already-formed clusters and other stations or clusters are redefined as the *minimum* of all possible pair-wise distances between members of the first cluster and the new station or cluster. This algorithm has the opposite tendency of the complete linkage algorithm. It tends to accrete stations onto previously formed clusters, even if these clusters are quite diffuse in species space, rather than form new and distinct clusters, as the complete linkage does.

Single linkage station membership in Cluster 1, an outer-shelf community, and Cluster 2, an inner-shelf community was identical to that of the complete linkage. Four of the remaining six stations were joined as pairs, and then each of these was accreted to the already formed inner-shelf community. These last six stations were those over the middle shelf which had formed a separate and distinct community in the complete linkage analysis. The similarity of the results of these two algorithms implies that communities identified by the dendrograms in Figures 5.2 and 5.3 are realistic interpretations of station relationships and community membership. Results from these two figures are not unduly bias by artifacts of the clustering algorithm.

The summer distribution of station cluster membership (Figure 5.1b and 5.3a and b) shows a similar cross-shelf trend to that seen during the winter. Both the binary and the frequency dendrograms identify an outer shelf community (Cluster 1). Binary taxonomic characteristics of this cluster (Table 5.5) show it to have the highest relative diversity, with all taxonomic groups represented. The mean frequency vector (Table 5.6) for stations in Cluster 1 shows a low relative proportion of euphausiids, chaetognaths, *Calanus pacificus*, and total Small Copepods but the highest relative proportion of amphipods, *E. bungii*, and *Metridia pacifica*.

Cluster 2 of both summer dendrograms is a mid-shelf community. These stations have an intermediate relative diversity (Table 5.5) with four taxonomic groups missing entirely. The mean frequency vector for this cluster (Table 5.6) shows these stations to have the highest proportions of euphausiids, chaetognaths, *Calanus pacificus* and total Large Copepods and the lowest proportions of *E.bungii*.

The remaining summer stations form a cluster (Cluster 3) representing an inner-shelf coastal community (Figure 5.1b) extending furthest offshore in the southern portion of the study area. The binary data matrix shows this community to have the lowest relative diversity (Table 5.5) with six of the eleven taxonomic groups absent entirely. The mean frequency vector (Table 5.6) for this cluster indicates a community characterized by the lowest proportion of total Large Copepods and amphipods and

	Station	TOM	Nc	Np	Ee	Mp	El	Ht	Gm	Cb	Lo	AMP
Cluster 1	1D	0	1	0	0	1	0	1	0	0	0	1
	1E	0	1	1	1	1	1	1	0	0	1	1
	2E	1	1	1	1	1	1	1	0	0	1	1
	3D2	1	1	1	1	1	1	1	0	0	1	1
	3E	1	1	1	1	1	1	1	0	1	1	1
	4D	1	1	1	1	1	0	1	0	1	1	1
	4D2	1	1	1	1	1	0	1	1	1	1	1
	4E	1	1	1	1	1	0	1	1	1	1	1
Cluster 2	2C	0	1	1	1	1	1	0	0	0	0	1
	2C2	0	1	0	0	1	1	0	0	0	0	1
	2D	0	1	1	0	1	1	0	0	0	0	1
	2D2	0	1	1	0	1	0	0	0	0	0	1
	3B	0	1	1	0	0	1	0	0	0	0	1
	3C	1	0	1	0	1	1	0	0	0	0	1
	3D	0	0	1	0	1	0	0	0	0	0	1
	4B	0	0	0	0	1	1	0	0	0	0	1
	4C	0	1	1	0	1	1	0	0	0	0	1
Cluster 3	2A	0	0	1	1	1	1	0	0	0	0	0
	2A2	0	1	1	1	1	1	0	0	0	0	0
	2B	0	1	1	1	1	1	0	0	0	0	0
	3A	0	1	0	0	0	1	0	0	0	0	0
	3A2	0	0	1	0	0	1	0	0	0	0	0
	3B2	0	0	0	0	1	0	0	0	0	0	0
	4A	0	0	0	0	1	1	0	0	0	0	0
	4A2	0	0	0	1	1	1	0	0	0	0	0

Table 5.5: Summer station binary data, grouped by cluster membership. Species abbreviations show presence (1) or absence (0).

	EUP	AMP	CH	LC	SC	Eb	Cp	Mp
Cluster 1	.015	.095	.030	.030	.023	.093	.015	.110
Cluster 2	.064	.021	.058	.070	.048	.011	.083	.007
Cluster 3	.038	.006	.030	.017	.048	.020	.017	.008

Table 5.6: Summer mean frequency vector for each cluster showing the component along each species axis.

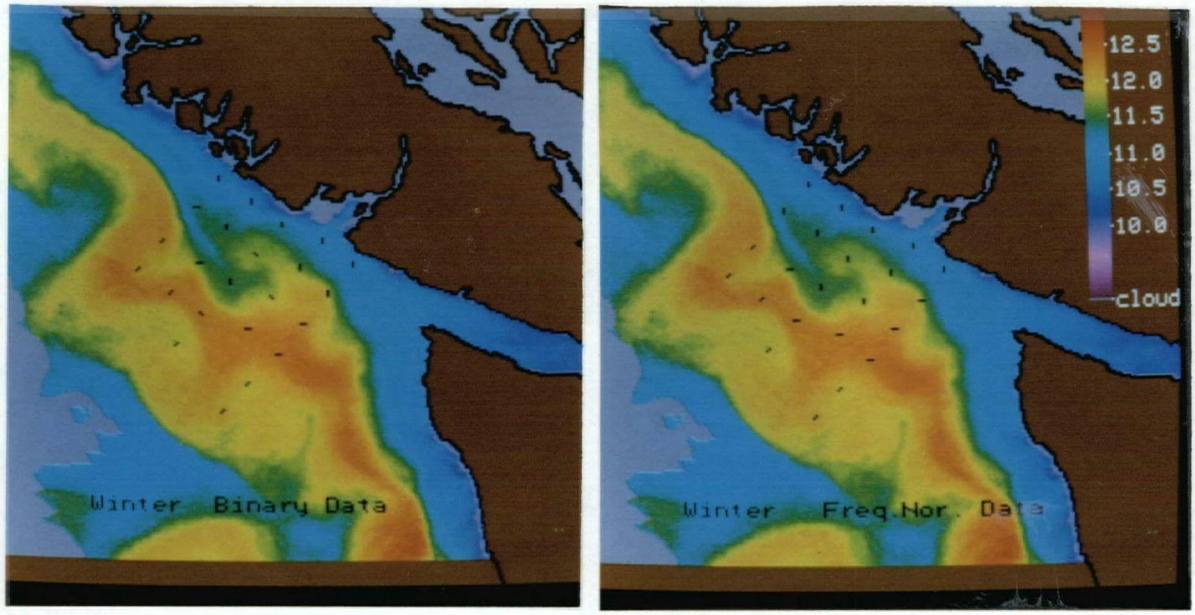

Figure 5.4: Winter mean satellite image showing the location and classification of winter stations according to a) the binary data and b) the frequency normalized data. The four communities identified by the winter binary data dendrogram and the three communities indentified by the frequency normalized dendrogram are indicated by the symbols shown in the dendrograms.

the highest proportion of total Small Copepods.

5.3 Community Relationship with Surface Temperature

A strong similarity between the spatial distribution of zooplankton community composition and satellite measured patterns of sea surface temperature, is evident during both winter and summer over shallower regions of the B.C. continental shelf (Figures 5.4a and b and 5.5a and b). In both seasons, communities associated with warmer water over the middle and outer portions of the shelf are different from communities present in colder water over the inner shelf. This indicates that patterns of community composition identified in this chapter are related to the hydrographic zonation and patterns of shelf circulation suggested in Chapter 3. The satellite data show, however, that the

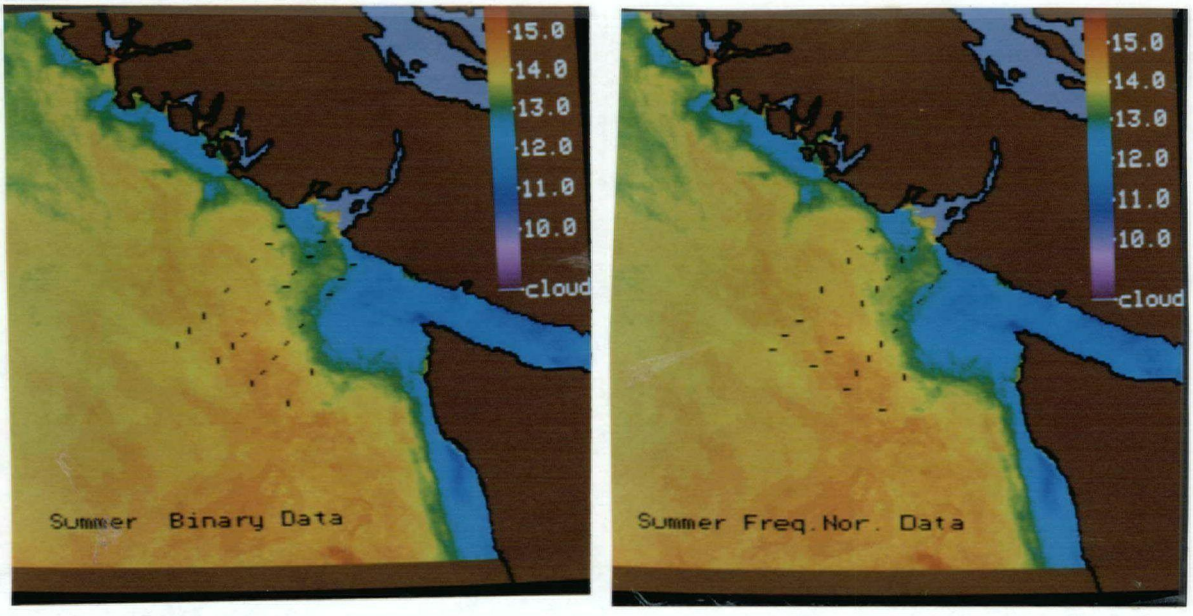

Figure 5.5: Summer mean satellite image showing the location and classification of summer stations according to a) the binary data and b) the frequency normalized data. The three communities identified by the summer binary data dendrogram and the frequency normalized dendrogram are indicated by the symbols shown in the dendrograms.

zooplankton community over the outer shelf is not well correlated with any single or identifiable thermal feature during either season.

The winter satellite image (Figure 5.4a and b) shows the inner-shelf zooplankton community (Cluster 2) to be associated with colder Vancouver Island Coastal Current water. Cluster analysis indicates that the frontal zone separating this water from warmer Davidson Current water over the middle and outer shelf is also a community boundary. Satellite images monitoring the position of this front (Figure 3.3) therefore identify the boundary between a winter coastal zooplankton community and a more oceanic zooplankton community. Community spatial patterns derived from both winter data matrices show that colder, coastal water extending offshore over La Perouse Bank retains a coastal type zooplankton community (Figure 5.4a and b). These figures show that the cross-shelf penetration of warmer Davidson Current water immediately south of La Perouse Bank is associated with a mid-shelf zooplankton community. The binary data (Figure 5.4a) divides this mid-shelf community into two groups. Cluster 4 is located around the outside edge of the cold tongue overlying La Perouse Bank. Cluster 3 is associated with warm water of the Davidson Current in the southern portion of the study area but is also present inshore of the major frontal zone at Leg 6, north of La Perouse Bank (Station 6B, Figures 5.1a and 5.4a). An explanation of this ambiguity is the lack of synopticity of the mean image shown in Figure 5.4. Warm water inshore of this frontal zone (extending north, inshore of the shallow bank) was more developed in individual images more concurrent with the actual sampling of this station. The mean image only weakly suggests this warmer extension. The suggested intrusion of Davidson Current water into near-shore deeper areas inshore of La Perouse Bank (Chapter 3) is supported by the presense of a mid-shelf community in the warmer water of this region at Station 4B (Figure 5.4a).

Winter zooplankton community boundaries on the outer shelf do not correspond to surface thermal patterns. The outer-shelf community (Cluster 1) occurs in both the main core of Davidson Current water, and in cooler, more stratified North Pacific

water to seaward (Figure 5.4a and b). This community shows a stronger association with bathymetry, generally located seaward of the 200 m depth contour (Figure 5.1a). These deeper stations will support both deeper living species and species whose life history pattern includes a deep vertical migration. Table 5.4 shows Cluster 1 has the highest proportions of euphausiids and *M.pacifica*, both known to be strong diel migrators. These stations also have the highest proportion of *E.bungii*, an ontogenetic migrator, which *Krause and Lewis (1979)* and *Lewis and Thomas (1986)* have shown to overwinter at depths greater than 100 m in B.C. coastal waters. The data indicate that the increased success of species such as these has a greater effect on patterns of community composition over the outer shelf than surface temperature patterns and hydrography.

Comparison of summer sea surface temperature patterns and zooplankton community composition (Figure 5.5a and b) reveals a distinct community associated with colder surface water of the inner shelf, and two communities associated with warmer water over the middle and outer shelf. The satellite images show that Cluster 3 occurs primarily in colder water identified as an upwelling zone in Chapter 3. This cluster most likely represents a community adapted to a coastal upwelling environment. The outer-shelf cluster (Cluster 1) is associated with warm and stratified offshore water (Figure 5.5a and b) and probably represents a community of oceanic origin. Stations between the upwelling region and the outer-shelf community represent a mid-shelf zooplankton community (Cluster 2) of intermediate taxonomic characteristics. This community occupies the shear zone between southward moving California Current System water along the outer shelf and northward moving Vancouver Island Coastal Current water along the inner shelf *(Hickey et al. in prep.)*. The cross-shelf pattern of this community reflects the cyclonic nature of shelf circulation in the vicinity of the eddy (Chapter 3). The community is stretched in a southerly direction across the shelf and around the cold water induced by upwelling within the eddy (Figure 5.5a and b). Satellite image derived motion vectors and in-situ buoy tracks *(Emery et al. 1986)* show this

to be the principal direction of summer surface advection on the shelf in the vicinity of the eddy.

The summer outer-shelf community pattern is not associated with any visible thermal feature in the satellite imagery (Figure 5.5a and b). Similarly, subsurface temperature profiles (Chapter 3) do not not show any discontinuity coincident with the community boundary between Clusters 1 and 2. While a discontinuity is known to exist in the current structure in this vicinity *(Freeland et al. 1984; Hickey et al. in prep)*, these data suggest that the community boundary might also be a result of increased depth and the coincident change in species distribution as seen in the winter data. The community pattern does show an association with the $200m$ contour (Figure 5.1b).

The association of winter and summer zooplankton communities with satellite measured sea surface temperature and depth was tested by analysis of variance. For each season, mean surface temperatures and depths associated with the zooplankton communities identified by both data matrices were significantly different (Table 5.7). A multiple comparison test (Scheffe's, from *Pollard, (1977)*) of the winter surface temperature means showed the inner-shelf community (Cluster 2) to be significantly colder than stations making up the more oceanic communities. Clusters 1 and 3, representing the outer and mid-shelf communities respectively, could not be distinguished on the basis of temperature. Multiple comparison of the mean depths, however, showed the outer-shelf community (Cluster 1) to be significantly different from the two communities closer to shore (Clusters 2 and 3), which were indistinguishable. Multiple comparison tests of the temperature and depth means for the summer communities showed similar relationships. The upwelling zone community (Cluster 3) had a significantly lower temperature than either of the more oceanic communities (Clusters 1 and 2), which were not significantly different. The mean depth occupied by the outer-shelf community was significantly different and greater than that of the two communities closer to shore, both of which, again, were not significantly different.

The association between patterns of sea surface temperature and spatial patterns

Winter Communities

Clustering	Variable tested	F(d.f.)	MCT
Freq. N.	SST	23.61(2,20)*	1-3, 2
Freq. N.	Depth	21.83(2,20)*	1, 2-3
Binary	SST	10.03(3,19)*	1-4-3, 2
Binary	Depth	13.95(3,19)*	1, 2-3-4

Summer Communities

Clustering	Variable tested	F(d.f.)	MCT
Freq. N.	SST	19.11(2,22)*	1-2, 3
Freq. N.	Depth	6.62(2,22)*	1, 2-3
Binary	SST	25.13(2,22)*	1-2, 3
Binary	Depth	6.14(2,22)*	1, 2-3

Table 5.7: Analysis of Variance results; SST is sea surface temperature, MCT indicates significantly different cluster means according to Scheffe's Multiple Comparison Test, d.f. are the degrees of freedom in the analysis of variance, and * indicates significance at the 0.95% level.

off community composition support *Mackas and Sefton's (1982)* contention that advection is primarily responsible for determining patterns of shelf zooplankton composition. Figures 5.4a and b show that this conclusion is also applicable to the winter shelf. The correlation of zooplankton community composition with temperature and salinity gradients normal to the coastline on the Scotia Shelf demonstrated a similar functional link between hydrographic processes and species distributions (*Tremblay and Roff 1983*). *Boucher et al. (1987)* use principal component analysis to show an association of surface zooplankton community composition with shelf and shelfbreak physical structure in the northern Mediterranean Sea. There is a contrast in the spatial scales of zooplankton community variability resolved by *Boucher et al. (1987)* ($\approx$ 4km after smoothing) and scales resolved by stations in Figure 5.1a and b ($\approx$ 20km). The detailed vertical hydrographic data presented by these authors illustrates the relationship between subsurface physical processes, surface structure, and the resultant zooplankton community patterns, consistent with relationships presented here. These data contrast with the results reported by *Star and Mullin (1981)* which indicated that patchiness of individual taxa in the North Pacific and California Current were not correlated with temperature and were most likely a result of intrinsic biological processes. This difference most likely illustrates the difference between an ecosystem primarily influenced by physical advective and mixing processes, and a more stable offshore ecosystem where biological processes become more important.

Although inferred from a limited taxonomic list, the relative diversity of the shelf communities reflects accepted biogeographical principles of community ecology. Community diversity in colder temperate waters will be lower than that of water of subtropical origin. Diversity in older, climax communities of physically stable regions is greater than that of younger communities in more physically dynamic areas *(McGowan 1977; Star and Mullin 1981)*. During both seasons, clusters forming near-shore communities had the lowest relative diversities. Figures 5.4 and 5.5 show these communities are associated with coldest water on the shelf. Outer-shelf communities in warmer water

of more oceanic origin had the highest diversities. In winter, the cold, inner-shelf Vancouver Island Coastal Current is of local (temperate) origin while the warmer Davidson Current water over the middle and outer shelf has a subtropical origin off the coast of California. Colder inner-shelf regions in summer were associated with localized coastal upwelling. Highly dynamic upwelling regions usually support a zooplankton community of relatively low diversity, composed of species adapted to exploit the widely fluctuating hydrographic conditions and food availabilities. Stratified water over the outer shelf originates in the North Pacific gyre which *McGowan (1977)* and *McGowan and Walker (1979)* describe as a geologically old ecosystem where community composition is determined predominantly by biological interactions rather than physical mixing or advective processes.

Taxonomic composition of the communities provides biological evidence of both the circulation patterns inferred from satellite and in-situ data in Chapter 3 and the origins of the principal hydrographic regimes on the shelf. *Corycaeus anglicus* is a common neritic species in British Columbian waters reaching high densities in estuarine conditions *(Lewis and Thomas 1986, Legare 1957).* The highest relative proportion of this species (Table 5.4) is in the near-shore community (Cluster 2) and associated with colder water (Figure 5.4b and Table 5.7) which has a strong estuarine influence (Chapter 3). Other winter communities are associated with warmer water of oceanic origin and have a lower proportion of this species. *Stone (1980)* and *Gardner (1982)* have shown that water of subtropical origin in B.C. coastal regions is associated with immigrant equatorial copepod species. These authors show that *C.bipinnata* is primarily associated with subtropical water and is evidence of equatorial water being advected north and onto the British Columbian shelf. The winter data (Table 5.4) show this species to be most common in Cluster 3. This mid-shelf community is associated with the warm core of Davidson Current water in the satellite image (Figure 5.4b). Summer data (Table 5.5) show that this species is only found at stations on the outer shelf in warmer water of oceanic origin (Figure 5.5a), and was never found in cooler, inner-shelf stations. Simi-

larly, *E.curticauda* is a oceanic, southerly species associated with northward intrusions of subtropical water *(Stone 1980)*. Winter data (Tables 5.3 and 5.4) shows this species to be present only in the community associated with warmer Davidson Current water of southern origin. It was not present in the zooplankton community of the Vancouver Island Coastal Current.

Chapter 6

CONCLUSIONS

Relationships between surface plankton distributions and physical processes on the B.C. continental shelf were strong enough to allow an interpolation of chlorophyll and zooplankton concentrations by thermal patterns visible in infrared satellite imagery. The success of these interpolations varied both in space and time, and also in their applicability to chlorophyll and zooplankton concentrations. Specific conclusions and qualifications to the general success of the interpolations are outlined below.

- The surface thermal signature of winter and summer mesoscale physical oceanographic processes on the southern British Columbia continental shelf were well defined in infrared satellite images.

- The winter shelf could be divided into four hydrographic zones on the basis of surface temperature and salinity properties. Vancouver Island Coastal Current water, Davidson Current water, the frontal zone separating these zones, and offshore North Pacific water, were each visible in the satellite imagery.

- Each winter hydrographic zone was associated with characteristic chlorophyll and zooplankton concentrations.

- Quantitative models relating winter plankton concentrations to the satellite imagery explained up to 54% of the chlorophyll variance and 49% of the $\log_e$ transformed zooplankton variance. Chlorophyll concentrations in North Pacific and

Davidson Current water were the most effectively modelled, with RMS differences between modelled and measured concentrations of 0.059 and 0.113mg $\cdot$ m^{-3} respectively. 'Plankton' images created from the means and coefficients of the models allowed a spatial representation of the surface plankton distribution and the model error.

- The association of characteristic plankton concentrations with hydrographic zones did not appear stable over time periods longer than six days, making concurrent sampling a necessity when using satellite images to monitor winter plankton distributions.

- The summer shelf could be divided into two hydrographic zones. An eddy over Juan de Fuca Canyon was associated with continuous upwelling throughout the study period and surface water remained cold. Other shelf regions were initially stratified with warm surface temperatures, but cooled rapidly during the sampling period in response to a wind event.

- Summer zooplankton concentrations did not show a consistent relationship with surface hydrographic properties but qualitative comparisons suggest that increased numbers were associated with both shallow banks and peaks in chlorophyll concentration around the eddy frontal zone.

- Relationships between summer surface chlorophyll concentrations and sea surface temperature followed previously established patterns for eastern boundary current upwelling regions. Coldest, most recently upwelled water was associated with concentrations below 6.0mg $\cdot$ m^{-3}, slightly warmer water within the upwelling region had maximum concentrations (above 12.0mg $\cdot$ m^{-3}), and warm stratified regions away from the upwelling had concentrations below 2.0mg $\cdot$ m^{-3}. Each of these regions was identifiable in the satellite imagery.

- The relationship between summer $\log_e$ transformed chlorophyll concentration and satellite temperature was quantified by a non-linear regression equation. A least-squares fit gaussian equation explained over 72% of the sampled $\log_e$ transformed chlorophyll variance. This allowed satellite images to produce realistic maps of surface chlorophyll distribution.

- Relationships between specific concentrations and thermal patterns remained stable over the 9 day summer sampling period despite dramatic changes in the sea surface temperature patterns induced by a wind event. However, the association of specific concentrations with specific temperatures changed. This implies that satellite image sequences showing changes in surface thermal pattern are as important in monitoring summer shelf chlorophyll patterns as measurements of sea surface temperature *per se*.

- Multivariate analysis of the zooplankton species distribution on the shelf revealed unambiguous spatial patterns of community composition. Over the middle and inner shelf, these patterns coincided with surface temperature zones identified in the satellite imagery. Analysis of these spatial patterns showed inner-shelf colder hydrographic zones during both seasons (Vancouver Island Coastal Current water, and upwelling water) were associated with a specific zooplankton community. Patterns over the middle shelf followed mesoscale physical features visible in the imagery and were consistent with established shelf advective fields. Patterns of community composition in water over the outer shelf seemed more closely related to bathymetry than surface temperature patterns.

Results of this research indicate that although both qualititive and quantitative relationships between hydrography, infrared satellite imagery, and biological distributions exist during both winter and summer, the form of this relationship is different. The demonstration of these relationships during the short winter and summer periods sampled in this study indicate that further data collection and analysis is warrented.

Three fundamental questions which this research raises are

1. Over how long a winter, or summer period are measured relationships valid?
2. To what extent are these seasonal relationships consistent from year to year?
3. How do the demonstrated winter and summer relationships fit into an overall seasonal pattern, specifically, transitions between the two?

The ability of satellite measured thermal patterns to explain a significant percentage of surface chlorophyll and zooplankton variance during both winter and summer indicates the value of infrared satellite images in extrapolating shelf biological distributions away from the limited spatial coverage obtainable by ships.

Chapter 7

BIBLIOGRAPHY

ABBOTT M.R. and P.M.ZION. 1985. Satellite observations of phytoplankton variability during an upwelling event. *Continental Shelf Research* 4:661-680.

ARMSTRONG F.A.J. C.R.STEARNS and J.D.H.STRICKLAND. 1967. The measurement of upwelling and subsequent biological processes by means of the Technicon Autoanalyser and associated equipment. *Deep Sea Research* 14:381-389.

ATKINSON L.P., K.H.BRINK, R.E.DAVIS, B.H.JONES, T.PALUSZKIEWICZ, and D.W.STUART. 1986. Mesoscale hydrographic variability in the vicinity of Points Conception and Arguello during April – May 1983: The OPUS 1983 experiment. *Journal of Geophysical Research* 91:12899-12918.

BOUCHER J., F.IBANEZ, and L.PRIEUR. 1987. Daily and seasonal variations in the spatial distribution of zooplankton populations in relation to the physical structure in the Ligurian Sea Front. *Journal of Marine Research* 45:133-173.

BOYD S.H., P.H.WIEBE, R.H.BACKUS, J.E.CRADDOCK and M.A.DAHER. 1986. Biomass in the micronekton in Gulf Stream ring 82-B and environs: changes with time. *Deep Sea Research* 33:1885-1905.

BREAKER L.C. 1981. The application of satellite remote sensing to west coast fisheries. Marine Technological Society Journal 15:32-40.

BRINK K.H., B.H.JONES, J.C.VAN LEER, C.N.K.MOOERS, D.W.STUART, M.R. STEVENSON, R.C. DUGDALE, and G.W.HEBURN. 1981. Physical and biological structure and variability in an upwelling center off Peru near 15°S during March 1977. In: Coastal Upwelling, F.A.Richards, (ed.), American Geophysical Union, Washington, D.C., pp. 473-495.

BROCCOLI OCEANOGRAPHIC INC. 1983. Ship of Opportunity. Report of Cruise 83-06 (November 1983), prepared by B.R.Dilke.

BROCCOLI OCEANOGRAPHIC INC. 1984. Ship of Opportunity. Report of Cruise 84-02 (July 9 to July 11, 1983), prepared by B.R.Dilke.

BROWN O.B., J.G.BRUCE, and R.H.EVANS. 1980. Evolution of sea surface temperature in the Somali Basin during the southwest monsoon of 1979. *Science* 209:595-597.

BROWN O.B., D.B.OLSEN, J.W.BROWN, and R.H.EVANS. 1983. Satellite infrared observation of the kinematics of a warm core ring. *Australian Journal Marine and Freshwater Research* 34:535-545.

CAMPBELL J.W. and W.E.ESAIAS. 1985. Spatial patterns in temperature and chlorophyll on Nantucket Shoals from airborne remote sensing data, May 7-9, 1981. *Journal of Marine Research* 43:139-161.

CASSIE R.M. 1962. Frequency distribution in the ecology of plankton and other organisms. *Journal of Animal Ecology* 31:65-92.

CHELTON D.B., P.A.BERNAL and J.A.McGOWAN. 1982. Large-scale interannual physical and biological interaction in the California Current. *Journal of Marine Research* 40:1095-1125.

COCHLAN W.P. 1986. Seasonal study of uptake and regeneration of nitrogen on the Scotian Shelf. *Continental Shelf Research* 5:555-577.

CONRAD J.W. 1980. Relationships between sea surface temperature and nutrients in satellite detected oceanic fronts. M.Sc. Thesis. Naval Postgraduate School, Monterey, California. 111p.

DENMAN K.L. 1976. Covariability of chlorophyll and temperature in the sea. *Deep Sea Research* 23:539-550.

DENMAN K.L. AND H.J.FREELAND. 1985. Correlation scales, objective mapping, and a statistical test of geostrophy over the continental shelf. *Journal of Marine Research* 43:517-539.

DENMAN K.L., D.L.MACKAS, H.J.FREELAND, M.J.AUSTIN, and S.H.HILL. 1981. Persistent upwelling and mesoscale zones of high productivity off the west coast of Vancouver Island, Canada. In: Coastal Upwelling, F.A.Richards (ed.), American Geophysical Union. Washington D.C.

DENMAN K.L. and T.PLATT. 1975. Coherences in the horizontal distribution of phytoplankton and temperature in the upper ocean. *Mem. Soc. Roy. Sci. Liege* 7:19-30.

DENMAN K.L. and T.M. POWELL. 1984. Effects of physical processes on planktonic ecosystems in the coastal ocean. *Oceanography and Marine Biology Annual Review* 22:125-168.

DESCHAMPS P.Y., R.FROUIN and L.WALD. 1981. Satellite determination of the mesoscale variability of the sea surface temperature. *Journal of Physical Oceanography* 10:961-970.

DODIMEAD A.J. and A.BALLANTYNE. 1980. Oceanographic observations during fisheries research surveys off the British Columbia Coast in 1979. Canada Data Report Fisheries and Aquatic Sciences. 210pp.

DOUGLAS M.L. and W.P.WICKETT. 1978 Temperature conditions on the shelf off Barkley Sound., Vancouver Island 1978. Canadian Fisheries Marine Survey Report 1492.

EMERY W.J. and K.HAMILTON. 1985. Atmospheric forcing of interannual variability in the northeast Pacific Ocean: connections with El Niño. *Journal of Geophysical Research* 90:857-868.

EMERY W.J. and M.IKEDA. 1983. A comparison of geometric correction methods for AVHRR imagery. *Canadian Journal of Remote Sensing* 10:46-56.

EMERY W.J. and L.A.MYSAK. 1980. Dynamical interpretation of satellite sensed thermal features off Vancouver Island. *Journal of Physical Oceanography* 10:961-970.

EMERY W.J., A.C.THOMAS, M.J.COLLINS, W.R.CRAWFORD and D.L.MACKAS. 1986. An objective method for computing advective surface velocities from sequential infrared satellite images. *Journal of Geophysical Research* 91:12856-12878.

EPPLEY R.W. and B.J.PETERSON. 1979. Particulate organic matter flux and planktonic new production in the deep ocean. *Nature* 282:677-680.

FASHAM M.J.R. and P.R.PUGH. 1976. Observations on the horizontal coherence of chlorophyll and temperature. *Deep Sea Research* 23:527-538.

FIEDLER P.C. 1984. Satellite observations of the 1982-83 El Niño along the U.S. Pacific coast. *Science* 224:1251-1254.

FOURNIER R.O., R.ERST, N.B.HARGREAVES, M.VAN DET, and D.DOUGLAS. 1984. Variability of chlorophyll *a* off southwestern Nova Scotia in late fall and its relationship to water column stability. *Canadian Journal of Fisheries and Aquatic Sciences* 41:1730-1738.

FOURNIER R.O., M.VAN DET, J.S.WILSON, and N.B.HARGREAVES. 1979. Influence of the shelf break front off Nova Scotia on phytoplankton standing stock in winter. *Journal of the Fisheries Research Board of Canada* 36:1228-1237.

FREELAND H.J. and K.L.DENMAN. 1982. A topographically controlled upwelling center off southern Vancouver Island. *Journal of Marine Research* 40:1069-1093.

FREELAND H.J., W.R.CRAWFORD, and R.E.THOMSON. 1984. Currents along the Pacific coast of Canada. *Atmosphere-Ocean* 22:151-172.

GAGLIARDINI D.A., H.KORSZENBAUM, R.LEGECKIS, and V.KLEMAS. 1984. Application of Landsat MSS, NOAA/TIROS AVHRR, and Nimbus CZCS to study the La Plata River and its interaction with the ocean. *Remote Sensing of the Environment* 15:21-36.

GARDNER G.A. 1982. Biological and hydrographical evidence for Pacific equatorial water on the continental shelf north of Vancouver Island, British Columbia. *Canadian Journal of Fisheries and Aquatic Sciences* 39:660-667.

GARVINE R.W. 1974. Dynamics of small scale oceanic fronts. *Journal of Physical Oceanography* 4:557-569.

HAGER S.W. L.I.GORDON and P.K.PARK. 1968. A practical manual for the use of Technicon Autoanalyser in seawater nutrient analysis. A final report to B.C.F. No. 14-17-0001-1759, Oct. 1968. Ref.68-33.

HALPERN D. 1976. Structure of a coastal upwelling event observed off Oregon during July 1973. *Deep Sea Research* 23:495-508.

HAURY L.R., J.J.SIMPSON, J.PELAEZ, C.J.KOBLINSKY, and D. WIESENHAHN. 1986. Biological consequences of a recurrent eddy off Point Conception, California. *Journal of Geophysical Research* 91:12937-12956.

HAYWARD T.L. and J.A.McGOWAN. 1985. Spatial patterns of chlorophyll, primary production, macrozooplankton biomass, and physical structure in the central North Pacific Ocean. *Journal of Plankton Research* 7:147-167.

HERLINVEAUX R.H. and J.P.TULLY. 1961. Some oceanographic features of Juan de Fuca Strait. *Journal of the Fisheries Research Board of Canada* 18:1027-1071.

HERMAN A.W., D.D.SAMEOTO, and A.R.LONGHURST. 1981. Vertical and horizontal patterns of copepods near the shelf break south of Nova Scotia. *Canadian Journal of Fisheries and Aquatic Sciences* 38:1065-1076.

HICKEY B.M. 1979. The California Current System - hypothesis and facts. *Progress in Oceanography* 8:191-279.

HICKEY B.M. 1981. Alongshore coherence on the Pacific Northwest continental shelf (January - April, 1975). *Journal of Physical Oceanography* 11:822-835.

HICKEY B.M., R.THOMSON, P.LeBLOND, and H.YIH. In Prep. A buoyancy driven coastal current.

HOLLIGAN P.M., R.P.HARRIS, R.C.NEWELL, D.S.HARBOUR, R.N.HEAD, E.A.S. LINLEY, M.I.LUCAS, P.R.G.TRANTER, and C.M.WEEKLEY. 1984. Vertical distribution and partitioning of organic carbon in mixed, frontal and stratified waters of the English Channel. *Marine Ecology Progress Series* 14:111-127.

HUYER A. 1977. Seasonal variation in temperature, salinity, and density over the continental shelf off Oregon. *Limnology and Oceanography* 22:442-453.

HUYER A., E.J.C.SOBEY and R.L.SMITH. 1979. The spring transition in currents over the Oregon continental shelf. *Journal of Geophysical Research* 84:6995-7011.

IKEDA M. and W.J.EMERY. 1984. A continental shelf upwelling event off Vancouver Island as revealed by satellite infrared imagery. *Journal of Marine Research* 42:303-317.

IKEDA M., W.J.EMERY and L.A.MYSAK. 1984a. Seasonal variability in meanders of the California Current System off Vancouver Island. *Journal of Geophysical Research* 89:3487-3505.

IKEDA M., L.A.MYSAK and W.J.EMERY. 1984b. Observation and modelling of satellite sensed meanders and eddies off Vancouver Island. *Journal of Physical Oceanography* 14:3-21.

JONES B.H., K.H.BRINK, R.C.DUGDALE, D.W.STUART, J.C.VAN LEER, D.BLASCO and J.C.KELLEY. 1983. Observations of a persistent upwelling center off Point Conception, California. In: Coastal Upwelling. E.Suess and J.Thiede (eds.), Plenum Press, New York, pp 37-60.

KATSAROS K. 1980. The aqueous thermal boundary layer. *Boundary-Layer Meteorology* 18:107.

KAWAMURA H., K.MIZUNO, and Y.TOBA. 1986. Formation process of a warm core ring in the Kuroshio-Oyashio frontal zone, Dec. 1981 - Oct. 1982. *Deep Sea Research* 33:1617-1640.

KRAUSE E.P. and A.G.LEWIS. 1979. Ontogenetic migration and distribution of *Eucalanus bungii* (Copepoda; Calanoida) in British Columbia waters. *Canadian Journal of Zoology* 57:2211-2222.

LANE R.K. 1961. A review of temperature and salinity structures in the approaches to Vancouver Island, British Columbia. *Journal of the Fisheries Research Board of Canada* 19:45-91.

LA PEROUSE PROJECT: 1985. First Annual Progress Report. March 1986. Unclassified Report, Department of Fisheries and Oceans, Canada. Project coordinators; D.M.Ware, Nanaimo Biological Station, Nanaimo, B.C., and R.E.Thomson, Institute of Ocean Sciences, Sidney, B.C..

LA PEROUSE PROJECT: 1986. Second Annual Progress Report. April 1987. Unclassified Report, Department of Fisheries and Oceans, Canada. Project coordinators; D.M.Ware, Nanaimo Biological Station, Nanaimo, B.C., and R.E.Thomson, Institute of Ocean Sciences, Sidney, B.C..

LARSEN P.F. 1985. Thermal satellite imagery applied to a littoral macrobenthos investigation in the Gulf of Maine. *International Journal of Remote Sensing* 6:919-926.

LASKER R., J.PALAEZ and R.M.LAURS. 1981. The use of satellite infrared imagery for describing ocean processes in relation to spawning of the northern anchovy. *Remote Sensing of the Environment* 11:439-453.

LAURS R.M., P.C.FIEDLER and D.R.MONTGOMERY. 1984. Albacore tuna catch distributions relative to environmental features observed from satellites. *Deep Sea Research* 31:1085-1099.

LA VIOLETTE P.E. 1984. The advection of submesoscale thermal features in the Alboran Sea gyre. *Journal of Physical Oceanography* 14:550-565.

LEGERE J.E.H. 1957. The qualitative and quantitative distribution of plankton in the Strait of Georgia in relation to certain environmental factors. *Journal of the Fisheries Research Board of Canada* 14:521-552.

LEGECKIS R. 1978. A survey of worldwide sea surface temperature fronts detected by environmental satellites. *Journal of Geophysical Research* 83:4501-4522.

LEGECKIS R. 1986. A satellite time series of sea surface temperature in the eastern equatorial Pacific Ocean, 1982-1986. *Journal of Geophysical Research* 91:12879-12886.

LEGECKIS R., and G.CRESSWELL. 1981. Satellite observations of sea surface temperature fronts off the coast of western and southern Australia. *Deep Sea Research* 28:297-306.

LEGECKIS R., and W.PICHEL. 1984. Monitoring of long waves in the eastern equatorial Pacific 1981-1983 using satellite multi-channel sea surface temperature charts. NOAA Tech. Rep. NESDIS 8, pp 1-19. NOAA, Washington, D.C..

LEGECKIS R., and G.REVERDIN. 1987. Long waves in the equatorial Atlantic Ocean during 1983. *Journal of Geophysical Research* 92:2835-2842.

LEGENDRE L. and S.DEMERS. 1984. Towards dynamic biological oceanography and limnology. *Canadian Journal of Fisheries and Aquatic Sciences* 41:2-19.

LEKAN J.F. and R.E.WILSON. 1978. Spatial variability of phytoplankton biomass in the surface waters of Long Island. *Estuarine Coastal and Shelf Science* 6:239-251.

LEWIS A.G. and W.R.CAVE. 1982. The biological importance of copper in oceans and estuaries. *Oceanography and Marine Biology Annual Review* 20: 471-695.

LEWIS A.G. and A.C.THOMAS. 1986. Tidal transport of planktonic copepods across the sill of a British Columbia fjord. *Journal of Plankton Research* 8:1079-1089.

LONGHURST A.R. 1981. Editor. Analysis of Marine Ecosystems, Academic Press, London, 741 pp..

LUTJHARMES J.R. 1981. Spatial scales and intensities of circulation in the ocean areas adjacent to South Africa. *Deep Sea Research* 28:1289-1302.

LYNN R.J. and J.SVEJKOVSKY. 1984. Remotely sensed sea surface temperature variability off California during a Santa Ana clearing. *Journal of Geophysical Research* 89:8151-8162.

MACISAAC J.J. and R.C.DUGDALE. 1969. The kinetics of nitrate and ammonia uptake by natural populations of marine phytoplankton. *Deep Sea Research* 16:45-57.

MACISAAC J.J. R.C.DUGDALE R.T.BARBER D.BLASCO and T.T.PACKARD. 1985. Primary production cycle in an upwelling center. *Deep Sea Research* 32:503-529.

MACKAS D.L. 1984. Spatial autocorrelation of plankton community composition in a continental shelf ecosystem. *Limnology and Oceanography* 29:451-471.

MACKAS D.L. K.L.DENMAN and M.R.ABBOTT. 1985. Plankton patchiness: biology in the physical vernacular. *Bulletin of Marine Science* 37:652-674.

MACKAS D.L. G.C.LOUTTIT and M.J.AUSTIN. 1980. Spatial distribution of zooplankton and phytoplankton in British Columbia coastal waters *Canadian Journal of Fisheries and Aquatic Sciences* 37:1476-1487.

MACKAS D.L. and H.A.SEFTON. 1982. Plankton species assemblages off southern Vancouver Island: geographic pattern and temperal variability. *Journal of Marine Research* 40:1173-1200.

MAUL G.A. and M.SIDRAN. 1973. Atmospheric effects on ocean surface temperature sensing from the NOAA satellite scanning radiometer. *Journal of Geophysical Research* 78:1909-1916.

McCLAIN C.R., L.J.PIETRAFESA and J.A.YODER. 1984. Observations of Gulf Stream induced and wind driven upwelling in the Georgia Bight using ocean colour and infrared imagery. *Journal of Geophysical Research* 89:3705-3723.

McCLAIN E.P. 1981. Split window and triple window sea surface temperature determination from satellite measurements. Mini-symposium on Application of Aerospace Remote Sensing in Marine Research. ICES Statutory Meeting.

McCLAIN E.P., W.G.PICHEL, C.C.WALTON, Z.AHMAD and J.SUTTON. 1983. Multi-channel improvements to satellite-derived global sea surface temperatures. *Advances in Space Research* 2:43-47.

McCLAIN E.P., W.G.PICHEL and C.C.WALTON. 1985. Comparative performance of AVHRR based multichannel sea surface temperatures. *Journal of Geophysical Research* 90:11587-11601.

McGOWAN J.A. 1977. What regulates pelagic community structure? In: Ocean sound scattering prediction. N.R.Anderson and B.J.Zahuranec (eds.) Plenum Press, New York.

McGOWAN J.A. and P.W.WALKER. 1979. Structure in the copepod community of the North Pacific Central Gyre. *Ecological Monographs* 49:195-226.

McMILLIN. 1980. The split-window retrieval algorithm for sea surface temperature derived from satellite measurements. In: Remote Sensing of Atmospheres and Oceans. A.Deepak (ed.), Academic Press, New York.

MILLARD S.P., J.R.YEARSLEY and D.P.LETTENMAIER. 1985. Space - time correlation and its effects on methods for detecting aquatic ecological change. *Canadian Journal of Fisheries and Aquatic Sciences* 42:1391-1400.

ODUM E.P. 1971. Fundamentals of Ecology. W.B. Saunders, Philadelphia.

OKUBO A. 1978. Horizontal dispersion and critical scales for phytoplankton patches. In: Spatial Patterns in Plankton Communities. J.H.Steele (ed.), Plenum Press. New York.

ORLOCI L. 1978. Multivariate Analysis in Vegetation Research. Dr.W.Junk - Publishers, The Hague.

PARSONS T.R., L.F.GIOVANDO and R.J.LEBRASSEUR. 1966. The advent of the spring bloom in the eastern subarctic Pacific Ocean. *Journal of the Fisheries Research Board of Canada* 23:539-546.

PARSONS T.R. and R.J.LEBRASSEUR. 1968. A discussion of some critical indices of primary and secondary production for large-scale ocean surveys. *Calif. Mar. Res. Comm., CalCOFI Rept. 12:54-63.*

PARSONS T.R. M.TAKAHASHI and B.HARGRAVE. 1984. Biological Oceanographic Processes. 3rd Edition. Pergamon Press.

PATHAK P.N. 1982. Comparisons of sea surface temperature observations from TIROS-N and ships in the North Indian Ocean during MONEX, (May – July 1979). *Remote Sensing of the Environment* 12:363-369.

PIELOU E.C. 1977. Mathematical Ecology. J.Wiley and Sons - Publishers, New York.

PIETRAFESA L.J. 1983. Shelfbreak circulation, fronts and physical oceanography: east and west coast perspectives. Society of Economic Paleontologists and Mineralogists, Special Publication No. 33, 233-250, June 1983.

PINGREE R.D., P.M.HOLLIGAN, G.T.MARDELL and R.N.HEAD. 1976. The influence of physical stability on spring, summer, and autumn phytoplankton blooms in the Celtic Sea. *Journal of the Marine Biological Assoc. of the U.K.* 56:845-873.

POLLARD J.H. 1977. A handbook of numerical and statistical techniques: with examples mainly from the life sciences. Univ. of Cambridge Press, Melbourne, New York.

POMEROY L.R., L.P.ATKINSON, J.O.BLANTON, W.B.CAMPBELL, T.R.JACOBSEN, K.H.KERRICK and A.M.WOOD. 1983. Microbial distribution and abundance in response to physical and biological processes on the continental shelf of southeastern U.S.A.. *Continental Shelf Research* 2:1-20.

RODEN G.I. and P.F.PASKAUSKY. 1978. Estimation of rates of frontogenesis and frontolysis in the North Pacific Ocean using satellite and surface meteorological data from Jan. 1977. *Journal of Geophysical Research* 83:4545-4550.

SCHLUESSEL P., H-Y. SHIN, W.J.EMERY and H.GRASSL. 1987. Comparison of satellite-derived sea surface temperatures with in-situ skin measurements. *Journal of Geophysical Research* 92:2859-2874.

SHANNON L.V., N.M.WALTERS, and S.A.MOSTERT. 1985. Satellite observations of surface temperature and near surface chlorophyll in the southern Benguela region. In: South African Ocean Colour and Upwelling Experiment. L.V.Shannon (ed.). Fisheries Research Institute, Cape Town, South Africa.

SIMPSON J.H., C.M.ALLEN and N.C.G.MORRIS. 1978. Fronts on the continental shelf. *Journal of Geophysical Research* 83:4607-4614.

SIMPSON J.J. 1983. Large scale thermal anomolies in the California Current during the 1982 – 1983 El Niño. Geophysical Research Letters 10:937-940.

SIMPSON J.J., C.J.KOBLINSKY, J.PELAEZ, L.R.HAURY, and D.WIESENHAHN. 1986. Temperature - plant pigment - optical relations in a recurrent offshore mesoscale eddy near Point Conception, California. *Journal of Geophysical Research* 91:12919-12936.

SMITH S.L. and JJ.VIDAL. 1984. Spatial and temporal effects of salinity, temperature and chlorophyll on the communities of zooplankton in the southeastern Bering Sea. *Journal of Marine Research* 42:221-257.

STAR J.L. and M.M.MULLIN. 1981. Zooplanktonic assemblages in three areas of the North Pacific as revealed by continuous horizontal transects. *Deep Sea Research* 28:1303-1322.

STEELE J.H. 1978. Editor. Spatial patterns in Plankton Communities. Plenum Press. New York. 470 pp.

STEELE J.H. and E.W.HENDERSON. 1979. Spatial patterns in North Sea plankton. *Deep Sea Research* 26:955-963.

STONE D.P. 1980. The distribution of zooplankton communities in a glacial runoff fjord and exchanges with the open sea. In; Fjord Oceanography, H.J.Freeland, D.M.Farmer, and C.D.Levings, (Eds.), NATO Conference Series IV: Marine Sciences, Vol. 4. Plenum Press. New York.

SUNDBY S. 1984. Influence of bottom topography on the circulation at the continental shelf off northern Norway. *Fiskeridir. Skr. Ser. Havunders.* 17:501-519.

TABATA S. and J.F.R.GOWER. 1980. A comparison of ship and satellite measurements of sea surface temperatures off the Pacific coast of Canada. *Journal of Geophysical Research* 85:6636-6648.

THOMSON R.E. 1981. Oceanography of the British Columbia coast. Can. Spec. Publ. 56, 291pp. Fish. Aquat. Sci., Ottawa, 1981.

THOMSON R.E. 1984. A cyclonic eddy over the continental margin of Vancouver Island: Evidence for baroclinic instability. *Journal of Physical Oceanography* 14:1326-1348.

THOMSON R.E. and J.F.R.GOWER. 1985. A wind induced mesoscale eddy over the Vancouver Island continental slope. *Journal of Geophysical Research* 90:8981-8993.

TRAGANZA E.D., V.M.SILVA, D.M.AUSTIN, W.L.HANSON and S.H.BRONSINK. 1983. Nutrient mapping and recurrence of coastal upwelling centers by satellite remote sensing: Its implication to primary production and the sediment record. In: Coastal Upwelling, F.A.Richards, (ed.), American Geophysical Union, Washington, D.C.

TREMBLAY M.J. and J.C.ROFF. 1983. Community gradients in the Scotian Shelf zooplankton. *Canadian Journal of Fisheries and Aquatic Sciences* 40:598-611.

TULLY J.P. 1942. Surface non-tidal currents in the approaches too Juan de Fuca Strait. *Journal of the Fisheries Research Board of Canada* 5:398-409.

WALTON C. 1980. Deriving sea surface temperatures from TIROS-N data. Remote sensing of Atmospheres and Oceans, A.Deepak (ed.) pp.547-579. Academic Press. New York.

WIEBE P.H., G.R.FLIERL, C.S.DAVIS, V.BARBER, and S.H.BOYD. 1985. Macrozooplankton biomass in Gulf Stream warm core rings: spatial distribution and temporal changes. *Journal of Geophysical Research* 90:8885-8901.

WILKERSON F.P. and R.C.DUGDALE. 1987. The use of large shipboard barrels and drifters to study the effects of coastal upwelling on phytoplankton dynamics. *Limnology and Oceanography* 32:368-382.

WISHNER K.A. and S.K.ALLISON. 1986. The distribution and abundance of copepods in relation to the physical structure of the Gulf Stream. *Deep Sea Research* 33:705-731.

ZIMMERMAN R.C. J.N.KREMER and R.C.DUGDALE. 1987. Acceleration of nutrient uptake by phytoplankton in a coastal upwelling ecosystem: A modelling analysis. *Limnology and Oceanography* 32:359-367.